UNIVERSITA' POLITECNICA DELLE MARCHE
Facoltà di Ingegneria

Corso di Laurea Magistrale in
INGEGNERIA CIVILE – Strutture

Tesi di Laurea:

BACK- ANALYSIS OF OFFSHORE STEEL PILE DRIVING RECORDS

ANALISI DEI RISULTATI DI BATTITURA DI PALI IN ACCIAIO IN MARE APERTO

Candidata:
Alessandra Pettinari

Relatore:
Prof. Paolo Ruggeri

Correlatore:
Ing. Andrea Foresi

Anno Accademico 2023-2024

Ai miei genitori e a mio fratello,

le uniche persone che ci hanno sempre creduto,

fin dal primo giorno, forse anche più di me.

SINTESI

La presente tesi riguarda l'analisi dei risultati di battitura di pali tubolari in acciaio in mare aperto, al fine di validare e ottimizzare le metodologie di calcolo presenti in letteratura. Lo studio è stato svolto in collaborazione con l'azienda SAIPEM S.p.A (sede di Fano).

Diversi sono i modelli attualmente in uso nell'industria offshore per valutare la resistenza del terreno all'infissione di un palo tubolare e tutti comportano elevate incertezze. A seconda delle condizioni del sito, si può avere sia una sovrastima che una sottostima della resistenza del terreno. Ciò può avere importanti conseguenze contrattuali e operative, ad esempio, nella scelta del battipalo (hammer) da utilizzare per l'installazione dei pali o nella definizione della sezione resistente del palo. Una sovrastima della resistenza all'infissione comporta infatti l'utilizzo di hammer più prestanti, di energie maggiori e quindi costi sicuramente più elevati. Al tempo stesso si potrebbe andare incontro ad un sovradimensionamento del palo: ad un battipalo più prestante corrisponde infatti un palo più robusto in modo da avere caratteristiche meccaniche adeguate a trasferire l'energia ricevuta al terreno.

Di contro, una sottostima può portare alla scelta di un battipalo inadeguato e comportare una condizione di "rifiuto" del palo, cioè ad un numero eccessivo di colpi per l'avanzamento o, addirittura, a una non penetrazione dello stesso. Lato struttura, inoltre, si potrebbe determinare un eccessivo stress sul palo (in quanto esso risulterebbe sottodimensionato in termini di spessore delle pareti e quindi di rigidezza e resistenza) o all'insorgenza di un danno da fatica.

In questa tesi, è stata effettuata una back analysis dei parametri registrati durante l'infissione di pali tubolari di grande diametro e lunghezza mediante il metodo dell'equazione d'onda, con l'ausilio del software GRLweap, per convalidare le formulazioni di letteratura al caso studio caratterizzato dalla presenza di argille calcaree. Dall'elaborazione dei dati si è osservato che questo particolare terreno manifesta sia basse resistenze all'infissione, come è risultato dalla battitura continua del palo (grazie al degrado dell'attrito laterale), sia un recupero di resistenza durante le interruzioni della battitura (a causa di saldature, mal funzionamento del battipalo, condizioni meteorologiche avverse), fenomeno questo che può anche portare a condizioni di rifiuto prematuro dei pali.

Lo studio è stato organizzato con una prima parte rivolta alla descrizione del processo di infissione e alla presentazione delle formulazioni esistenti per la corretta stima della

resistenza che il terreno offre alla penetrazione del palo, raccogliendo ed esaminando la letteratura disponibile. I metodi studiati e analizzati sono:

- Metodo di Stevens: basato sull'analisi di piattaforme installate nell'area del Golfo Persico, considerando due possibili comportamenti della punta di un palo tubolare, a punta chiusa (plugged) o a punta aperta (unplugged).
- Metodo di Alm & Hamre: basato sulla stima della resistenza del terreno a partire dalla prova penetrometrica statica (CPT). È un metodo tarato sui terreni del Mar del Nord e quindi tende a sovrastimare la resistenza all'avanzamento rispetto a quella riscontrata nell'area di interesse.
- Metodo della "percentuale della capacità assiale".

Per ottenere le informazioni necessarie a raggiungere gli obiettivi prefissati, il lavoro di tesi è stato suddiviso in una serie di fasi successive:

1. Per iniziare, sulla base dei dati in nostro possesso, provenienti da indagini geofisiche, geologiche e geotecniche, è stato valutato il modello stratigrafico del terreno in riferimento al caso di studio: argille calcaree intervallate da depositi sabbiosi.
2. Nello step successivo, i valori monitorati dalla società responsabile del programma di indagine geognostica (Fugro) durante l'infissione del palo, in termini di numero di colpi, energia del martello e sollecitazioni sul palo (tensioni e compressioni) sono stati utilizzati per due analisi, condotte mediante un software che simula la risposta di un palo elastico in un mezzo elasto-plastico-viscoso sotto l'impatto di un battipalo (GRLweap) e specificamente:

   - "Analisi della capacità portante (bearing analysis)": fornisce, a partire dal numero di colpi registrati durante l'infissione, una stima della resistenza del terreno alla penetrazione del palo.

   - "Analisi di infiggibilità (drivability analysis)": fornisce, a partire dal modello geotecnico del terreno (caratterizzato sia dal punto di vista statico che dinamico) e dall'assunzione di un'energia mediata rispetto ai valori reali monitorati, una valutazione del numero di colpi necessari all'infissione, da confrontare poi con quelli reali.
3. Successivamente sono stati modificati i parametri dinamici del terreno (in termini di smorzamento) per considerare eventuali stop durante l'installazione del palo, in

modo da ottenere la migliore corrispondenza tra i parametri registrati e quelli derivanti dall'analisi.

4. Per concludere, i risultati ottenuti sono stati confrontati con i dati reali, concentrando l'attenzione sul fenomeno di degrado della resistenza durante un'installazione continua e sul recupero della resistenza durante i periodi di interruzione.

Un grande supporto a questa tesi è dato dalla presenza di un monitoraggio dinamico dei pali. I pali delle piattaforme prese in esame sono tutti strumentati con accelerometri ed estensimetri che restituiscono in output i parametri dinamici misurati durante l'installazione. Questi dati successivamente sono stati elaborati con un noto metodo analitico di analisi dinamica basato sui risultati di infissione del palo (CAPWAP: Case Pile Wave Analysis Program) in modo da stimare i valori di capacità laterale, alla punta e i parametri dinamici del terreno (smorzamento e soglia plastica).

Grazie a questi dati è stato possibile calibrare il modello, elaborato con il software GRLweap, ed ottenere una buona corrispondenza tra i valori calcolati e i valori monitorati.

Il programma simula ciò che accade nel battipalo, nel palo e nel terreno durante e subito dopo l'impatto dello strumento. A tal fine il palo è modellato da una serie di masse rigide collegate da molle elastiche in modo da considerare sia l'inerzia che l'elasticità della pila.

I pali tubolari in esame sono caratterizzati da lunghezze importanti (dell'ordine dei 200 m) in quanto si devono raggiungere profondità di penetrazione nel fondale dell'ordine dei 130 m. Il motivo di questa elevata dimensione dipende dai carichi molto elevati, dati dalla piattaforma e dalle sollecitazioni ambientali e, soprattutto, dalla natura del terreno, che, nel sito preso in esame (Golfo Persico), è costituito da argilla con resistenza non drenata bassa, come spesso succede in ambiente Offshore. A causa di queste caratteristiche geometriche, i pali in mare aperto non sono mai installati in un'unica soluzione, ma sono costituiti da un corpo principale (lead section) e da spezzoni aggiuntivi (add on) saldati sul posto.

L'hammer, in particolare la massa (ram) e il dispositivo a contatto con la testa del palo (anvil) sono generalmente elementi rigidi e sono rappresentati semplicemente dalle loro masse.

Il terreno è rappresentato in termini statici e dinamici. Il processo di infissione genera sollecitazioni dinamiche lungo il fusto e sulla punta del palo.

Il palo è quindi modellato come una serie di molle elasto-plastiche che si deformano in maniera elastica fino a un valore massimo di spostamento che corrisponde allo snervamento (quake) e da uno smorzatore viscoso che simula una resistenza direttamente proporzionale

alla velocità associata al segmento di palo durante la battitura ed è rappresentato dal parametro di smorzamento (damping).

A conclusione del lavoro si è dimostrato che, nonostante intorno ai parametri dinamici (damping e quake) ci sia una grande incertezza, tramite una back analysis dei risultati monitorati è stato possibile trovare i valori che meglio rappresentano il comportamento dinamico del terreno e che potranno essere riutilizzati in progetti futuri dell'azienda in situazioni caratterizzate dalla stessa stratigrafia del sito preso in esame.

I principali risultati di questo lavoro sono riportati di seguito:

- I valori della capacità interpolata (valutata con analisi GRLweap) trovano una buona corrispondenza con i valori monitorati utilizzando un fattore di smorzamento (damping) compreso tra 0.4 s/m e 0.7 s/m. Questi valori confermano quanto rilevato da Delimi e da Clavaud, nell'area del Golfo Persico, in presenza di pali di grande diametro e terreno con elevato contenuto di carbonato. Sono inoltre anche in linea con le assunzioni di Smith, che prevede l'utilizzo di uno smorzamento pari a 0.65 s/m per terreni argillosi e 0.16 s/m per terreni prevalentemente sabbiosi.

  In corrispondenza dei periodi di interruzioni dall'installazione (con il fenomeno di set-up, cioè il recupero di capacità portante che si verifica dopo l'installazione), il fattore di damping tende a diminuire.
- Le argille calcaree hanno mostrato una elevata degradazione durante l'infissione:
  - In corrispondenza della profondità di penetrazione del secondo add-on (EOD_P3), la resistenza mobilizzata è compresa tra il 40 e il 70% della resistenza stimata nell'ipotesi di installazione continua (cioè, della capacità assiale statica del palo ridotta con un coefficiente di degradazione) e tra il 20 e il 30% della capacità assiale statica.
  - Per l'infissione dell'ultima sezione (fino alla penetrazione obiettivo del palo) è stato osservato un aumento della resistenza del terreno rispetto all'infissione fino alla sezione P3. La resistenza mobilizzata è compresa tra l' 80% e il 130% della resistenza valutata per simulare l'installazione continua (cioè, della capacità assiale statica del palo ridotta con un coefficiente di degradazione) e tra il 20% e il 40% della capacità assiale statica.

- Grazie al fenomeno del set-up il palo ha recuperato e sviluppato la sua capacità portante:
    - In corrispondenza dell'ultima saldatura, considerando il periodo di stop di tre/quattro giorni (BOD_P4), la resistenza mobilizzata è compresa tra l' 80% e il 130% della resistenza valutata nell'ipotesi di installazione continua (cioè, della capacità assiale statica del palo ridotta con un coefficiente di degradazione) e tra il 40% e il 60% della capacità assiale statica del palo.

LIST OF FIGURES

LIST OF TABLES

CONTENTS

CHAPTER 1: INTRODUCTION

1.1. ABOUT THIS THESIS

Drivability prediction models currently used in the offshore industry may involve large uncertainties. Depending on the soil conditions, this can yield to either over-estimate or under-estimate the driving resistances likely to be encountered at a site. This can have important contractual and operational consequences when considering the selection of hammers to be used for pile installation.

An over-estimate of it can lead to a definition of more powerful hammer or of an oversized pile; that means higher costs. On the other hand, an under-estimate of it results in possibilities of pile refusal (because of a definition of a less powerful hammer) or pile overstress or fatigue damage. In this last case a drilling operation can be necessary to install the pile (more expensive that drivability installation).

The scope of drivability analysis is to select the hammer able to drive a pile up to the target penetration in any conditions (continuous or restart mode) without experiencing premature refusal, without overstressing the pile due to static and dynamic stresses and without fatigue damage.

In this thesis, a back-analysis of pile driving records by means of the wave equation method (with the software GRLweap) was carried out to validate the pile drivability model for offshore clays, taking into account both the low driving resistances observed during continuous driving (thanks to the friction degradation) and the set-up effect during driving interruptions (due to welding; hammer braking; bad weather conditions), which can lead to premature refusal of piles.

It is easily understood that, after the piles have been driven, the “observed” soil resistance to driving (SRD) can be backcalculated from driving blow counts by the wave equation analyses. This “reversed” calculation procedure allows the actual soil resistance to be compared to the predicted SRD range.

This back-analysis is only valid if:

- Similar quake and damping parameters are used in both analyses

- The actual driving energy transferred to the pile is known with accuracy (by pile monitoring).

1.2. PURPOSE AND SCOPE

This thesis aims at:

- Estimating of maximum driving resistance, likely to be encountered, based on back-analysis of pile driving records (blow counts).
- Estimating of soil parameters to find a match between the calculated and monitoring blow counts.
- Estimating of soil driving resistance based on CPT method.
- Estimating of effect occurred from friction degradation phenomenon during pile installation (possibly yielding low driving blow counts during continuous driving) and set-up effect during driving interruptions (which can lead to premature refusal of pile).

In order to estimate the driving resistance that a given pile-hammer-soil system can overcome, we must determine:

- pile dimensions (diameter, wall thickness, length) and penetration

- hammer characteristics (efficiency and driving energy transferred to the pile)

- quake and damping properties of the soil.

Drivability analysis must be conservative but not too conservative because it can lead to the mobilization of too large hammers and concern about the ultimate capacity in relation with the very low blow counts obtained.

1.3. THESIS ORGANIZATION

The contents of the thesis are organized in the following chapters:

- ***Chapter 1 (Introduction)*:** introduction of the work, including purposes and the thesis organization.
- ***Chapter 2 (Phenomenology):*** general presentation of the topic of offshore pile installation, possible problems during pile driving and some remedial actions. In this

chapter it is introducing some important aspects that are going to be treated during the thesis such as the static soil resistance to driving and the dynamic characterization (in terms of quake and damping). Techniques for monitoring offshore piles and the CAPWAP procedure for estimating soil resistance to driving are then reported.

- ***Chapter 3 (Case studies):*** presentation of the case studies: focus on the characterization of the study area, of the pile data, soil data and hammer data for pile installation. In this chapter the field data are also presented: a graphical illustration of the observed parameters along the pile in terms of blows count, compressive stress on the pile and hammer energy.
- ***Chapter 4 (Methodology):*** detailed description of the procedure used in GRLweap and presentation of the two analyses for pile installation, bearing and drivability analyses. It is also reported another program that can be used to carry out the same analysis.
- ***Chapter 5 (Results):*** results of the comparison between observed and calculated values of capacity and blow count considering both analyses, bearing and drivability. Then, the results of CPT method and the influence of set-up phenomenon in the prediction of blow counts and SRD are presented and discussed.

  Also, a statistical representation through histograms is provided to show the differences between measured and calculated SRD.
- ***Chapter 6 (Conclusions and future studies):*** conclusions and recommendations for further studies.

CHAPTER 2: PHENOMENOLOGY

2.1 OFFSHORE ENGINEERING

Offshore Engineering is the engineering discipline that deals with the design and construction of structures intended to work in a stationary position in the ocean environment. The majority of offshore structures are designed for various purposes like oil drilling, gas extraction, and renewable energy production. Recent advancements have led to innovative designs and improved installation processes. There are various types of offshore structures listed below [4]:

- Fixed platform: are directly anchored to the seabed, typically used in shallow waters (up to 150 meters deep). They consist of a jacket made of tubular steel members and are used for drilling and production operations.
- Compliant towers: are slender, flexible structures, suitable for depths between 150 and 900 meters. They can withstand significant lateral forces, making them ideal for areas with strong currents and high winds. These towers are assembled onshore, then floated and towed to the site. The base is secured to the seabed with piles.
- Semi-submersible Platforms: are floating structures, supported by pontoons submerged below the water surface. They are stable and suitable for deep-water operations (up to 3000 meters).

-Floating Production Systems (FPS): are ship-shaped vessels used for the processing and storage of oil and gas. They are flexible and can be relocated.

-Tension-leg Platforms (TLP): are floating platforms tethered to the seabed by vertical tendons, minimizing vertical movement. They are suitable for depths up to 2000 meters.

-Renewable Energy Structures: these include structures for wind, wave, and tidal energy. Floating wind turbines are becoming increasingly popular in deep-water locations.

Then, another important component of offshore world is the pipeline that is useful to bring oil and gas onshore.

The field of offshore structures is evolving rapidly, with new technologies enhancing efficiency, safety, and environmental sustainability. Each type of structure has unique characteristics and installation processes, tailored to specific operational requirements and environmental conditions.

As the demand for offshore resources and renewable energy grows, these structures will continue to play a pivotal role in global energy strategies.

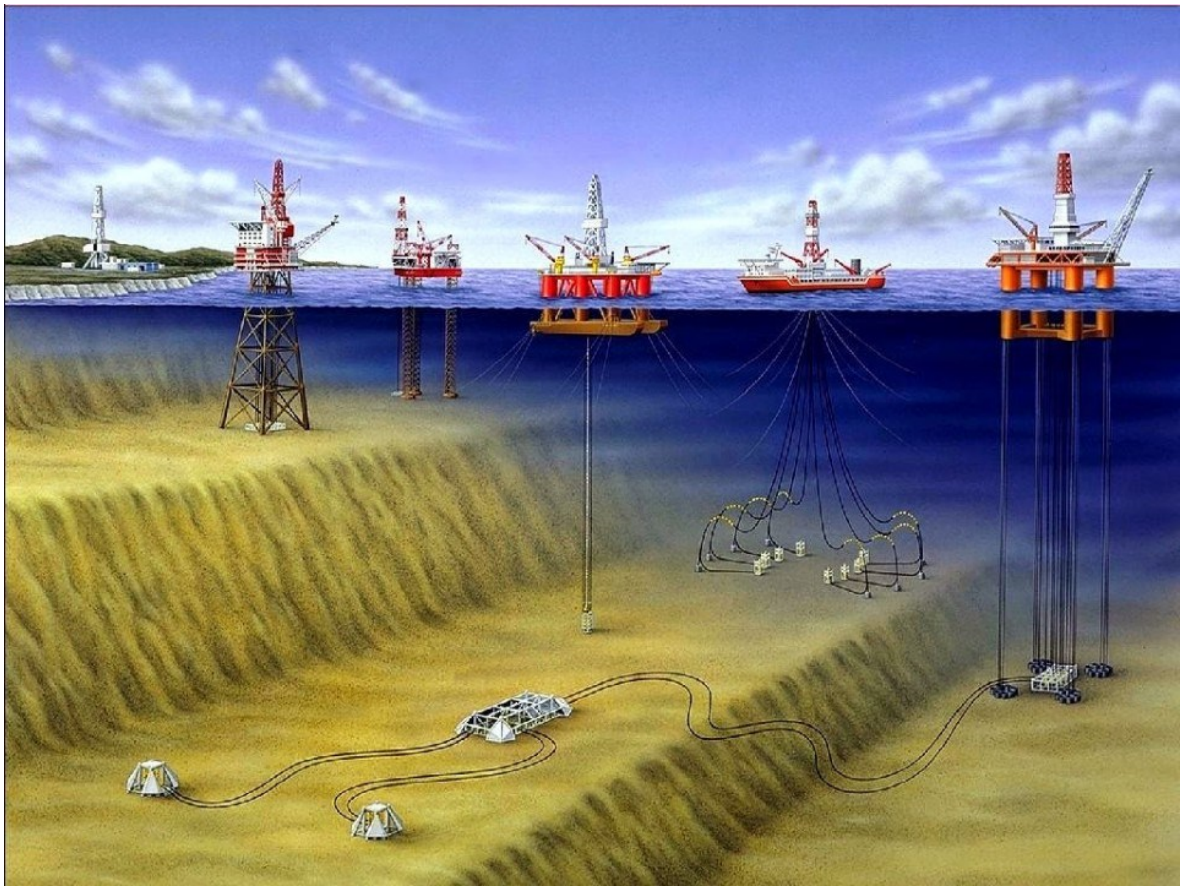

Figure 1 Offshore world

2.1.1 TYPICAL ACTIONS IN THE OFFSHORE ENVIRONMENT

Loads on offshore structures are in general gravity loads, environmental loads and seismic loads. Gravity loads arise from dead weight of structure and facilities either permanent or temporary; they include [5]:

- Structural Dead Load: include all fixed items in the platform deck and jacket. It includes all primary steel structural members and secondary structural items. The primary structural steel members are automatically calculated based on the structural information in the model when a computer program is used to analyze the structure. Differently, the weight of the secondary structural steel items shall be calculated applied to the structural model at appropriate locations.

- Facility Dead Loads: the structure built either for driving or wellhead type platform or for process type platform supports various equipment and facilities. The weight of such items shall be calculated and applied at the appropriate locations according to the design of the structure.
- Fluid Loads: they are weight of fluid on the platform during operation. This may include all the fluid in the equipment and piping.
- Live Loads: they are defined as movable loads and are temporary in nature.

Seismic loads arise from gravity loads and are a derived type.

Environmental loads play a major role in governing the design of offshore structures. Before starting the design of any structure, accurate prediction of environmental loads is important. Various environmental loads acting on the offshore platform are listed below:

- Wind Loads: it shall be calculated as per API RP2A guidelines. The total force of wind on the platform can be calculated as:

$$f_x = F_w \cdot A_x \cdot C_s$$

$$f_y = F_w \cdot A_y \cdot C_s$$

  Where F_w is the wind pressure, C_s is a shape coefficient that can be selected from API RP2A guidelines and A is the wind blockage area.

- Wave and Current Loads: there are two ways of applying it. The first one is called Design wave method; in this case a discrete set of design waves (maximum) and associated periods are selected to generate loads on the structure. These loads are used to compute the response of the structure. The second one is called the spectral method: in this case an energy spectrum of the sea-state for the location are taken and a transfer function for the response will be generated.

  The period of wind generated waves in the open sea can be in the order of 2 to 20 s. These waves are called gravity waves and contain most of the wave energy. Maximum wave shall be used for the design of offshore structures.
- Ice Loads: for structures located in Polar regions and cold countries, they shall be considered in the design.
- Buoyancy load: as offshore jackets are partially or fully submerged, they are subjected to hydrostatic pressures due to the weight of the water above it and due to the movement of water around the members resulting from wave actions.

According to API-RP2A [6] environmental loads, except for earthquake, should be combined in a manner consistent with the probability of their simultaneous occurrence during the loading condition being considered.

Earthquake load, where applicable, should be imposed on the platform as a separate environmental loading condition.

2.2 STEEL OFFSHORE FIXED PLATFORMS

Offshore platforms are extensively used to explore, drill, produce, storage, and transport ocean oil and/or gas resources in different depths.

The most widely used platform type is the steel jacket structure. This consist of a welded tubular steel space frame (jacket) supported on a piled foundation.

The jacket (sub-structure) is used to support the platform topsides (e.g. deck) above the water and serves as a template for pile driving.

Typical steel offshore platform installed are:

- 4 legged jacket platform (as shown in Figure 2)
- 6 legged jacket platform

The jacket size and weight vary with the water depth and the topsides weight.

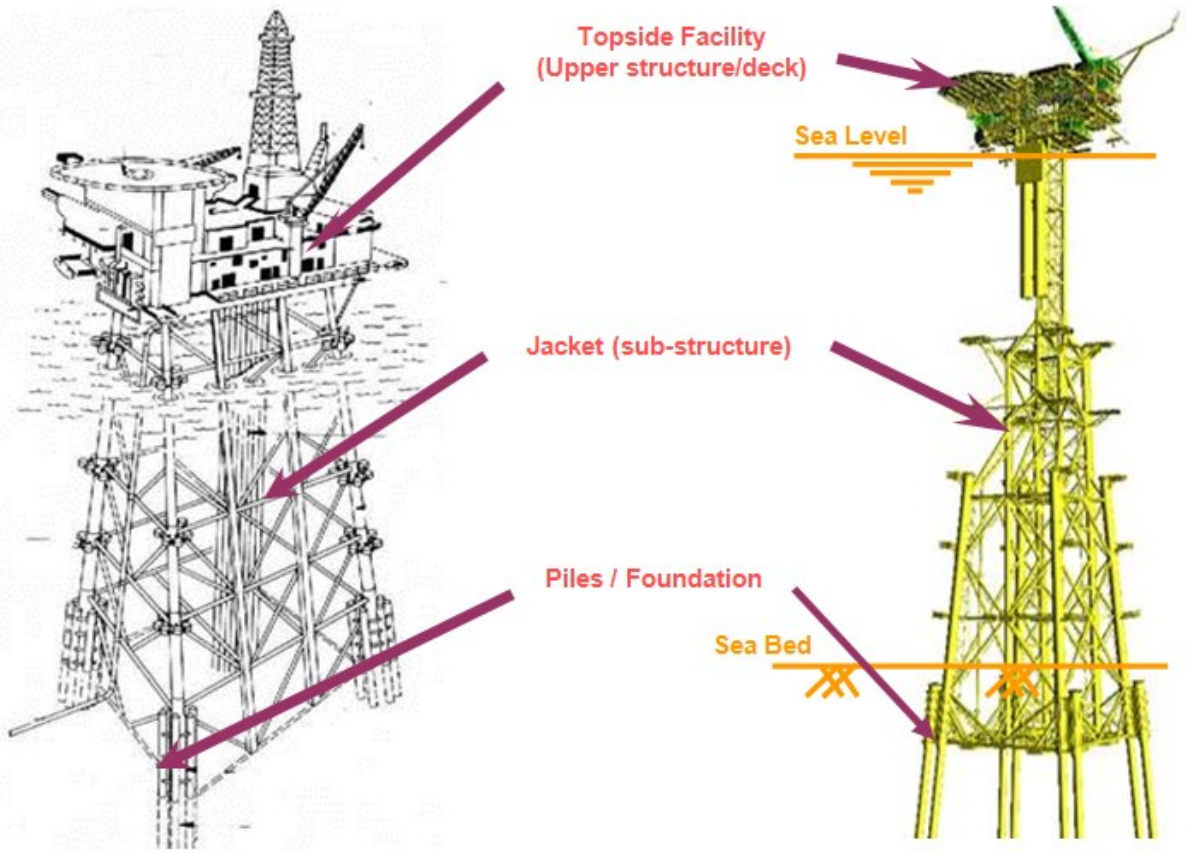

Figure 2 Example of four-legged platform

Offshore platforms commonly adopt open ended steel piles characterized by large diameter and length.

Based on their purposes, piles can be categorized as:

- Foundation pile: its main purpose is to carry out the full weight and acting loads of an offshore structure against all external forces and anchor the platform to the seafloor.
- Conductor pile: is only a template guide for the drill string that will reach the well of the gas or oil fluid.

2.3 PILE DATA

Offshore platforms commonly use open ended steel piles. Based on their purposes, piles can be categorized as foundation piles.

Foundation pile main purpose is to carry out the full weight and acting loads of an offshore structure against all external forces and anchor the platform to the seabed.

There are several types of foundation piles commonly used in offshore. Those are main piles, skirt piles, suction piles, pin piles and anchor piles as shown in Figure 3.

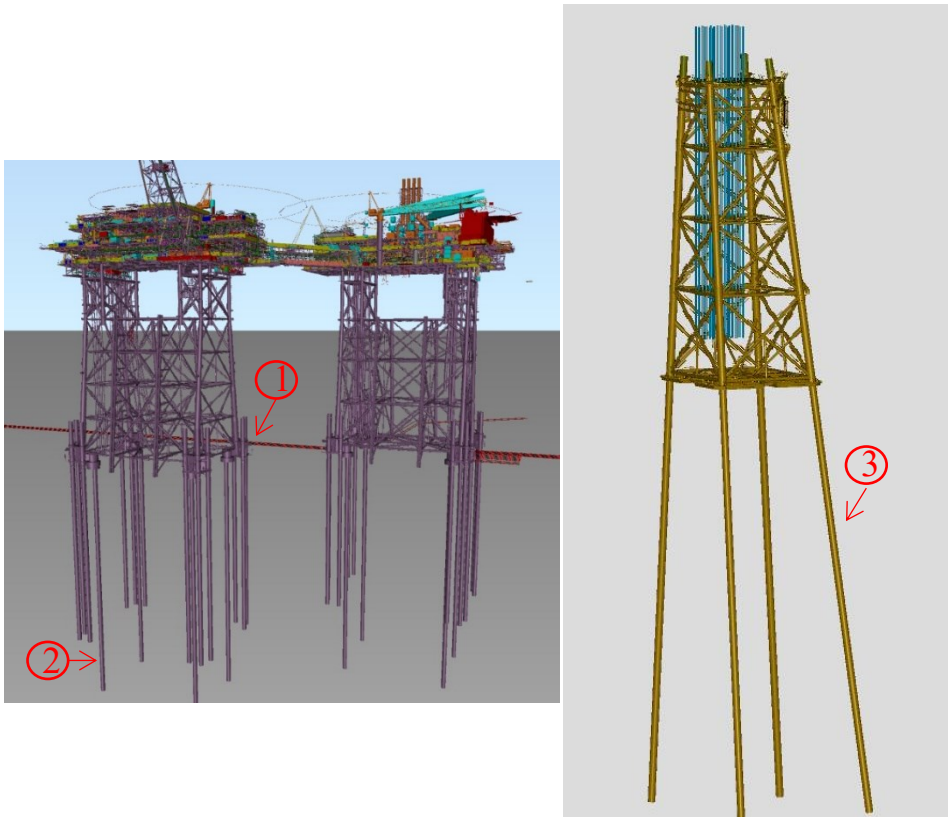

Figure 3 Foundation pile: 1) skirt pile; 2) pin pile; 3) main pile.

A **Skirt pile** is a foundation pile that is installed inside a sleeve welded around the jacket leg. It is installed in vertical position (pile batter is conservatively assumed 1°) and it consists usually of one section only. Finally, a final connection is made by grouting the annulus space between pile sleeve and skirt pile.

Pin pile is a large diameter foundation pile (72" ÷ 96") driven through the soil using a template guide to guarantee the verticality and the correct positioning. Usually, it has a conical reduction.

Suction pile is a large diameter pile with a relatively short penetration (one or two times the pile diameter) mostly used as mooring anchors or as foundation system for subsea structures in deep water condition. It offers several advantages e.g. installation that relies on pumps rather than underwater hammer. Installation starts with the pile penetration under self-weight

and then the reduction of water pressure under the caisson cap creating a downward differential force.

Anchor pile is a driven short-pile that can be used as foundation piles for pipeline shore-pulling or subsea structures foundation.

These piles are usually made by one section and installed in vertical position. Generally, they have small design penetrations (10m - 20m).

Main piles are those foundation piles with multiple sections which are driven to seabed through the jacket legs. The number of sections may vary and, generally, it depends on the water depth and target penetration depth. The pile is usually a slender long steel cylinder; it is divided into uniform pile and non-uniform pile if the geometry (diameter and wall thickness) varies along pile length: usually, on the vicinity of seabed, the pile wall thickness is thickened for resisting to the lateral load. On the top of jacket leg, it can be treated as well.

2.4 GEOTECHNICAL DESIGN OF PILE

Pile capacity for axial compression relates to the axial resistance of a pile subjected to compressive loads along the pile axis. Usually, foundation piles gain the ultimate capacity at a certain period after driving.

The ultimate pile axial capacity can be computed using the following equation:

$$Q_d = Q_f + Q_p = f \cdot A_s + qA_p \qquad \text{Eq. 1}$$

Where:

- Q_d is the ultimate axial pile capacity
- Q_f is the total shaft friction resistance
- Q_p is the total end bearing resistance
- f is the unit shaft friction capacity
- A_s is the side surface area of pile
- q is the unit end bearing capacity
- A_p is the end area of pile

Static pile capacity of tubular piles should be calculated considering two possible conditions which are plugged and unplugged (Figure 4), depending on the behaviour of the pile tip.

For plugged condition, the internal shaft resistance exceeds the end bearing capacity of the pile tip gross area, so that the entire pile capacity includes the shaft friction on external side and the end bearing resistance of the pile tip gross area.

For unplugged condition, shaft resistance acting on both sides of pile (external and internal) and pile tip annulus area should be considered.

- For unplugged condition:

$$Q_d = Q_{f,ext} + Q_{f,int} + Q_{p,annulus} \quad \text{Eq. 2}$$

where:

$Q_{f,ext}$ is the external shaft friction

$Q_{f,int}$ is the internal shaft friction or end bearing of the plug soil, whichever is less

$Q_{p,annulus}$ is the annulus end bearing.

- For plugged condition:

$$Q_d = Q_{f,ext} + Q_{p,gross} \quad \text{Eq. 3}$$

where:

$Q_{p,gross}$ is the gross end bearing

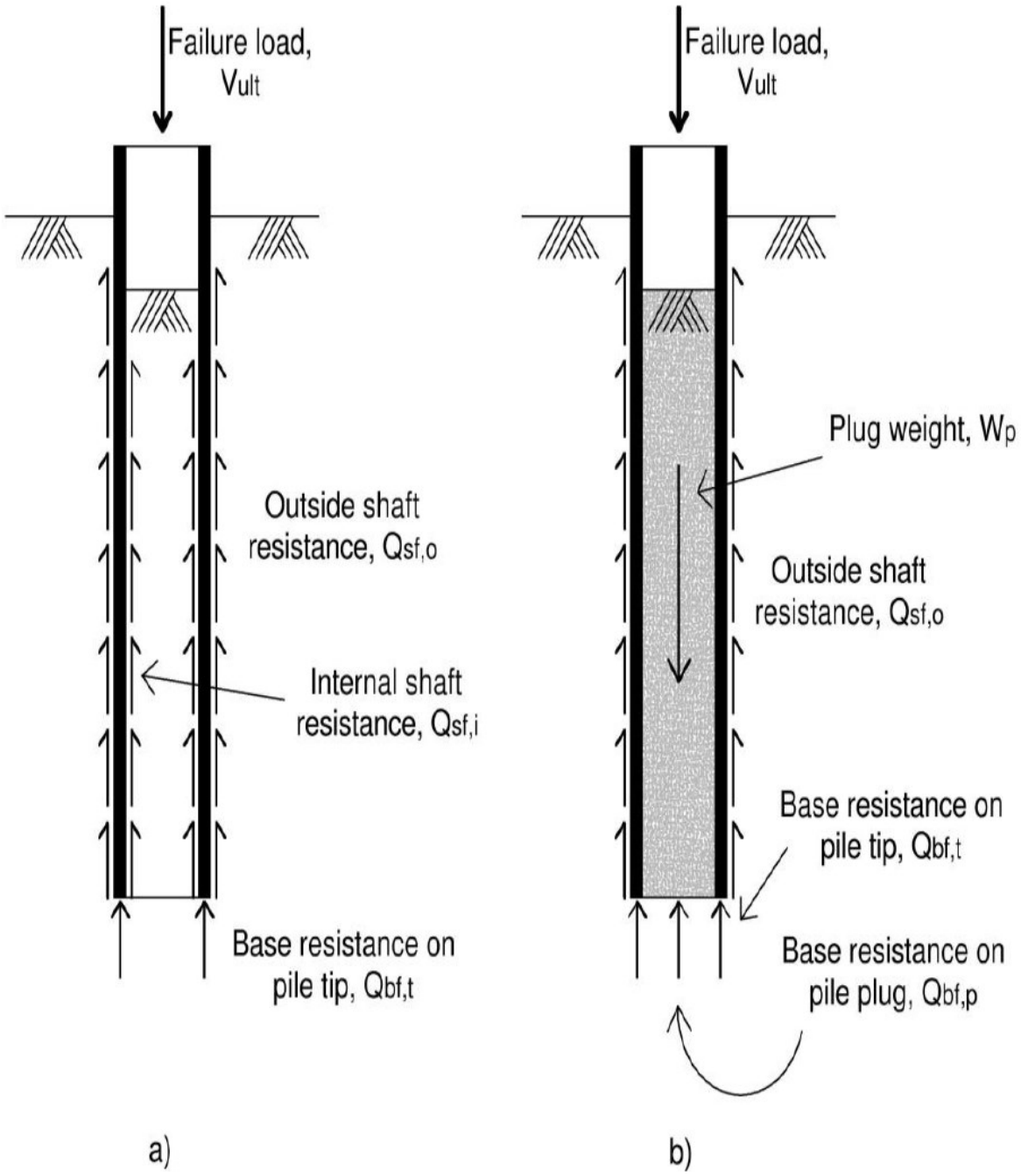

Figure 4 Open-ended pile failure mechanism (a) unplugged behaviour (b) plugged behaviour

The unit shaft friction and the unit end bearing depend on the soil type.

The unit shaft resistance is usually calculated as a long-term shaft resistance value using standard static geotechnical procedures (API recommended practice 2A-WSD) [7]:

- For Cohesionless soil:

$$f = \beta \cdot \sigma'_{V0} < f_{lim}$$ Eq. 4

where:

β = shaft friction factor for sands

σ_0' = effective overburden pressure at point in question

Recommended values of β and f_{lim} can be taken in the table below:

Relative Density[a]	Soil Description	Shaft Friction Factor[b] β (-)	Limiting Shaft Friction Values kPa (kips/ft^2)	End Bearing Factor N_q (-)	Limiting Unit End Bearing Values MPa (kips/ft^2)
Very loose Loose Loose Medium dense Dense	Sand Sand Sand-silt[c] Silt Silt	Not applicable[d]	Not applicable[d]	Not applicable[d]	Not applicable[d]
Medium dense	Sand-silt[c]	0.29	67 (1.4)	12	3 (60)
Medium dense Dense	Sand Sand-silt[c]	0.37	81 (1.7)	20	5 (100)
Dense Very dense	Sand Sand-silt[c]	0.46	96 (2.0)	40	10 (200)
Very dense	Sand	0.56	115 (2.4)	50	12 (250)

NOTE The parameters listed in this table are intended as guidelines only. Where detailed information, such as CPT records, strength tests on high quality samples, model tests, or pile driving performance, is available, other values may be justified.

[a] The definitions for the relative density percentage description are as follows:
- Very loose, 0 – 15;
- Loose, 15 – 35;
- Medium dense, 35 – 65;
- Dense, 65 – 85;
- Very dense, 85 – 100.

[b] The shaft friction factor β (equivalent to the "K tan δ" term used in previous editions of API 2A-WSD) is introduced in this document to avoid confusion with the δ parameter used in the Annex.

[c] Sand-silt includes those soils with significant fractions of both sand and silt. Strength values generally increase with increasing sand fractions and decrease with increasing silt fractions.

[d] Design parameters given in previous editions of API 2A-WSD for these soil/relative density combinations may be unconservative. Hence, it is recommended to use CPT-based methods from the annex for these soils.

Figure 5 Recommended values of β and f_{lim} and N_q.

- For cohesive soil:

$$f = \alpha \cdot S_u$$ Eq. 5

where:

S_u = undrained shear strength of the soil at the point in question

α = adhesion factor, dimensionless

$$\alpha = \begin{cases} 0.5 \cdot \psi^{-0.5} & se\ \psi \leq 1 \\ 0.5 \cdot \psi^{-0.25} & se\ \psi > 1 \end{cases}$$ Eq. 6

α should not exceed 1.0. For under consolidated clays (clays with excess pore pressures undergoing active consolidation), α can usually be taken as 1.0.

ψ = strength ratio, dimensionless

$$\psi = \frac{C_u}{\sigma_0'} \qquad \text{Eq. 7}$$

σ_0' = effective overburden pressure at point in question

ψ is an indirect measure of over consolidation ratio. For rough approximation:

- $\psi \leq 0.2$ for under consolidated clay and normally consolidated clay;
- $\psi > 0.2$ for over consolidated clay;

Unit toe resistance is also calculated in a static formula as a long-term value. Normally, it is not assumed that the toe resistance changes significantly due to driving.

- For cohesionless soil it can be calculated by the following equation:

$$q = N_q \cdot \sigma'_{V0} < q_{lim} \qquad \text{Eq. 8}$$

where:

N_q = bearing capacity factor (Recommended values of N_q and q_{lim} can be taken in table above).

σ_0' = effective overburden pressure at point in question

- For cohesive soil:

$$q = 9 \cdot S_u \qquad \text{Eq. 9}$$

where:

S_u = undrained shear strength

2.5 PILE DRIVABILITY

The scope of pile drivability analysis is to assess if a selected hammer is able to drive a pile up to the target penetration in any conditions (continuous or restart mode) without experiencing premature refusal and without overstressing the pile due to static and dynamic stresses and without fatigue damage.

The pile drivability study consists of four main phases:

- Estimation of the soil resistance to driving (SRD) versus depth based on soil properties at the site.

- Estimation of relevant dynamic soil properties (damping and quake)
- Estimation of self-weight penetration (from resistances value calculated from API formulations)
- Evaluation of blow-counts and hammer energy versus depth

Figure 6 shows the pile driveability analysis flow chart.

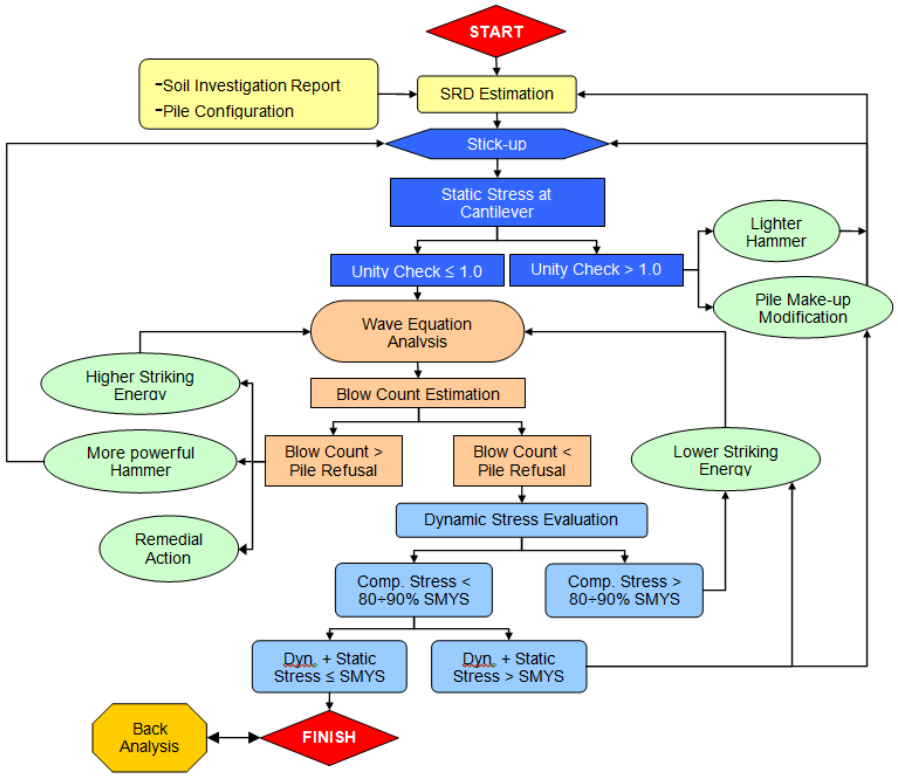

Figure 6 – Driveability analysis flow chart

Drivability analysis starts with collecting the following information:

- Soil parameters: usually from geotechnical, soil investigation report.
- Drawings: piles, platform, and any other useful drawing.
- Pile material: SMYS (Specified Minimum Yield Strength).
- Other installation requirements: available hammer, installation sequence and any other useful information from the installation procedure.

After all information has been gathered, the next step is estimating soil resistance to driving (SRD). The SRD estimation is necessary to calculate the self-weight penetration of pile (SWP) and as an input for the wave equation analysis. Self-weight penetration needs to be

known because it influences the pile free standing length. Longer pile free standing length will have a bigger static stress at the cantilever section.

Static stress on the pile (bending and axial compressive stress) is due to its own weight and hammer weight. Static stress calculation is called stick-up analysis. During driving, each pile is subjected to:

- Self-weight load
- Hammer and other installation equipment weight
- Environmental loads (waves, currents, wind)

These loads may be limiting factors in establishing the maximum length of the add-ons or the suitable hammer for the piles in order not to damage the pile. So, a stick-up analysis is necessary to guarantee pile integrity during the installation operations.

It is necessary to verify that the static stresses due to this load must be less than the Specified Minimum Yield Strength.

Once the stick-up analysis unity checks are satisfied [7], wave equation analysis can be performed to estimate blow count and dynamic stress.

Dynamic stress is the compressive stress on the pile that occurs during driving due to hammer impact.

The pile driveability analysis is satisfied when the following conditions are achieved:

- Stick-up unity checks < 1
- Estimation blow count < refusal criteria (for hydraulic hammer the refusal is for 800 blows/m)
- Dynamic stress < 80÷90% SMYS (Specified Minimum Yield Strength)
- Static plus dynamic stress ≤ SMYS (Specified Minimum Yield Strength)

The resistance of the soil encountered by the pile during driving may be divided in two parts:

- a static part, i.e. the static resistance to driving (SRD);
- a velocity or displacement rate dependent part, called the damping.

It is usual for a SRD model to be used with an accompanying set of standard quake and damping values: the quake values are the displacements required to achieve the yield; the dynamic forces and viscous rate effects are represented by the damping that is used to model

the velocity or displacement rate dependent part of the soil total resistance to driving. This dynamic aspect will be analysed in Section 2.9.

2.6 HAMMER DATA

The hammer is the machine used to drive the pile into the soil up to the desired depth. Depending on its use during the installation campaign, a hammer could be:

- **Main** hammer: can drive up the pile to the target penetration in any condition (continuous and restart).
- **Back-up** hammer: can replace the main hammer with the same energy or more powerful.
- **Contingency** hammer: is a powerful hammer to be used in case of the following contingency circumstances:

  - soil resistance in field higher than expected

  - unexpected main hammer refusal

  - main / backup hammer damage

There are four types of main hammers (depending on the source of energy):

- Hydraulic Hammer (impact hammer): specifications are given in Section 3.2.3
- Diesel Hammer (impact hammer): they can be used only above water; can drive vertical or battered piles. They are less efficient than hydraulic hammers in terms energy transferred to the pile; generally, the striking energy can be set to only four fixed values; the gradual regulation of the striking energy is possible thanks to an additional device to be installed in the hammer.

  It uses diesel combustion under the ram to provide the upward movement to the ram. This type of hammers presents some advantages such as its light weight, solid construction and they do not need additional external power supply.

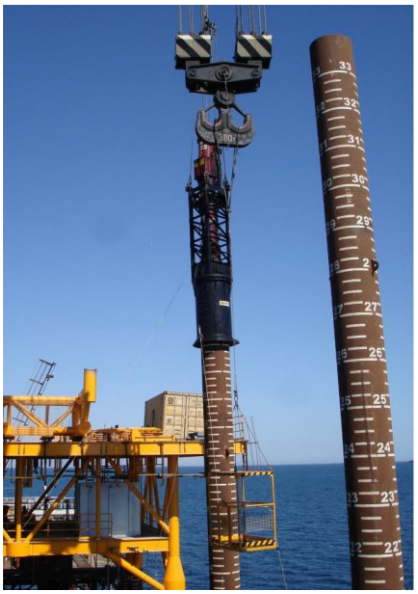

Figure 7 Diesel hammer

- Steam Hammer (impact hammer): This type of hammer can be used only above the water, to drive battered (10° max. reasonable value) or vertical piles. Steam hammers efficiency range from 0.6 to 0.85 normally. The striking energy can be varied from 25 % (minimum) to 100 % of nominal value modifying the stroke (acting on the steam inlet pressure-valve) of the falling weight inside the hammer cylinder. The hammer stroke and start/stop control system are mounted to the resting hammer crosshead. These hammers are very tall and heavy (e.g. 18m x 158 t).

  In this case the ram is attached to a steam engine that pulls the ram up. Therefore, when the valves are switched, the ram goes up before it starts the downward movement. Shortly before the impact, the valves are switched again generating an upward force on the ram and a new cycle is started. When the valves are switched too early, it will cushion the impact and some energy will be lost (preadmission).

Figure 8 Steam hammer

- Vibration Hammer (non-impact hammer): This type of hammer is generally use for onshore/nearshore applications. For offshore, it only efficient for driving the piles with short penetrations. Vibratory hammers are relatively effective and easy to install, and it can also be adapted to work underwater with an additional underwater kit.

The following table contains a summary of all types of hammers and their specification.

Table 1 Summary hammer

DESCRIPTION	**TYPES OF HAMMER**			
	Hydraulic	**Steam**	**Diesel**	**Vibration**
Efficiency	0.85-0.95	0.60-0.85	0.80-0.90	Up to 1
Above / Under Water Driving	Both (equipped with underwater ballast for driving below water)	Above water ONLY	Above water ONLY	Both
Energy Setting	0÷100%	0÷100%	4 settings only*	0÷100%
Blow Count Record	Automatic	Manual	Manual	(Vibration per minute)

2.7 POSSIBLE PROBLEMS DURING PILE DRIVING

In the past few years, several oil companies had to face serious platform installation problems due to major difficulties encountered during pile driving operations. Four types of problems have been identified:

1. **Hammer refusal:** Development of strong set-up effects in hard clays during add-on welding may can lead to premature refusal of piles. Interruptions in pile driving are followed by strong set-up effects. Redriving the pile after a few hours or days may result in a soil resistance to driving much higher than the value recorded before stopping. The values of the soil resistance at time of redriving are often close to the calculated values of the pile static resistance. This suggests that the material may recover its original strength properties.
2. **Pile free fall:** pile run could be described as non-controlled sudden descent of the pile already placed inside of jacket leg. In most of the cases it occurs when pile, passing through soil, enters into a layer softer than the layer above. The occurrence of a pile run typically occurs when the bearing capacity of the soil is insufficient to counteract the combined weight of the pile, the hammer and the inertia generated by the hammer's impact. Once the pile starts moving, along with the impact hammer resting on it, gravity accelerates its descent, subjecting it to additional forces that demand an even higher bearing capacity to halt the movement. This motion cannot be stopped until the pile's toe reaches a depth where the bearing capacity exceeds the downward force applied.

   As piles continue to grow in size, the required bearing capacity to prevent uncontrolled penetration increases as well.

   Consequently, under the same soil conditions, a larger pile will exhibit significantly greater self-weight penetration compared to a smaller pile. Additionally, larger and heavier piles carry more inertia when set in motion, making it more challenging to halt their self-penetration process once initiated.

   The most problematic soil layer consists of dense sand with thick layers of soft clay underneath.

   Therefore, "soft" soil layers that would traditionally provide adequate bearing capacity for smaller piles can now pose a pile run risk when dealing with modern and much larger

piles.

Consequences of the potentially occurred pile run are as follows:

- Loss of pile.
- Damage of structure (jacket).
- Damage of lifting equipment.
- Damage of Crane system.

3. **Pile tip damage:** it has become of particular concern for the offshore industry due to the extensive use of large diameter, thin-walled piles for monopiles and jacket structures. The potential for damage has increased in recent developments due to the occurrence of embedded boulders within the seabed sediments or partially weathered soft rocks.
4. **Soil degradation:** the soil resistance during continuous driving is very low and increases slowly with depth. The analysis of dynamic records indicates a strong degradation of the skin friction under the cumulative effect of the hammer blows.

   After several hundred consecutive blows, the dynamic skin friction may locally drop to about one fifth of the static value. More details of this phenomenon are reported in Section 2.8.3 and 3.1.1.

2.7.1 REMEDIAL ACTIONS

Mitigations that could be implemented to avoid pile free fall are:

- controlled slack of the rigging;
- well defined soil profile.

In case that there is a situation where the 1st layer is hard, followed by a soft layer and followed again by a hard one, it is necessary to evaluate during the design and installation engineering phase if the pile self-weight is sufficient to overcome initial penetration through the hard layer and following soft layer.

From some experiences, risk of pile run can be observed for first 30-40m of soil profile. Once pile is reaching 30-40m penetration, risk of pile run is significantly reduced.

As a summary, it is suggested to perform detailed pile installation analysis in order to mitigate risks of pile run. Nowadays, with availability of vibro hammer, it is possible to

overcome complex soil profile situations by using vibro hammer for initial phase of pile installation, in order to assure safe pile installation in shallow soil profiles.

Furthermore, nobody can guarantee that in field everything will go according to the plan, therefore sometimes even if the pile driveability analysis has been well performed, hammer refusal can still occur during driving.

In case of unexpected refusal during driving, the following actions can be done as remedial actions:

- Change the hammer with more powerful hammer (if any).
- Perform drilling: drilling through the pile and/or under the pile driving shoe and subsequently drive the pile to target penetration.
- Estimate the actual pile capacity based on driving records back analysis and investigate if the achieved penetration guarantees the required design capacity of the pile.

API standards code for example provides general refusal criteria but also each manufacturer provides limiting criteria in use of their equipment that must be followed.

Furthermore, the risk of pile tip damage can be reduced with a better soil investigation and using a local pile tip thickening (usually referred to as a "driving shoe"). It could be employed to improve drivability, to provide reinforcement against local hard spots, such as boulders, and to reduce tip stresses.

The shoe is an internal wall thickening which can in some cases also reduce the internal skin friction and by consequence the overall resistance to driving. Generally, the shoe consists of a length of pile at the tip which is increased in thickness by up to say 50%.

2.8 SOIL RESISTANCE TO DRIVING (SRD)

The soil static resistance to driving (SRD) is the profile of shaft and toe resistance developed during pile installation and its estimation is required to perform a driveability study.

A SRD profile differs from a static capacity profile in that it models the cumulative increase in shaft capacity with further pile penetration and has a toe resistance associated with each driving increment, as opposed to a static profile with a single base resistance. Moreover, they differ in terms of time, degree of mobilization and consolidation.

Below it is providing a detailed description of the main methodologies available in literature for the estimation of the soil static resistance to driving (SRD):

- Stevens method, including Semple and Gemeinhardt's and Puech recommendation
- Alm & Hamre method
- Percentage of axial capacity

The Stevens method was derived from back analyses of driving data for relatively shallow penetrations (16 m to 51 m) and relatively small diameters (30 in to 42 in OD).

For deeper penetrations more friction degradation will occur and the plugging mode during driving is unlikely. Plugging mode is also unlikely because of the relatively large diameters considered.

General comments on the provided SRD profiles are as follows:

- low estimate SRD is expected during continuous driving due to degradation effects.
- high estimate SRD is expected after an important driving interruption due to set-up effects.

2.8.1 Stevens Method

Stevens' method was developed in 1982 from field measurements of pile driving during installation of a number of small platforms in the Arabian Gulf across a variety of soil conditions including carbonate sand and calcarenite.

SRD should be computed for both, unplugged and plugged pile conditions:

- UNPLUGGED: when at pile cores, relative movement between pile and soil occurs both on the outside and inside the pile wall. Skin friction is developed on both outside and inside pile wall. The end bearing area is equal to the cross-sectional area of steel at the pile tip.

$$SRD = Q_{f,ext} + Q_{f,int} + Q_{p,annulus} = \sum(f_{ext} \cdot A_{ext}) + \sum(f_{int} \cdot A_{int}) + q \cdot A_w \quad \text{Eq. 10}$$

where:

$Q_{f,ext}$ = external shaft friction

$Q_{f,int}$ = internal shaft friction

$Q_{p,annulus}$ = annulus end bearing

f_{ext} = unit shaft friction on external wall during driving

f_{int} = unit shaft friction on internal wall during driving

A_{ext} = external wall area of pile

A_{int} = internal wall area of pile

q = unit end bearing during bearing

A_w = cross-sectional area at pile tip

- PLUGGED: when a pile plugs, the soil plug moves with the pile during driving. Skin friction is mobilized only on the outer wall; the end bearing area is the gross area of the pile.

$$SRD = Q_{f,ext} + Q_{p,gross} = f_{ext} \cdot A_{ext} + q \cdot A_p \qquad \text{Eq. 11}$$

where:

$Q_{f,ext}$ = external shaft friction

$Q_{p,gross}$ = gross end bearing

f_{ext} = unit shaft friction during driving

A_{ext} = external wall area of pile

q = unit end bearing during bearing

A_p = gross cross-sectional area at pile tip

For both conditions, plugged and unplugged, a lower and upper bound of the SRD should be computed considering the following recommendations provided by Stevens:

Table 2 – Stevens' method – Unit shaft friction & unit end bearing – CLAY

		Unit Skin Friction, f	**Unit End Bearing, q**
UNPLUGGED	LOWER BOUND	$f_{int} = 0.5 \cdot \alpha \cdot S_U \cdot F_p$ $f_{ext} = \alpha \cdot S_U \cdot F_p$	$q = 9 \cdot S_U$
	UPPER BOUND	$f_{int} = f_{ext} = \alpha \cdot S_U \cdot F_p$	$q = 9 \cdot S_U$
PLUGGED	LOWER BOUND	$f_{ext} = \alpha \cdot S_U \cdot F_p$	$q = 9 \cdot S_U$
	UPPER BOUND	$f_{ext} = \alpha \cdot S_U \cdot F_p$	$q = 15 \cdot S_U$

Table 3 – Stevens' method – Unit shaft friction & unit end bearing – SAND

		Unit Skin Friction, f	**Unit End Bearing, q**
UNPLUGGED	LOWER BOUND	$f_{int} = f_{ext} = 0.7 \cdot \sigma_0' \cdot tan\,\delta \leq f_{lim}$	$q = N_q \cdot \sigma_0' \leq q_{lim}$
	UPPER BOUND	$f_{int} = f_{ext} = 0.7 \cdot \sigma_0' \cdot tan\,\delta \leq f_{lim}$	$q = N_q \cdot \sigma_0' \leq q_{lim}$
PLUGGED	LOWER BOUND	$f_{ext} = 0.7 \cdot \sigma_0' \cdot tan\,\delta \leq f_{lim}$	$q = N_q \cdot \sigma_0' \leq q_{lim}$
	UPPER BOUND	$f_{ext} = 1.3 \cdot 0.7 \cdot \sigma_0' \cdot tan\,\delta \leq f_{lim}$	$q = 1.5 \cdot N_q \cdot \sigma_0' \leq q_{lim}$

where:

S_u = undrained shear strength

δ = friction angle between the soil and pile wall, equal to $\phi - 5^\circ$

ϕ = soil internal friction angle

σ_0' = effective overburden pressure

N_q = dimensionless factor

f_{lim} = unit skin friction limitation for cohesionless soil, taken from section 2.4

q_{lim} = unit end bearing limitation for cohesionless soil, taken from section 2.4

α = adhesion factor, dimensionless

FP = pile capacity factor, equal to $\lambda \cdot (OCR)^{0.3}$

$$FP = \lambda \cdot (OCR)^{0.3} \qquad \text{Eq. 12}$$

λ = empirical factor (Stevens assumes $\lambda = 0.5$)

OCR = soil over consolidation ratio

If not available, Stevens suggests estimating OCR value with reference to Semple and Gemeinhardt's recommendation

$$\frac{S_U}{S_{U,NC}} = (OCR)^{0.85} \qquad \text{Eq. 13}$$

S_U = actual undrained shear strength of clay having a given index of plasticity I_P

$S_{U,NC}$= undrained shear strength of the same clay if normally consolidated; according to Skempton relationship: $S_{U,NC} = (0.11 + 0.0037 I_P) \cdot \sigma_0'$

When plasticity data are unavailable, the ratio $S_U/S_{U,NC}$ for a lean clay may be taken as 0.2 and the submerged unit weight of a stiff clay as 10 kN/m³. Hence $S_{U,NC}$ in kPa is twice the depth in m. For a stiff, lean clay the OCR may be estimated as:

$$OCR = 0.45 \cdot \left(\frac{S_U}{Z}\right)^{1.2} \qquad \text{Eq. 14}$$

Stevens recommends that the unit skin friction for piles driven in rock layers is computed assuming sand parameters since it is expected that rock layer is fractured during pile driving and rock is reduced to granular material.

Unit end bearing is limited to values given for granular soil if rock is poor to fair quality (Rock Quality designation RDQ ≤ 75%); in case of more competent rock (RDQ > 75%), unit end bearing can be computed using following equation:

$$q_p = 3 \cdot u \qquad \text{Eq. 15}$$

where u is the compressive strength of rock.

Puech adapted the method developed by Stevens to cope with the soil conditions encountered in the Southern part of the Gulf of Guinea. Puech proposed to modify the λ factor in Eq. 12 as follows:

- The lower bound of soil resistance to driving should be computed using $\lambda = 0.2$.
- The upper bound of soil resistance to driving should be computed using $\lambda = 0.5$.

Puech expected that for long driving sequences, the blowcount will tend to come near the lower bound.

The above recommendations are valid for driving in stiff to hard clay.

2.8.2 Alm & Hamre Method

The pile driveability problems in hard clays offshore include:

- The friction degradation with very low driving resistances during continuous driving.
- Strong and rapid set-up effects after driving interruptions which may lead to premature refusal of piles.

In 1998, Alm & Hamre presented a model for driveability predictions based on the friction fatigue concept; in 2001, the method was improved and updated by the same authors based on a more complete database: the soil resistance to driving has been directly correlated to the cone penetration test (CPT) measurements.

The reference database includes installation data from a variety of soil conditions representing the North Sea soils (16 different locations). The database consists of piles with diameters ranging from 72" to 108", but the installation data from 30" conductors in one location were included for comparison.

Being the CPT data directly used as input in the calculation of the SRD, the site data interpretation (particularly the selection of the undrained shear strength profile) is removed from the engineering process and the uncertainty reduced. On the other side, since the CPT sleeve friction is required for assessing the SRD in clay, attention should be given to obtain reliable sleeve friction profiles.

The major contribution to SRD is due to side friction and a realistic model for friction during driving has been based on the friction fatigue concept both in sand and clay.

The SRD calculation is based on three steps:

- Calculation of the unit skin friction during driving (f_d) and unit end bearing strength (q_d) during driving.
- Calculation of BE SRD (best estimate) for unplugged mode.
- Calculation of HE SRD (high estimate) applying an amplification factor of 1.25 to the BE SRD to consider possible soil variability.

The first step is the calculation of the Unit Skin Friction During Continuous Driving.

The following formulation is used for cohesive and frictional soils:

$$f_d = f_{sres} + (f_{si} - f_{sres}) \cdot e^{k \cdot (d \cdot p)} \qquad \text{Eq. 16}$$

where:

f_d = unit skin friction during driving [kPa];

f_{sres} = residual unit skin friction [kPa];

f_{si} = initial unit skin friction [kPa];

k = shape factor for degradation [-];

d = depth to the top of the actual sublayer [m];

p = pile tip penetration [m].

The shape factor is calculated as follow:

$$k = \sqrt{\frac{q_T}{\sigma'_{V0}}}/80 \quad \text{Eq. 17}$$

where:

q_T = CPT total cone resistance at the considered depth [kPa];

σ'_{v0} = vertical effective stress [kPa].

With this formulation, a rapid degradation will occur for dense sand, while the opposite will be the case for soft clays.

The unit skin friction inside (f_i) and outside (f_o) the pile wall is calculated as follow:

In cohesive soils:

$$f_i = f_o = f_d \quad \text{Eq. 18}$$

In frictional soils:

$$f_i = f_o = 0.5\ f_d \quad \text{Eq. 19}$$

For cohesive soils, the initial skin friction is taken as the recorded CPT sleeve friction, while the residual skin friction is a function of the normalized total cone resistance:

$$f_{si} = f_{s-CPT} \quad \text{Eq. 20}$$

$$f_{sres} = 0.004 \cdot q_T \cdot (1 - 0.0025 \frac{q_T}{\sigma'_{V0}}) \quad \text{Eq. 21}$$

where:

$f_{s\text{-}CPT}$ = CPT sleeve friction at the considered depth [kPa];

q_T = CPT total cone resistance at the considered depth [kPa];

σ'_{v0} = vertical effective stress [kPa].

For frictional soils, the initial skin friction is calculated as follow (no upper limit on unit friction is included):

$$f_{si} = K \cdot \sigma'_{V0} \cdot \tan(\delta) \quad \text{Eq. 22}$$

where:

K = coefficient of lateral earth pressure [-];

σ'_{v0} = vertical effective stress [kPa];

δ = soil-steel friction angle, taken as the internal effective friction angle φ' – 5 [deg].

The lateral stress coefficient K is directly linked to the cone resistance as presented by Jardine & Chow (1996) using the following formulation:

$$K \cdot \sigma'_{V0} = 0.0132 \cdot q_T \cdot \left(\frac{\sigma'_{v0}}{p_a}\right)^{0.13} \quad \text{Eq. 23}$$

where:

q_T = CPT total cone resistance at the considered depth [kPa];

p_a = atmospheric pressure = 100 kPa;

σ'_{v0} = vertical effective stress [kPa].

The residual pile shaft friction is calculated as follow:

$$f_{sres} = 0.2\ f_{si} \quad \text{Eq. 24}$$

The second step is the calculation of the unit end bearing q_d.

The formulation that can be used for cohesive soils is the follower:

$$q_d = 0.6\ q_T \quad \text{Eq. 25}$$

where:

q_T = CPT total cone resistance for unit end bearing.

Instead, the unit end bearing for frictional soils is calculated as follow:

$$q_d = 0.15 \cdot q_T \cdot \left(\frac{q_T}{\sigma'_{v0}}\right)^{0.2} \quad \text{Eq. 26}$$

where:

q_T = CPT total cone resistance at the considered depth [kPa];

σ'_{v0} = vertical effective stress [kPa].

The ultimate shaft capacity and end-bearing capacity are then calculated by the integration of the unit side friction and the unit base resistance.

$$F_i = \pi \cdot (OD - 2WT) \cdot f_i \cdot z \quad \text{Eq. 27}$$

Where

-F_i is the total skin friction inside the pile wall

-OD is the outside diameter of pile

-WT is the wall thickness

- f_i is the unit skin friction inside the pile wall; the formulation is reported above.

$$F_o = \pi \cdot OD \cdot f_o \cdot z \quad \text{Eq. 28}$$

Where

-F_o is the total skin friction outside the pile wall

-OD is the outside diameter of pile

- f_o is the unit skin friction outside the pile wall; the formulation is reported above.

$$Q_{tip} = A_{steel} \cdot q_d = (\pi \cdot q_d \cdot (OD^2 - (OD - 2WT)^2)/4z \quad \text{Eq. 29}$$

Where

-Q_{tip} is the end-bearing capacity

-OD is the outside diameter of pile

-WT is the wall thickness

- q_d is the unit end bearing.

Finally, the SRD is calculated by the sum of the shaft capacity and the end-bearing capacity.

$$SRD = Q_{tip} + F_o + F_i \quad \text{Eq. 30}$$

2.8.3 Percentage of axial capacity

To predict the soil resistance to driving during continuous driving most of better known methods are broadly based on modifications to pile static axial capacity calculations estimated with API formulation, considering a friction degradation factor.

Delimi, Maron and Clavaud used a selected set of pile monitoring data in calcareous clay to derive it.

It was observed (as showed in Figure 9) that the degradation factor decreases with pile penetration: 0.45 to 0.78 at shallow depths up to 60m then decreasing linearly to 0.1 to 0.25 at around 140 m. During continuous driving there is a higher loss of soil resistance to driving due to this phenomenon.

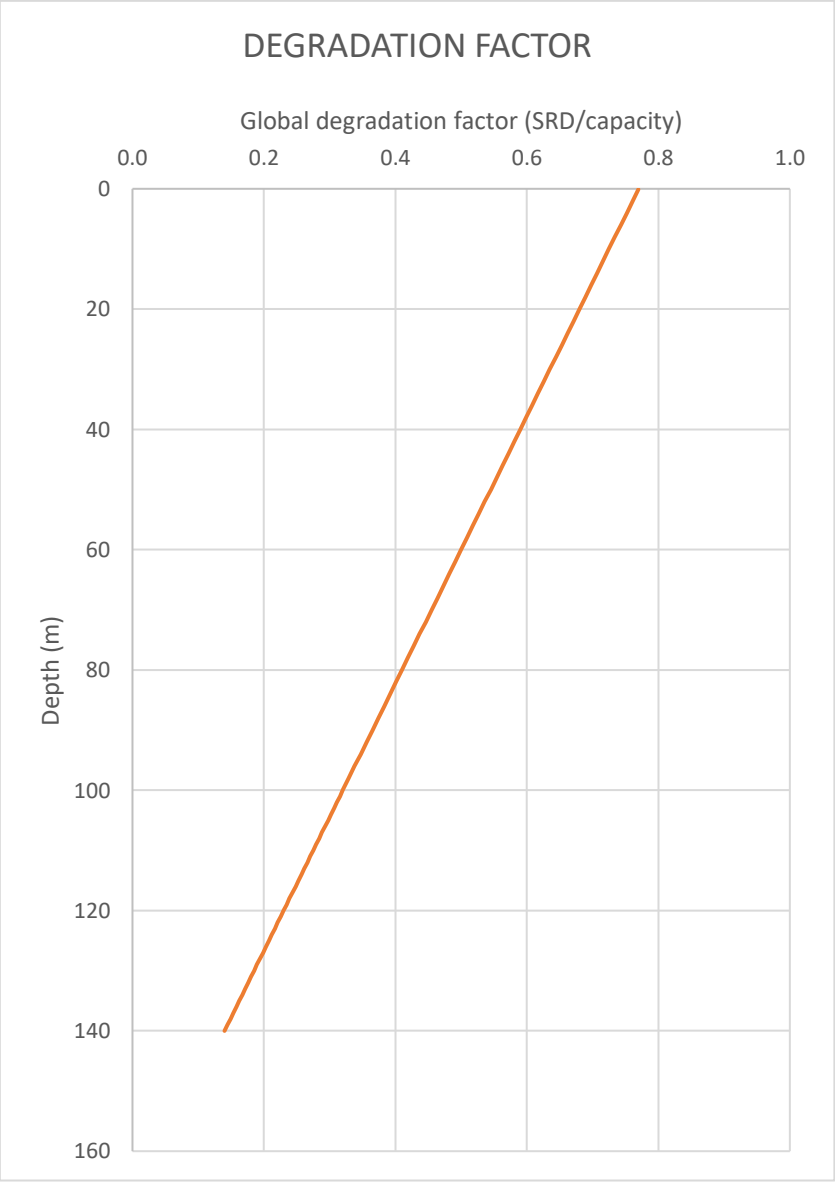

Figure 9 Global degradation factor versus depth - continuous driving

The continuous driving can be calculated with the following equation:

$$SRD = GDF \cdot \sum_{i=0}^{Z} f_{plug,i} \cdot P + GDF \cdot q \cdot A \qquad \text{Eq. 31}$$

Where:

- GDF is the global degradation factor. It is calculated with the formulation below, to replicate the correct trend: GDF = (-0.0045 · z + 0.77)

- $f_{plug,i}$ is the shaft resistance in clay and in sand; formulations are reported in Section 2.4
- q is the unit end bearing in clay and in sand; formulations are reported in Section 2.4
- P is the perimeter of pile P = π · OD · WT.
- A is the external pile area A = π · (OD - 2WT)^2/4.

2.9 QUAKE AND DAMPING

The pile driving process generates dynamic soil stresses along the pile shaft and at the pile toe during the propagation of the stress wave. Thus, is necessary the modelling of the dynamic response of the soil around.

The amplitude of a stress wave decreases as the wave travels through the soil. Viscous damping is often conventionally used to represent the dissipation of elastic energy.

Prediction of soil drivability is based on driving resistance models consisting of a static resistance part (SRD) and some damping contribution which together form the dynamic resistance.

In simplified approaches, the soil during driving is modelled as a series of spring and dashpot. The spring can deform elastically to a maximum value called “quake” after which there is no additional resistance from continued deformation.

The resistance of the dashpot is assumed to be directly proportional to the velocity of the associated segment during the displacement and is the damping.

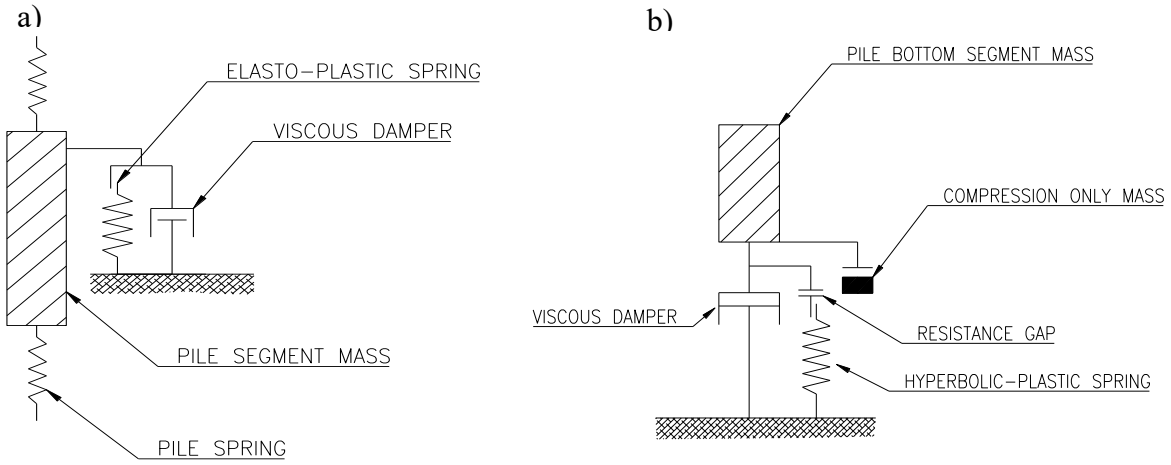

Figure 10 a) Model for pile shaft; b) Model for pile toe.

Smith (1960) modelled the total resistance (static and dynamic) mobilized during driving dynamic loading as:

$$R_t = R_s(1 + Jv) \qquad \text{Eq. 32}$$

Where:

- R_t is the total resistance to driving
- R_s is the static resistance part (SRD)
- J is the damping factor
- v is the velocity of a pile segment during a given time interval.

The total resistance is the sum of the static resistance R_s and dynamic resistance R_d. The latter is the product of damping factor times pile velocity times the static resistance. The static resistance is not constant. It is thought to increase from zero to a maximum R_{ud} value. The Smith approach substitutes the ultimate resistance R_{uf} for R_s which then makes the damping approach linear.

$$R_t = R_{ud}(1 + Jv) \qquad \text{Eq. 33}$$

R_{ud} is the ultimate static resistance (is the failure load) determined in a dynamic loading test after accounting for damping $R_d = R_{ud}\, J\, v$

Being the static resistance usually the major contribution in the total dynamic resistance, the uncertainty in the static resistance contribution exceeds by far the uncertainty in the damping contribution.

The dynamic soil parameters (quake and damping) are an integral part of any pile driveability assessment, and it is common for an SRD model to have a set of associated quake values and damping factors.

The typical value for shaft and toe quake is 2.54 mm.

On the other hand, the typical value for the toe damping is 0.5 s/m. The shaft damping depends on the different models adopted for SRD. The recommended skin damping parameters to use are:

- 0.16 s/m, for sand layers
- 0.65 s/m for clay layers
- For mixed soil, intermediate values may be used:
    - a sandy silt or clayey sand may be modelled with 0.33 s/m
    - a cohesive silt or a sandy clay with 0.5 s/m.

If we consider the Alm & Hamre model, they recommend a shaft damping of 0.25 s/m for both sand and clay.

2.10 SET-UP

Every time the driving operations have to restart at a certain depth for any reason, special consideration shall be given to the possible SET-UP effects occurred in the soil (gain of capacity over time after installation). The main reason of this gain is the greater dissipation of pore water pressure.

For the calculation of the SRD at full set-up after driving interruptions, Puech proposed a procedure where the following empirical factor λ is used in the equation 11 [8]:

Table 4 Proposed set of λ value

	Upper bound SRD	Lower bound SRD
λ_{max}	0.5	0.2
$\lambda_{residual}$	0.25	0.05

Set-up effects means that at a certain value of penetration, the blowcount was for example as low as 10-15 bl/0.25m. After some time (for example 10 hour) interruption for welding the last add-on element, driving could not be resumed because of the quick increase in resistance.

The set-up factor F_{su} was defined by the following expression:

$$F_{su} = \frac{(SRD)_r}{(SRD)_c} \qquad \text{Eq. 34}$$

Where:

- $(SRD)_c$ is the resistance during continuous driving
- $(SRD)_r$ is the resistance at the time pile driving is resumed.

Empirical formulations that attempt to predict how capacity will be regained as a function of time after driving have been proposed in the literature. For example, Skov et al. [9] presented an equation that assumes a linear capacity increase with the logarithm of time. Considering that the static capacity is a function of the waiting time since pile installation, t_w, and considering a reference capacity $R_u(t_o)$ determined at a relatively short time, t_o, after installation, the equation would be:

$$R_u(t_w) = R_u(t_0) \cdot [1 + A \log_{10}(t_w/t_0)] \qquad \text{Eq. 35}$$

The factor A is the relative increase of the static capacity during a 10 fold waiting time increase. The authors suggested A= 0.2 for sand (t_o = ½ day) and A = 0.6 for clay (t_o = 1 day). In the case of clay, for example, if after 1 day of waiting, the reference capacity $R_u(t_o)$ is 100 tons, then it will be 160 tons after 10 days, and 220 tons after 100 days.

2.11 MONITORING

Pile driving process is usually monitored by recording the force and the velocity to which the pile is subjected during the impact. Pile driving monitoring can be compared as each blow was a dynamic pile test.

The aims of pile driving monitoring [2] are the following:

- Establish the pile ultimate bearing capacity and confirm pile design assumptions;
- Evaluate pile fatigue resulting from the driving process;
- Allow the calibration of a model for the back analysis of non-instrumented piles.

The pile is monitored by Pile Driving Analyser (PDA) which is a data acquisition system. Two pairs of strain gauges and accelerometers are usually placed 1.5 to 2 pile diameters below the pile head in order to record the velocity and force applied in the pile due to the impact. Both pairs of strain gauges are attached to the two opposite side of the pile near the pile head.

Dynamic testing in offshore conditions requires special waterproofing sensors and cables.

The transducers are connected to the PDA system where the data is recorded for further analysis in the office. The interpretation of the results is based on the wave equation approach.

Because of stress wave effects caused by the rapid loading of the pile, the estimated bearing capacity does not resemble the static load-displacement curve. Hence, in order to obtain the static load-displacement curve it is necessary to remove dynamic effects of both the pile and the soil. This calculation is usually performed by a signal matching analysis. CAPWAP is the most used program for the calculation of the static load-displacement curve from dynamic pile testing.

2.11.1 CAPWAP ANALYSIS

CAPWAP analysis is considered to be a standard procedure for the pile capacity evaluation from dynamic pile testing data. This software is based on a signal matching analysis.

To perform the CAPWAP analysis, the pile segment below the control point is modelled in the form of a series of lump masses and springs. The soil resistance is modelled both along the side and at the toe as an elastic-plastic spring and linear dashpot. This model is similar to the one proposed by Smith (1960), where for every mass the soil model [10] included three unknows: soil stiffness, static capacity and a damping factor.

Considering the problem to be solved, when a dynamic test is performed two measurements at the pile top are recorded, the deformation and the acceleration. Afterwards, the force and the velocity present in the pile are deduced from the deformation and acceleration measures.

In a CAPWAP analysis, the measured velocity at the pile top is treated as an input quantity. Hence, the measured velocity signal is imposed on the top element in the model.

The static and the dynamic soil parameters should then be determined so that when the velocity is applied at the top element, the force calculated at that point will be the same as the measured force. The solution is therefore achieved by an iteration process until the

measured and the calculated force signals match. This procedure is named as inverse analysis or signal matching analysis. The traditional signal matching technique can be summarized as following:

- Data input – select a record with appropriate data quality;
- Data check and adjustment;
- Check and change resistance distribution;
- Check damping and quake parameters;
- Find the values that produce the best match.

The soil resistance acting at some location along the pile under impact during CAPWAP analysis can be expressed [10] as follow:

$$R(t) = f_{gl}R_s(t) + R_d(t) \quad \text{Eq. 36}$$

Where:

- f_{gl} is a gain/loss factor
- R_s is the long-term static resistance (LTSR)
- R_d is the dynamic or velocity dependent component.

During pile driving the soil properties change and the pile encounters the Static Resistance to Driving (SRD), that it is see as a product between $f_{gl}\ and\ R_s(t)$.

For shaft resistance, f_{gl} usually is the inverse of soil set-up factor, fs. It expresses the gain of shaft resistance after initial driving ends and is almost always greater than unity.

For end bearing, f_{gl} is the inverse of a degradation factor f_t. It expresses a loss of end bearing after driving and is therefore less than unity. So, in general, the gain/loss factor reduces shaft resistance and increases end bearing during initial pile installation from the long term expected service conditions.

The CAPWAP results include total capacity incorporating its distribution along the shaft and toe, a load-set curve for the short duration dynamic test at the time of testing, dynamic resistance (damping component) and the stiffness of the static resistance components.

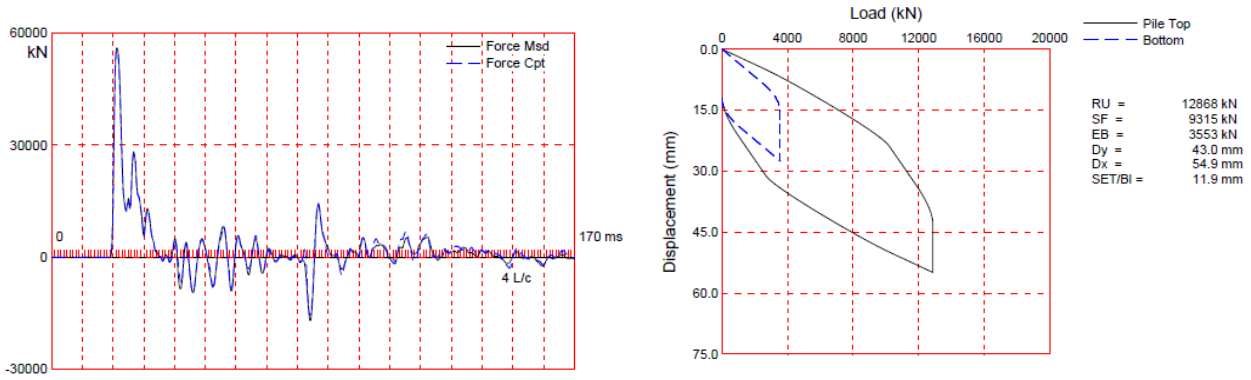

Figure 11 Measured force at pile top (on the left) and simulated static load-set curve (on the right)

2.12INSTALLATION OPERATIONS

Below, a general description of a Foundation Pile installation is provided; the following main steps are identified:

1. Moving piles from cargo barge to installation vessel (or upending directly on the bear cage (external clamp, providing temporary connection and alignment of a pile add-on with a pile string prior welding. Bear cage holds two piles which are to be welded through bear cage window).
2. Upending Lead section.
3. Stabbing Lead section inside the jacket leg.
4. Lifting, upending and stabbing 1st add-on and weld:
    - Fit up/alignment can be performed either by bear cage or turnbuckles.
5. Welding is done either in manual mode (SMAW) or semi-automatic mode (FCAW) or a mix of both systems. The weld integrity is checked by Ultrasonic Testing (UT) and/or Magnetic Particle Inspection (MPI) and/or Radiographic testing (RT).
6. Remove the Bear Cage/turnbuckles from the piles.
7. Install the hammer on pile top.
8. Drive pile up to the foreseen intermediate penetration.
9. Perform cut-off of damaged part due to hammer's impact.
10. The same installation procedure will be repeated for each add-on up to reach the design penetration.

11. Jacket levelling.
12. Upon completion of the pile driving and levelling, the piles are welded to the jacket on top of legs (shims or collars).

The Figures below show the pile installation process.

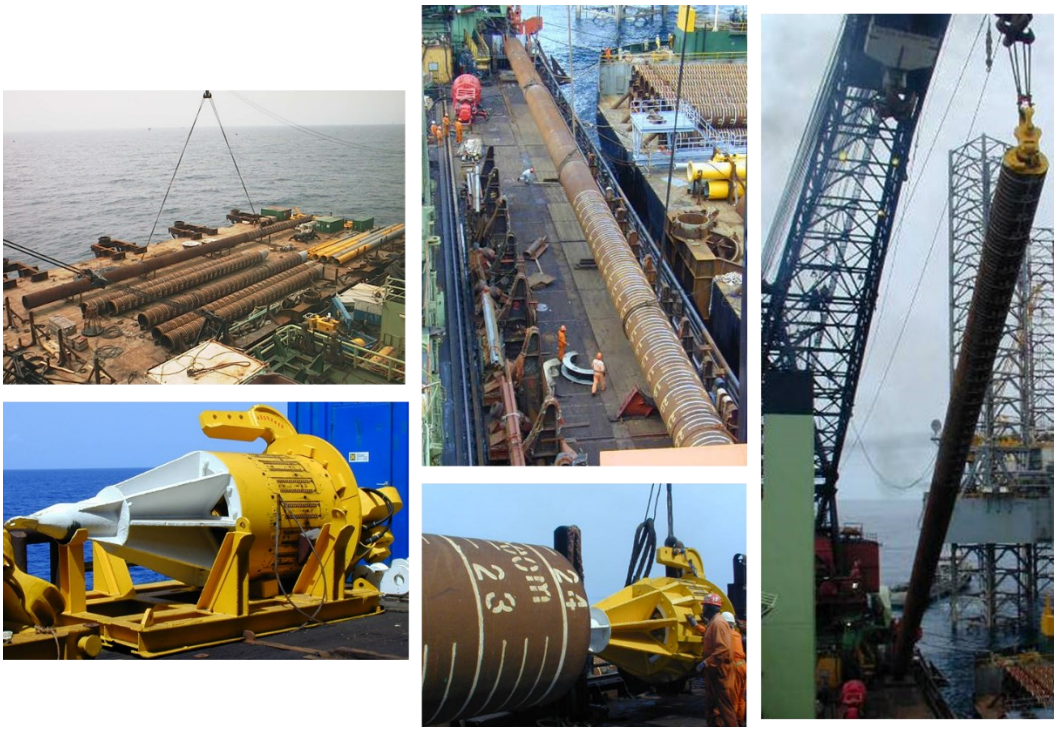

Figure 12 First and second steps

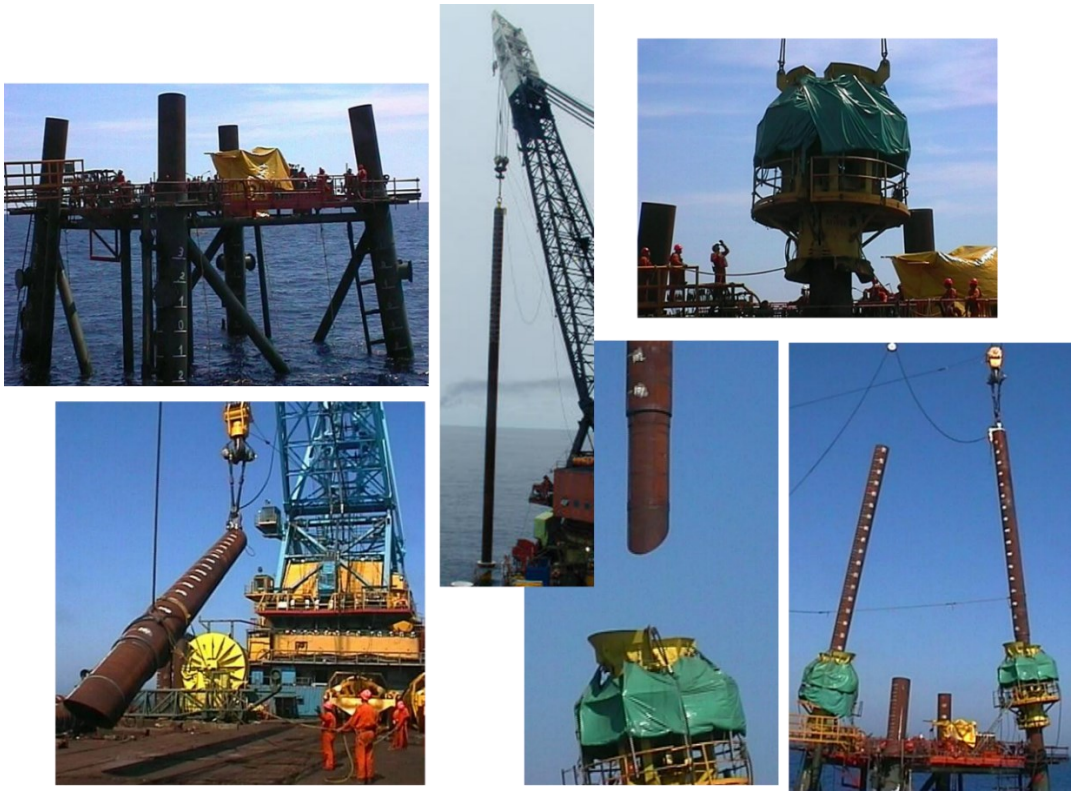

Figure 13 From 3 to 6 step.

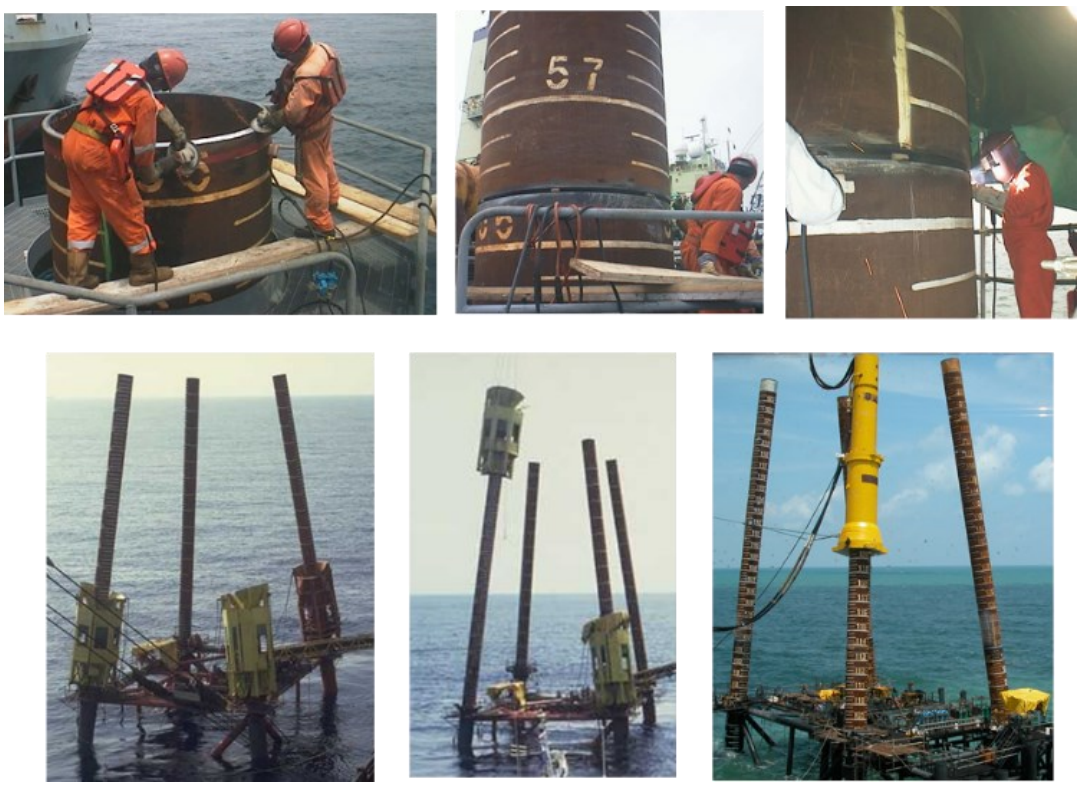

Figure 14 The last steps.

2.13 STATE OF THE ART

Calcareous soils with a significant content of calcium particles exist in many offshore environments. These soils show a particular behavior that has been recently investigated by many authors. They often exhibit a dynamic and static behavior that is different from that observed in other soils, especially if they are driven by hammer impact.

The figure below [11] shows how in all this type of soils the resistance decreases during driving attributed to the friction degradation and increases during driving interruptions, based on a so-called Soil Setup Time, (the time required for the soil resistance to increase from SRD to SSR). The set-up effect suggests that the loss of shaft capacity is only temporary, and the soil may recover its initial strength properties; because of this behaviour, hammer refusal can occur and can lead to premature refusal of piles.

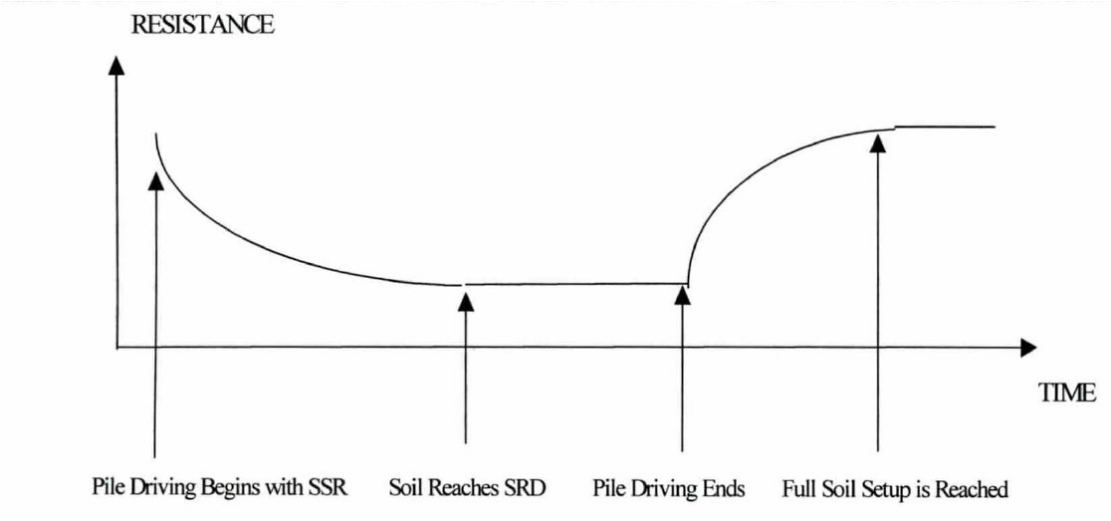

Figure 15 Variation of static resistance to driving

The first aspect of interest of pile driving in calcareous soils is the strength degradation.

The reduced SRD in cemented calcareous sands is generally attributed to a crushing of the soil particles, as it is said in Murff (1985) [1].

For other soils, the degradation of resistance may be caused by pore water pressure increase, soil remoulding and soil fatigue.

Installation of piles by impact hammer always caused changes in pore water pressure and in soil structure. The increase of pore water pressures reduces the effective stresses in the soil and therefore the shaft resistance. In sandy soils with good drainage, there may only be a

small temporary increase of pore water pressure; however, well graded sandy soils with some silt and clay may exhibit very significant increases in pore water pressure and, consequently, large loss of the shaft resistance.

In cohesive soils, temporary soil strength losses occur because of pore water pressure increases and soil remolding.

Actually, Chow has shown that not only cemented sands, but also dense marine sands develop an arching mechanism around the pile which explains why sometimes a relatively low friction in sands during pile installation is observed.

Once the excess pore water pressures dissipate, the effective stresses increases and the pile regains its strength. That is called set-up process.

To estimate how much strength has been regained, restrike tests are done.

Hussein in 1988 reported that restrike tests conducted on main piles, indicated setup gains up to 10 times above the soil resistance to driving under the first restrike blow [1].

However, he noticed that, for the second restrike blow, the soil strength was only one half and after the 20^{th} blow all of strength regained by the soil during the waiting period was lost.

It can be assumed that the first restrike blow not only encountered setup strength but also a peak frictional strength; later, blows encountered a reduced setup strength and only a residual soil strength.

Hussein claims that set-up strength assessment by restrike test should always be done with instrumentation because relying on the strength only to restrike blow count may indicate a so called “false setup” since hammers do not perform well under the early restrike blows.

Experimentation in 1997 showed the following assumptions that should be made for the calculation of unit shaft resistance and end bearing:

- In the calcareous clay, shaft resistance (SSR) is 2% of p_c (cone penetration test data) and end bearing is 40% of p_c. To calculate the shaft resistance to driving (SRD) a set-up factor 2.5 can be adopted. So, it was assumed that the calcareous clay had 40% of its static resistance during driving.
- In the calcareous and cemented sand, shaft resistance (SSR) is 0.5% of p_c limited to 30 MPa and unit end bearing was set to 100% p_c, limited to 150 MPa. In this case

the set-up factor that can be assumed is 1.5. This is equivalent to assume that the calcareous sand had 67% of its static resistance during driving.

With the assumption above he obtained a good agreement between the trends of the observed and computed blow counts during driving.

The set-up is a phenomenon useful to recover the soil strength. Several authors over the years have addressed this topic. Camp, in 1992, referring to some static and dynamic tests showed that piles with sand overburden reach earlier a higher strength compared to piles with clay overburden, for the same set-up time.

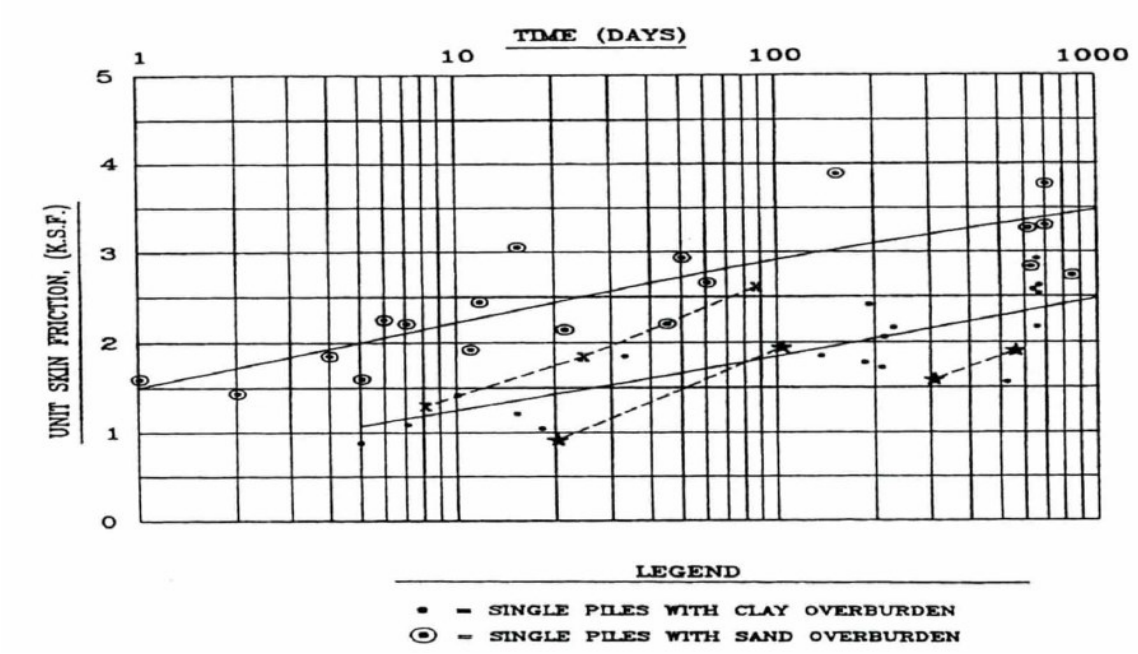

Figure 16 Capacity development with time (Camp)

Piles with sand overburden had average unit skin friction values of 70 kPa one day after installation and 168 kPa after 1000 days of waiting. For piles with clay overburden the average skin friction increased from 50 kPa after 5 days to 120 kPa after 1000 days.

The difference in performance was attributed to a slower drainage in the case of piles with clay overburden.

When no dynamic measurements are taken during the installation of the piles, the procedure Blow Count-Depth Matching (BCDM) [3] is useful for bearing capacity assessment. It

requires knowledge of the blow count vs depth including hammer model, hammer energy setting and the duration of driving interruptions.

It also attempts to predict long-term bearing capacity from soil setup effects occurring during interruptions of pile driving. Of course, far reaching assumptions must be made regarding the hammer driving system and the soil behaviour, limiting the reliability of this approach.

In Figure 17 the flowchart of the method is reported.

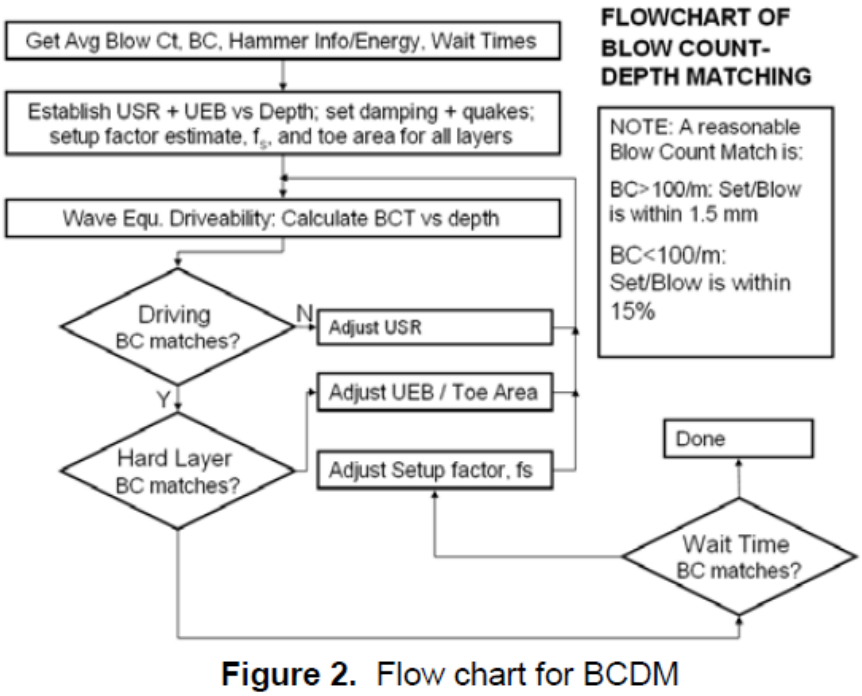

Figure 2. Flow chart for BCDM

Figure 17 Flow chart of blow count-depth matching

The basis for calculating long term capacity using this BCDM procedure is a complete blow count vs depth record, the hammer model and its energy setting and furthermore, driving interruption durations or restrike waiting times must be documented.

As a first step, the static soil resistance, the associated dynamic soil resistance parameters (quake and damping) and the soil setup factors for the various layers have to be evaluated.

Then, driveability analysis is performed which will produce an estimate of blow count vs depth.

This result should include “before” and “after” driving interruption analyses for the same depth for which GRLWEAP would produce the corresponding blow count changes. The

“after” waiting analyses generally correspond to a partial soil setup situation which allows for a refinement of the long-term unit shaft resistance values while the blow counts during continuous driving help establish the setup factors for the shaft resistance. Sudden changes in blow count are interpreted as changes in end bearing. Again, it will be necessary to modify both unit end bearing and toe area values to match those portions of the driving record.

CHAPTER 3: CASE STUDIES

3.1 THE STUDY AREA

The Arabian Gulf is a shallow elongated basin of Late Pliocene to Early Pleistocene age. The basin is asymmetric, with a gentle slope on the Arabian side, a much steeper slope on the Iranian side.

Figure 18 Arabian Gulf

According to Walkden and Williams (1998), the Gulf experienced the interaction of some equally important depositional systems throughout Pleistocene-Holocene time. A variety of depositional, erosional and diagenetic processes have been active in this area over a relatively short geological time. The record represents a complex interaction between fluvial erosion, aeolian deflation and redeposition, wind-driven marine processes, sea level fluctuations and evaporite diagenesis.

Due to the wide variation in the types of material and the processes to which they were subjected after deposition, the materials show highly variability in strength and type within relatively short distances.

Sometimes surface sands are cemented to a thin ‘caprock’. These hard layers, which can overlie loose sands and soft muds, were formed in relatively recent times. Small changes in

sea level exposed the sand, leading to the evaporation of water and allowing chemical carbonate cementation.

Cementation and lithification commonly affect the deeper (e.g. Pleistocene) soil of the Gulf as well.

The soil units were differentiated using geotechnical criteria. This includes soil composition, geotechnical properties and behaviour as determined by laboratory tests and interpretation of CPT results.

Because of erosion of overlaying layers, Arabian Gulf soils have generally experienced an effective vertical stress higher than the current one. An over-consolidation is also due to desiccation, often accompanied by a chemical action causing weak cementation. This occurs during repeated cycles of subaerial exposure and submerging when the vertical effective stress is respectively increased and then reduced. This complex stress history has resulted in over-consolidated competent Pleistocene soils with lateral effective stresses significantly higher than those found in normally consolidated soils.

Generally, finer-grained sediments are observed in deeper water farther from shoreline, and relatively stronger sediments are observed in shallower water nearer shoreline. Finer grained sediments are more easily transported by moving fluids such as currents and wave action. This suggests relatively low current influence and that shallower water is subject to increased wave action.

3.1.1 CALCAREOUS CLAY

The high carbonate contents (average 82% and maximum 98%) in the sediments found in the area suggest that most of the deposits are of marine origin.

Interpretation of carbonate content has significant effect on the reduction of the unit skin friction. This is particularly important when assessing axial pile capacity. Carbonate content was measured by performing rapid carbonate content tests.

Cohesive layers were described as ‘calcareous clays’ and ‘carbonate clays’ when the measured carbonate content is within in the range of 10 % to 50 % and 50 % to 100 %, respectively.

Non-cohesive layers were described as ‘siliceous carbonate’ for sand/silt strata with carbonate content in the range of 50 % to 90 %.

3.1.1.2 PILE INSTALLATION IN CALCAREOUS CLAY

Calcareous soils, characterized by a significant content of calcium particles, exhibit a dynamic and static behavior that is distinctly different from that observed in other soils, especially when piles are installed by hammer impact. Loss of bearing capacity due to the pile installation process and either full or only partial regain of capacity by setup, are phenomena largely affected by the mineral contents or structural properties of the soil grains [11].

Loss of soil resistance during and after installation is normally called degradation and usually attributed to the following phenomena:

- Increment of porewater pressure which decrease the soil's effective stress and therefore shaft resistance during installation.
- Liquefaction in loose granular soils due to the dynamic pile motions
- Soil remolding as is frequently found in clays or thixotropic materials
- Soil fatigue
- Loss of cemented structure in calcareous soils.

The setup is defined as a gain of bearing capacity occurring after installation and the main reason is:

- Dissipation of pore water pressure

Delimi, Maron and Clavaud [1] used a selected set of pile monitoring data in calcareous clay to derive specific parameters and support the drivability assessment of pile.

It was observed (as showed in Figure 19 that the degradation factor decreases with pile penetration: 0.45 to 0.6 at shallow depths up to 60 m then decreasing linearly to 0.1 to 0.25 at around 140 m. During continuous driving there is a higher loss of soil resistance to driving due to this phenomenon.

The global degradation factor is calculated with the formulation below, to replicate the correct trend:

$$GDF = (-0.0045 \cdot z + 0.77) \quad \text{Eq. 37}$$

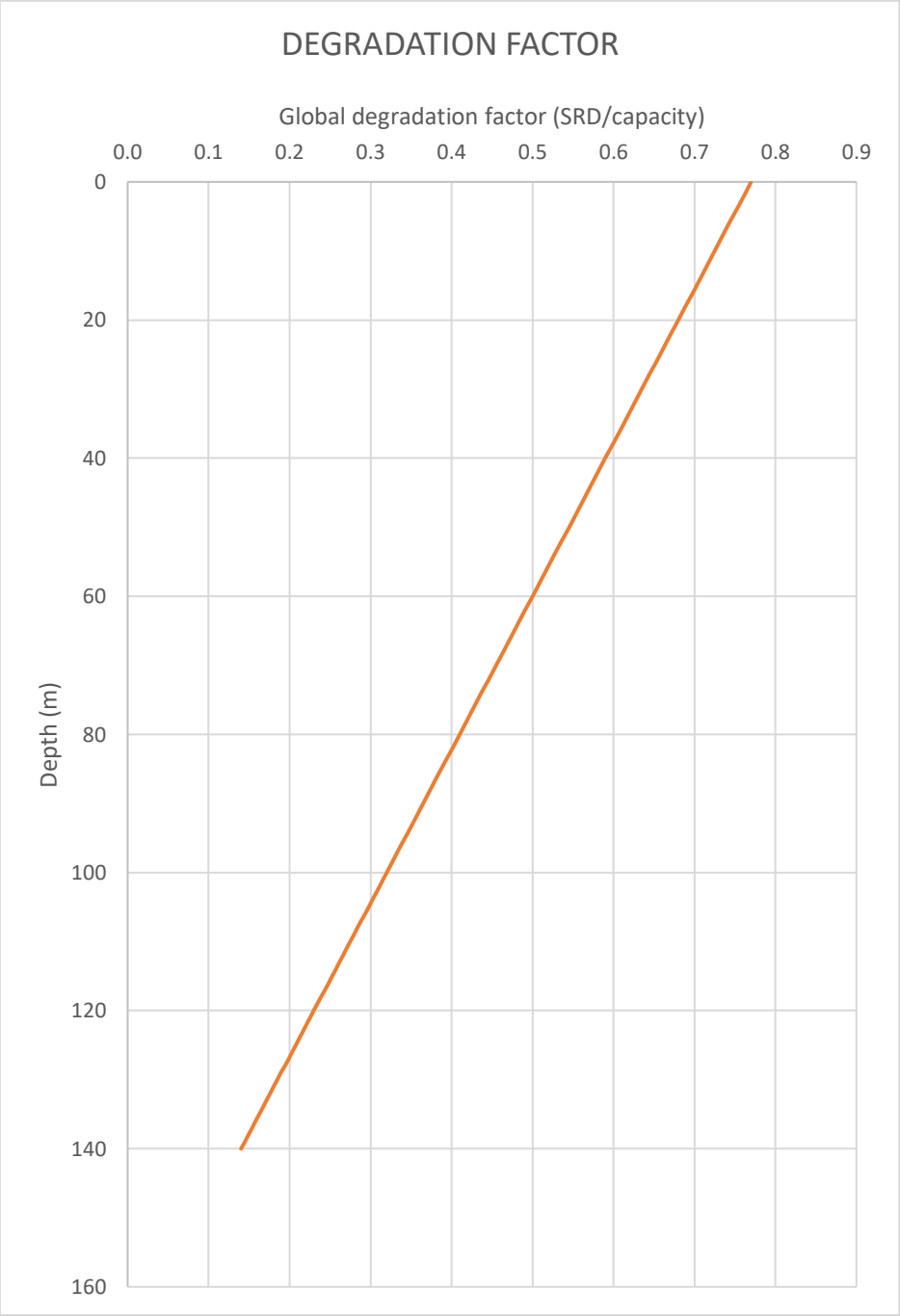

Figure 19 Global degradation factor versus depth - continuous driving

Instead, the set-up effect was found to develop from 2.5 after 24 hours interruption to 4 after 5 days interruption.

The shaft damping was observed to be around 0.7 s/m at the end of continuous driving and 0.4 s/m at restart after driving interruption.

3.2 DATA

This section presents the basic information to be used for the driving analysis:

- pile data, in particular main pile.
- soil data
- hydraulic hammer

3.2.1 MAIN PILE

Main piles are those foundation piles with multiple sections which are driven to seabed through the jacket legs. The number of sections may vary generally, depending on the water depth and target penetration depth. The pile is usually a slender long steel cylinder; it is divided into uniform pile and non-uniform pile if the geometry (diameter and wall thickness) vary along pile length: usually, on the vicinity of seabed, pile wall thickness is thickened to improve lateral resistance.

The pile modelling input parameters are:

- Pile outside diameter (OD)
- Pile wall thickness (W.T.)
- Target penetration (TP)
- Water depth (WD)
- True batter
- Final assembled pile length
- Pile section area: it is the cross-sectional area of the pile; for non-uniform pile it varying along pile length
- specific weight: the steel unit weight in the air must be given as input even if the pile is under water. This value is used for the calculation of masses to model the pile.
- Perimeter, used to calculate the shaft resistance in drivability analysis.
- Cut-off length
- Final cut-off length
- Driving shoe details
- Stopper elevation on the pile sections

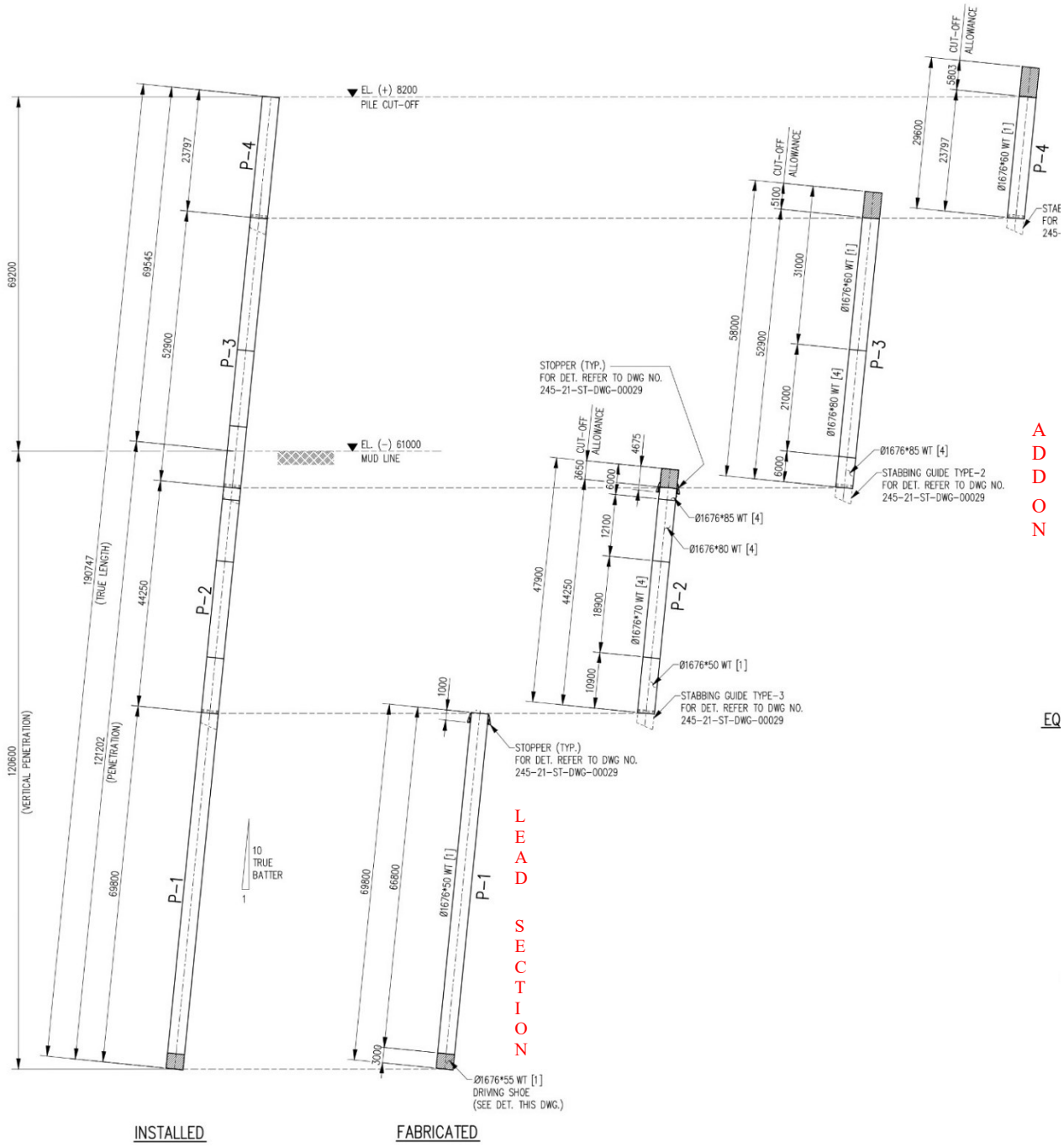

Figure 20 Main pile detail

The picture in Figure 20 shows the pile under consideration. There were four sections assembled into 190.747m length of main pile. The first section which is on the bottom of main pile is called lead section, and the other three pile sections above the lead section are called 1st add-on, 2nd add-on, and so on. In this case, lead section is sometimes equipped with a driving shoe.

The driving shoe is the thickened section at the pile tip of lead section that help piles to penetrate through hard layers or to reduce driving resistance for reaching deeper penetrations.

Another input parameter is the cut-off. It is an allowance length removed from the top of each pile section once driven to eliminate the material damaged by the hammer at the impact point (typical value: 0.5÷1.5 m). The final cut-off is the length of the last pile section to be cut (or to leave uncut) to reach the final main pile design elevation.

The inclination of the main piles depends on the jackets legs that can be vertical, battered or a mix of both.

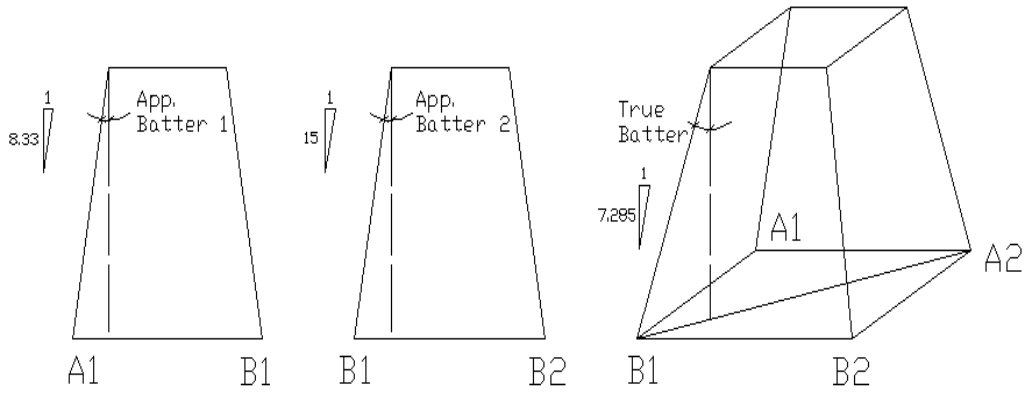

Figure 21 Apparent and true batter

The apparent batter is the pile inclination referred to the direction normal to the mudline in the plane that passes through each jacket side. Each main pile can have up to 2 different apparent batters.

The true batter is the pile inclination referred to the direction normal to the mudline in the plan that passes through pile and the vertical direction normal to the mudline.

3.2.2 SOIL DATA

A detailed knowledge of the soil conditions at the piles locations is necessary for a good piles Design and Installation Engineering processes and allows to mitigate many of the associated risks.

Site specific investigation data should be provided for the proposed structure site. The information should include the results of the offshore site investigation and the laboratory testing report. Geophysical data may also be available.

In general, for pile engineering purpose, the soil can be categorized in two main types which are:

- Cohesive Soil (Clay)
- Cohesionless Soil (Sand)

The first one is composed by fines soil particles (diameter < 0.002 mm); this gives the soil a plasticity or ability to be modelled.

The important design parameters for the follow analysis are:

- Submerged weight (γ'): Soil unit weight calculated as saturated unit weight (γ_{sat}) – water unit weight (γ_{water}). Generally, γ_{water} is taken as 10 kN/m³.
- Undrained Shear Strength (S_u)

Cohesionless soil is composed of individual soil particles that rearrange when loaded. This soil can only be held together by effective stresses. The important design parameters are:

- Submerged unit weight (γ')
- Soil internal friction angle (φ'): it can be directly estimated from the shear box test results. It should be noted that friction angles cannot be derived from CPTs due to the nature of the carbonate soils.

Soil data considered for the embedment calculation are summarized in Table 5 and the following points must also be considered:

- Plasticity index (IP)
- Limiting unit skin friction (f_{lim})
- Limiting unit end bearing (q_{lim})
- End bearing factor (N_q)
- Skin friction factor (β)
- friction angle between the soil and pile wall (δ), equal to $\phi - 5^\circ$

To determine all parameters, some tests were carried out.

The geotechnical investigation for all jacket location includes a single borehole with alternate CPT and sampling up to a final length of 130.1 m.

Output details of the borehole is reported in , il mio punto debole e il mio punto di riferimento. Ti ringrazio per non avermi lasciata mai sola, per non essere né avanti né indietro, ma accanto ad ogni mio passo. Alla nostra telepatia, al nostro essere troppo simili

in troppe cose, alla tua dolcezza e alla tua pazienza che in quest'ultimo periodo troppa ce n'è voluta. Alla nostra felicità, ai nostri successi e ai nostri progetti e traguardi, che insieme, mano per la mano, abbiamo conquistato e riusciremo a conquistare.

Siete esattamente quello che ho sempre desiderato, siete la parte mancante che completa il mio cuore. Noi siamo una squadra e ogni mia vittoria è anche la vostra.

Vi voglio bene.

APPENDIX A.

On-site data acquisition was carried out from the DPSV Fugro Adventurer.

Geotechnical testing was performed onboard the DPSV Fugro Adventurer's laboratory immediately following recovering of the samples.

Offshore laboratory testing comprises:

- Classification Testing: Particle Size Distribution, Water Content, Unit Weight, Atterberg Limits, Carbonate Content, and Visual Inspection.
- Strength Testing: Labvane (LV), Torvane (TV), Pocket Penetrometer (PP), Unconsolidated

  Undrained (UU) Triaxial Test and Point Load Test (PLT).

The general stratigraphy identified at all the jacket location is described below and includes soil composition, geotechnical properties and behaviour as determined by laboratory tests and interpretation of CPT results.

Table 5 Soil data detail

Depth		SOIL	γ'	IP	S_{u_top}	S_{ugrad}	ϕ	δ	f_{lim}	N_q	q_{lim}	β
from	to	TYPE										
[m]	[m]	-	[kN/m³]	[-]	kPa	kPa/m	[deg]	[deg]	[kPa]	[-]	[kPa]	-
0.0	1.1	SAND	9.0				20.0	15.0	15.0	8.0	900.0	0.21
1.1	14.1	CLAY	8.0	16.0	45	1.9						
14.1	15.6	SAND	9.0				20.0	15.0	15.0	8.0	1800.0	0.21
15.6	16.7	CLAY	9.0	11.0	70	0						
16.7	18.6	SAND	12.0				35.0	30.0	15.0	20.0	8300.0	0.21
18.6	32.1	CLAY	9.0	21.0	70	3.3						
32.1	33.4	SAND	9.0	-			40.0	35.0	25.0	8.0	5400.0	0.56
33.4	42.1	CLAY	9.0	21.0	118	3						
42.1	44.2	SAND	9.5				20.0	15.0	15.0	8.0	1800.0	0.21
44.2	68.0	CLAY	10.0	21.0	152	3						
68.0	76.3	CLAY	10.0	19.0	225	0						
76.3	79.5	SAND	10.5				20	15.0	15.0	8.0	3000.0	0.21
79.5	106.0	CLAY	10.0	19	300	0						
106.0	130.0	CLAY	10.0	19	330	0						

For assessing unit weight, two approaches were considered:

1. measuring the volume and weight of a sample with an estimated degree of saturation
2. calculating the unit weight from measurements of solid particle density and water content.

The first approach is called volume-mass calculation. It is normally applicable to cohesive material as the degree of saturation cannot be measured accurately when the sampled soil is cohesionless. However, unit weights were also determined using volume mass calculation by accurately measuring dimensions and weight.

The second approach is less reliable for cemented sand/rock layers as normal water content measurement is not suitable for cemented sand, hence giving a larger scatter. Best estimate particle density value of 2.65 Mg/m^3 was used in order to determine unit weight.

To estimate S_u, following tests were performed and interpreted:

- Unconsolidated Undrained triaxial test (UU);

- Cone Penetration Test (CPT) (indirect measurement): shear strength can be inferred from CPT net cone resistance (q_n) results, upon definition of an appropriate N_k factor. At this location, N_k factors of 15 and 25 were selected. Generally, shear strength inferred from CPTs are in agreement with laboratory test results.

- Pocket Penetrometer (PP): these results show a high degree of scatter. Substantial influence is due to the inclusion of sand. Interpretation of PP results was therefore done with caution.

Figure 22 includes the interpreted undrained shear strength from CPTs, using the selected N_k factors of 15 and 25.

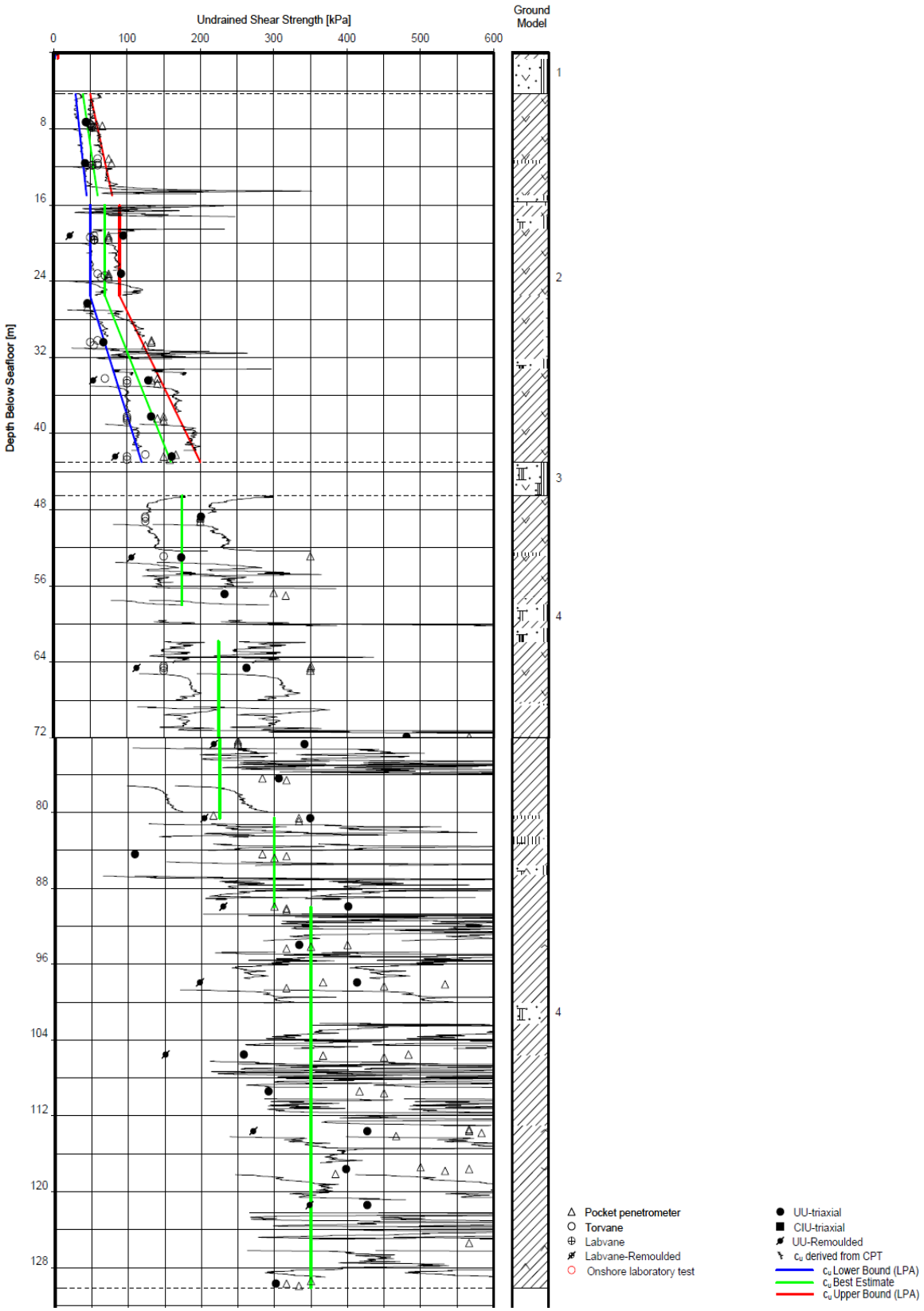

Figure 22 Undrained Shear Strength vs depth

One of the most important parameters is the evaluation of carbonate content. It has significant effect on pile design as carbonate cohesionless materials are susceptible to particle crushing, and hence reducing considerably the friction. This is particularly important when assessing axial pile capacity.

Carbonate content was measured by performing rapid carbonate content tests. Result of measurements are presented in Figure 23.

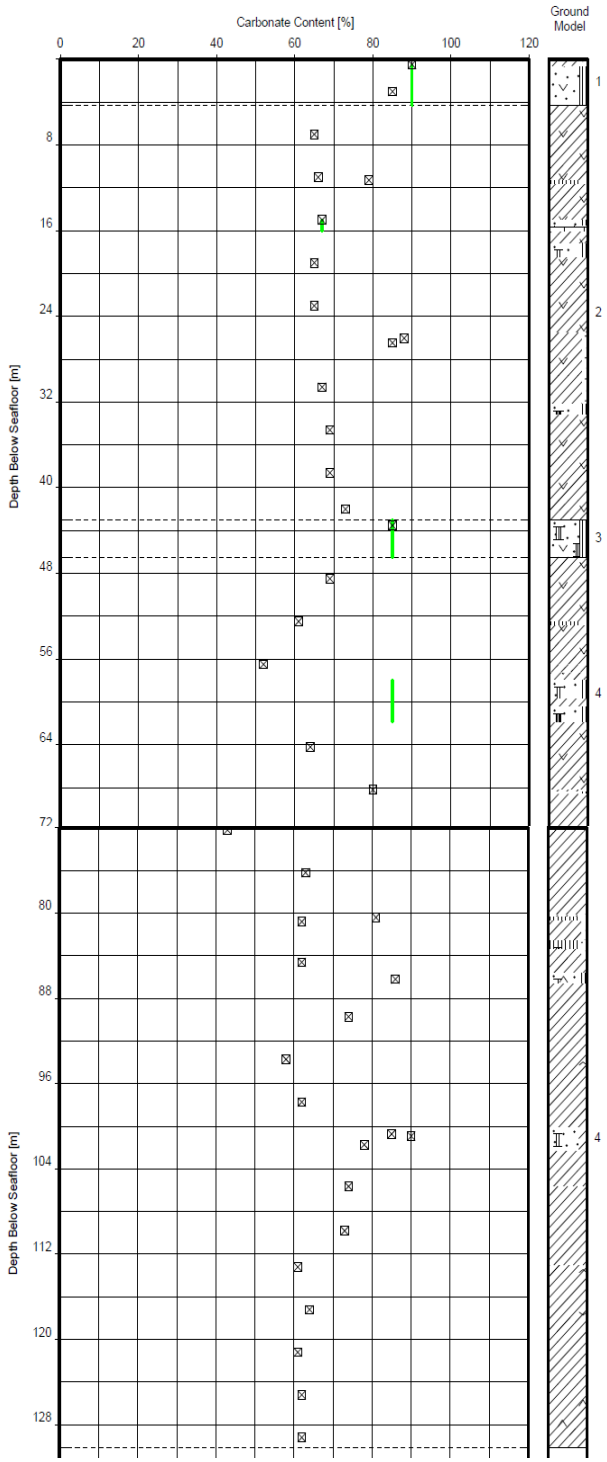

Figure 23 Carbonate content best estimate and carbonate content derived from rapid tests

It includes a constant fit of carbonate content per unit versus depth (best estimate value) for frictional layers.

The measured carbonate content varies between 60% and 90%. Cohesive layers were described as “calcareous clays” and “carbonate clays” when the measured carbonate content

is within in the range of 10% to 50% and 50% to 100%, respectively. Non-cohesive layers were described as ‘siliceous carbonate’ for sand/silt strata with carbonate content in the range of 50% to 90%.

We can conclude that at this location soils mainly consist of firm to very hard carbonate clay interbedded by slightly to moderately cemented carbonate sand down to maximum exploration depth of 130.1 m.

To estimate the soil resistance to driving with Alm & Hamre Method, a CPT tests is necessary. The following figure show the cone tip resistance vs depth. A peak on tip resistance is a sign of a sand intersection, as confirmed by borehole.

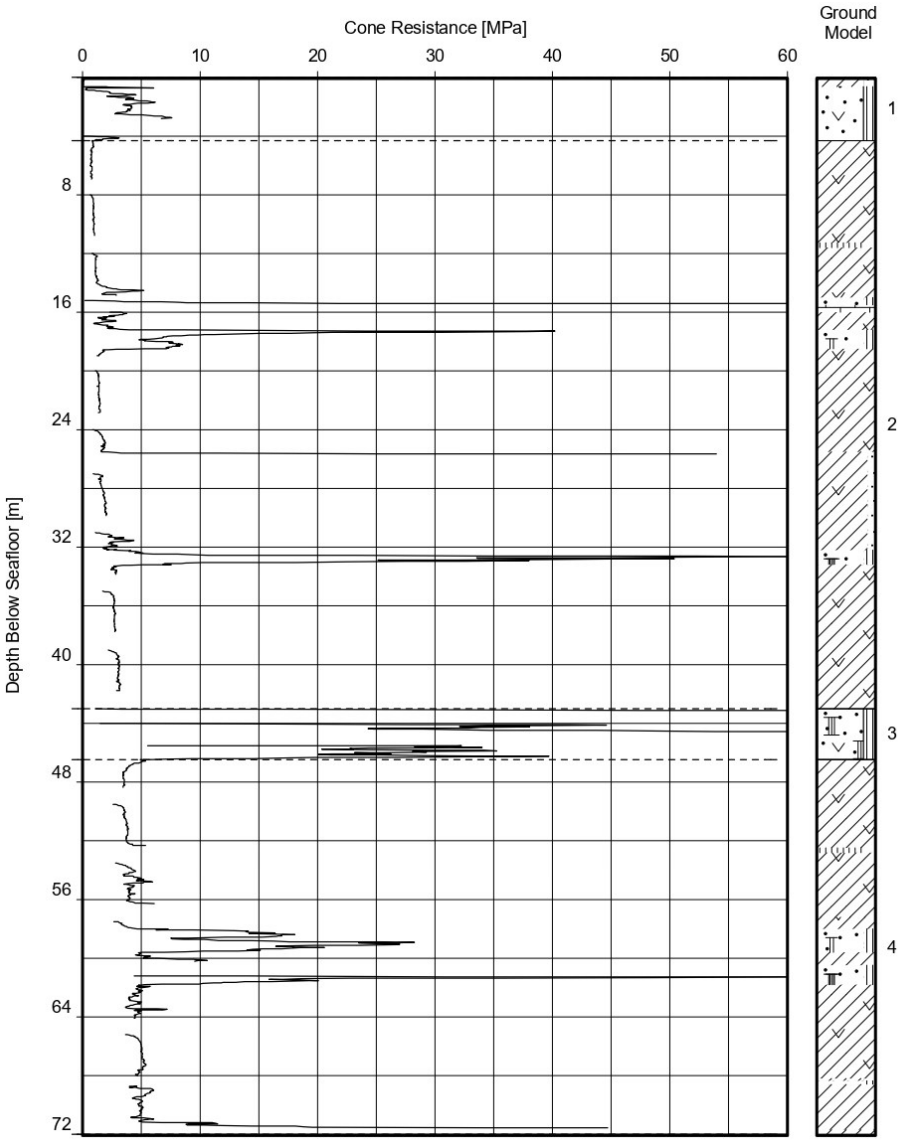

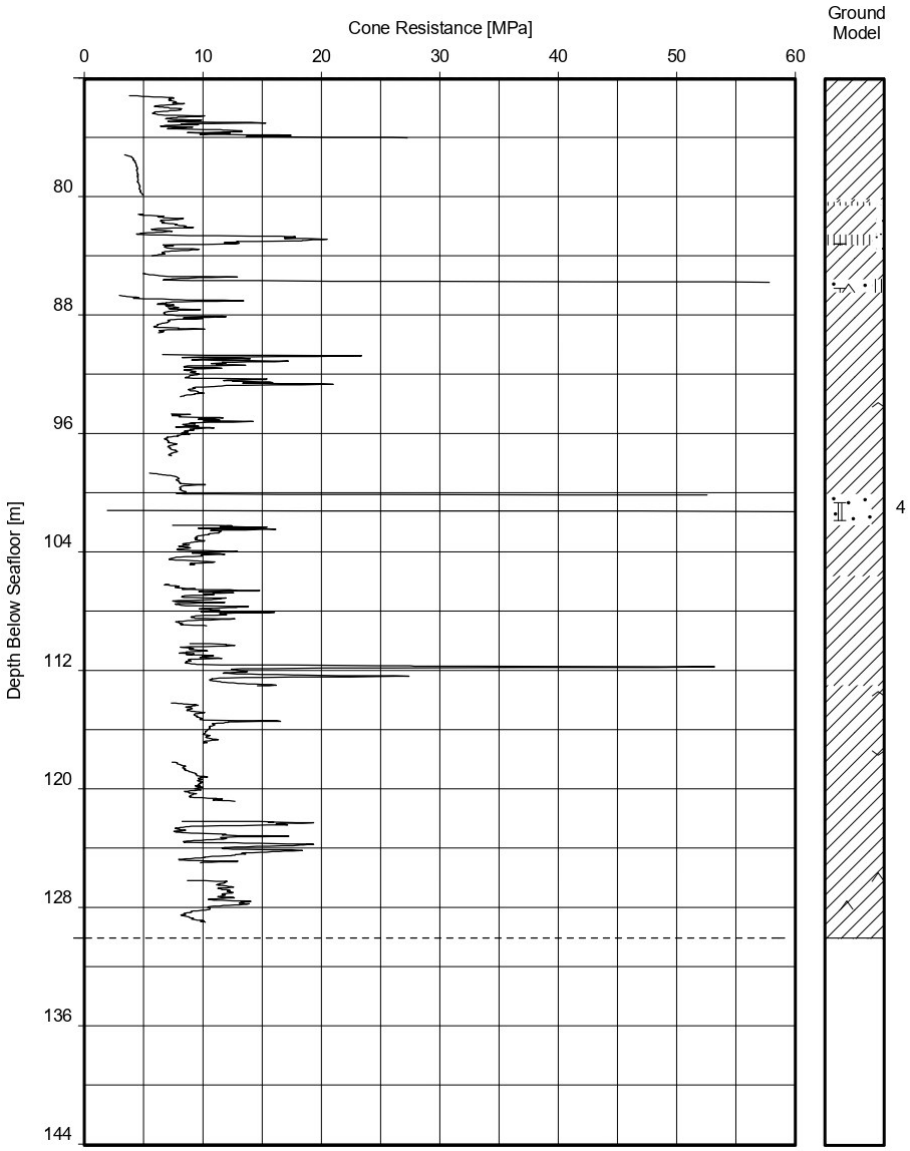

Figure 24 Cone tip resistance vs depth.

3.2.3 HYDRAULIC HAMMER

In this case study only hydraulic hammer was used. This type of hammer can be used both above and under water, to drive battered or vertical piles. It is more efficient than steam and diesel hammer, so the energy transferred to the pile is higher. The striking energy can be varied from a single blow to 100% of nominal value modifying the stroke of the ram inside the hammer housing.

Each pile driving parameter (number of hammer blows per linear unit of pile penetration (bl/25cm or bl/m;); striking energy, energy produced by hammer's machinery; penetration

depth, etc.) can be recorded by this type of hammer and saved as a text-file, however manual blow count recording has to be performed on board in any case.

The efficiency of a Menck Hammer (in water) is about 0.95 in continuous driving mode and 0.85 in restart (after add-on welding, after 12-24 hrs of driving stop, etc.). Above water the efficiency can be more than 1.

To operate below water the hammer is provided with a device, called Under Water Ballast (UB), an additional device needed to compensate the weight loss under water. If used, the weight of under-water ballast should be considered.

These hammers are very tall (~10 m to 20 m) and heavy (~15 t to 300 t),

Hydraulic hammers are equipped with anvil, that is the part of hammer that contacts with the top of pile. There are two types of anvil for hydraulic hammer: flat and dome anvil.

Then there is the ram: it is the part of hammer that moves up and down to generate the striking energy.

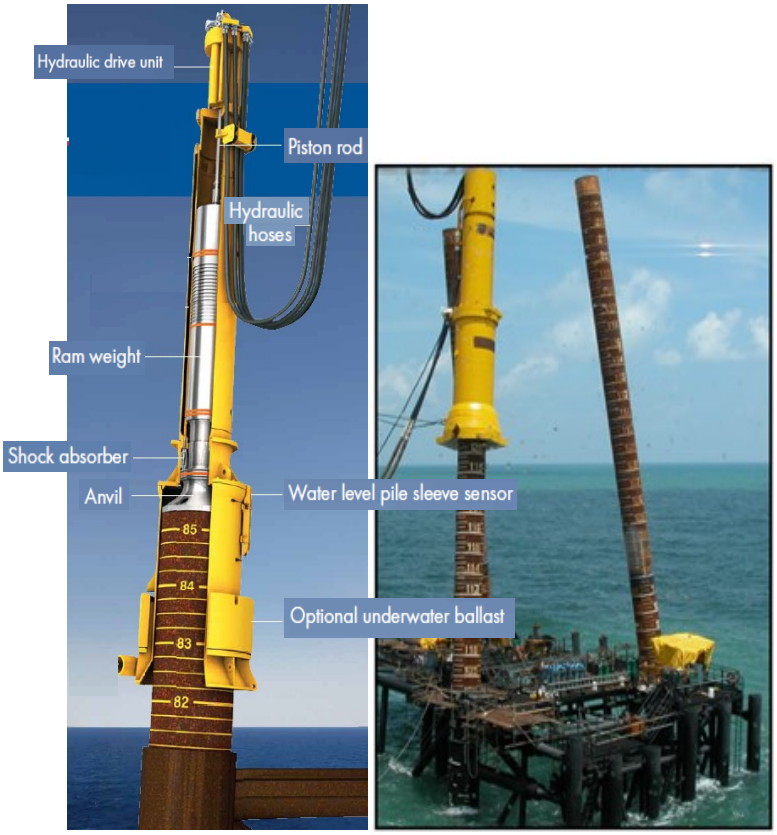

Figure 25 Hydraulic hammer

Another important factor to be considered is the hammer refusal.

It is the point where the pile driving with a considered hammer must be stopped and other methods instituted (e.g. drilling system or using a powerful hammer).

Typically, the refusal criteria is defined as a certain number of blows over a certain penetration and depends on the hammer type. For hydraulic hammer the refusal criteria is 800 bl/m.

3.3 FIELD DATA

Field data are divided into two components:

- Monitoring of blow counts, hammer energy and compressive stress vs depth
- Pile dynamic monitoring carried out during pile installation.

Pile Dynamic Monitoring (PDM) has the following objectives and advantages:

- Monitoring of the induced stresses during driving to ensure pile structural integrity and to prevent for pile damages and potential associated downtime during installation.
- Providing information on soil resistance at the time of monitoring and on driving system performance.
- Verification on pile capacity and pile acceptance, at the end of driving.
- Optimization for future projects: comparison of predicted with measured soil resistance to driving (BACK-ANALYSIS).

Figure 26 Data acquisition system

The force and the velocity signals measured by the strain gauges and accelerometers (as show in Figure 26) in the real pile dynamic test are represented in Figure 27. The measured signals are influenced not only by the hammer blow but also by the wave reflections that occur due to the soil resistance. Thus, these signals represent the effects to which the pile is submitted during the dynamic test.

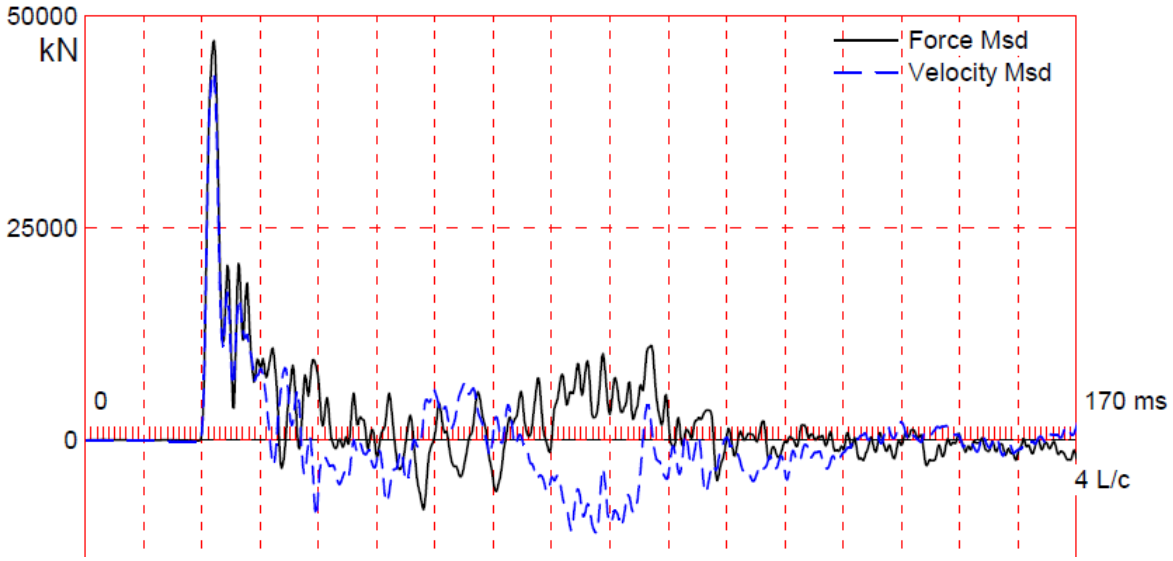

Figure 27 Measured force and velocity.

3.4 FUGRO DATA

3.4.1 DRIVING RECORDS

Thus, while dynamic monitoring was initially limited to a basic Case Method bearing capacity, transferred energy and pile top force result, the range of possible PDA (reported in Section 2.11.1) calculated outputs now includes (in addition to obvious results like maxima of acceleration, velocity, displacement):

- Maximum tension stresses
- Compression stress at the pile bottom
- Blow count

Results of driving records are reported in the figure below.

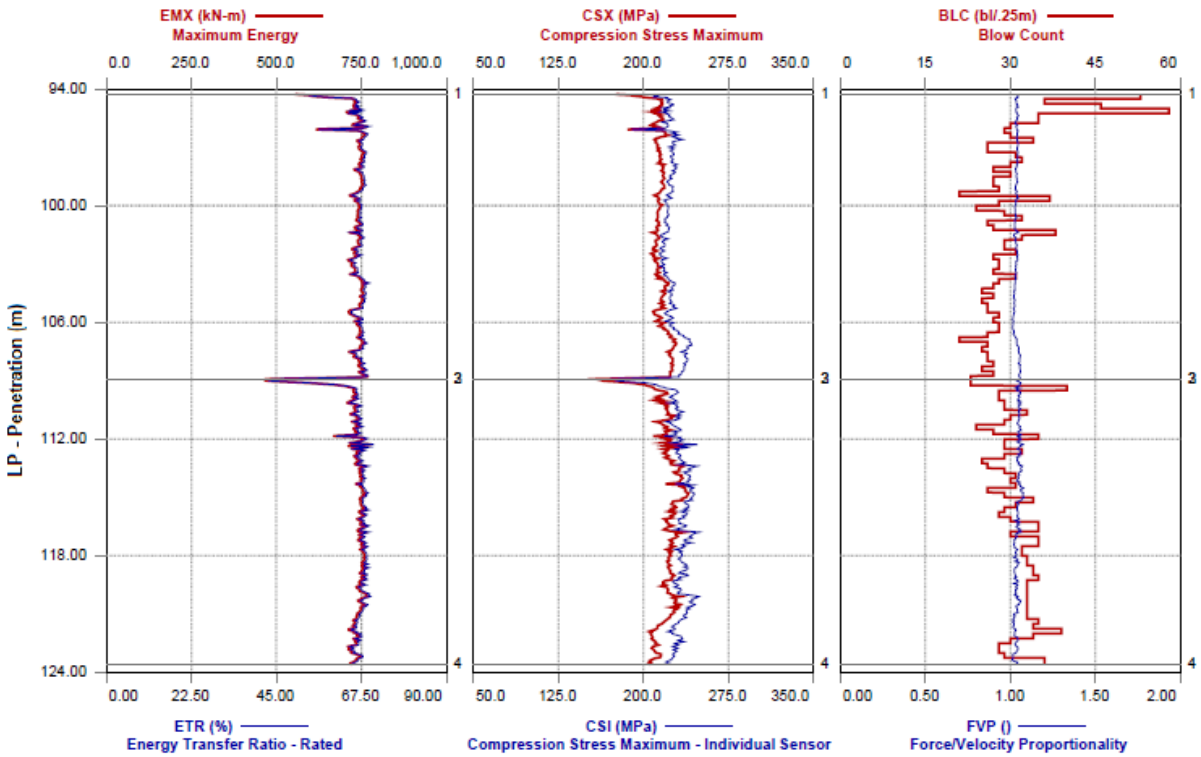

Figure 28 Driving Fugro records (blow counts, compression stress and maximum energy vs depth)

3.4.2 CAPWAP

The digitized record was then further processed on a main frame computer using the CAse Pile Wave Analysis Program (CAPWAP). This ‘‘signal matching’’ program input the velocity, assumed a soil model, and calculated the force required to keep the system in dynamic equilibrium; the soil model was iteratively adjusted to produce the best match between computed and measured force (Rausche, 1972). Because of this more intensive numerical analysis in CAPWAP, the correlation of predicted capacity to measured static load test results was better than the simple Case Method result from the PDA, and became standard practice for a well performed dynamic test.

CAPWAP can compute the forces and motions at locations along the pile with about the same precision as could be measured.

Thanks to CAPWAP Smith damping factor and quake are available and they are showed in the histogram diagram.

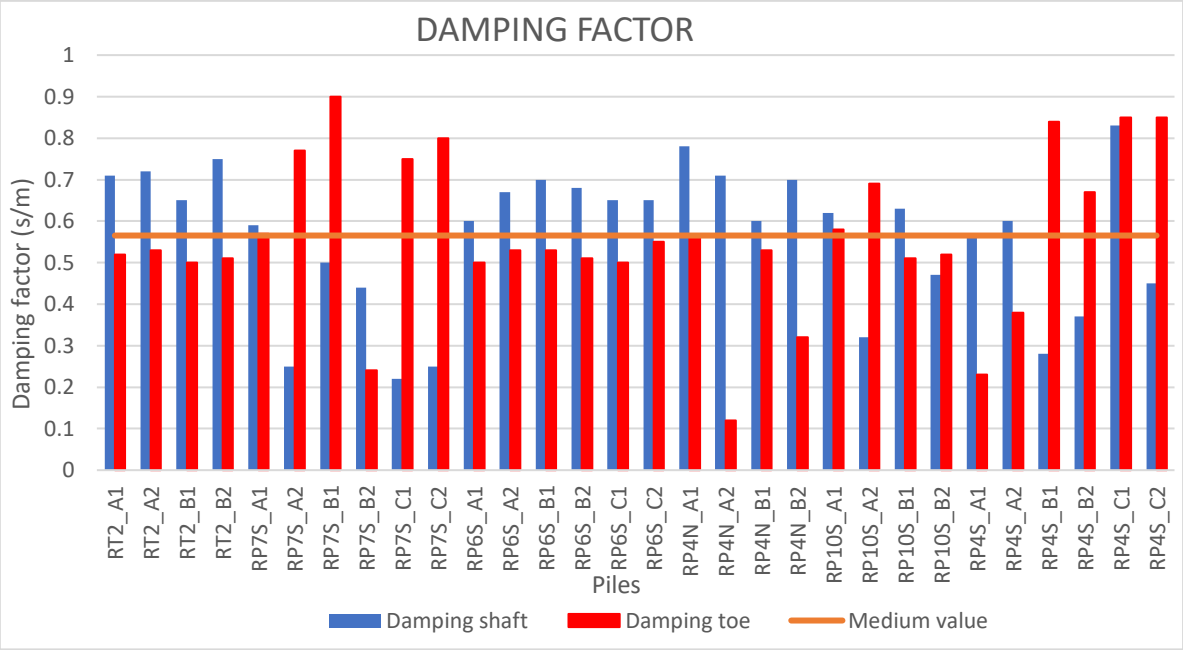

Figure 29 Damping factor for all jacket

For the analysis reported in the sections below, it is used a medium, constant damping factor of 0.57 s/m for the first analysis and for a better match, it is changed to a variable damping factor.

Thanks to Pile Dynamic Monitoring, also a damping factor at restart was measured (Figure 30).

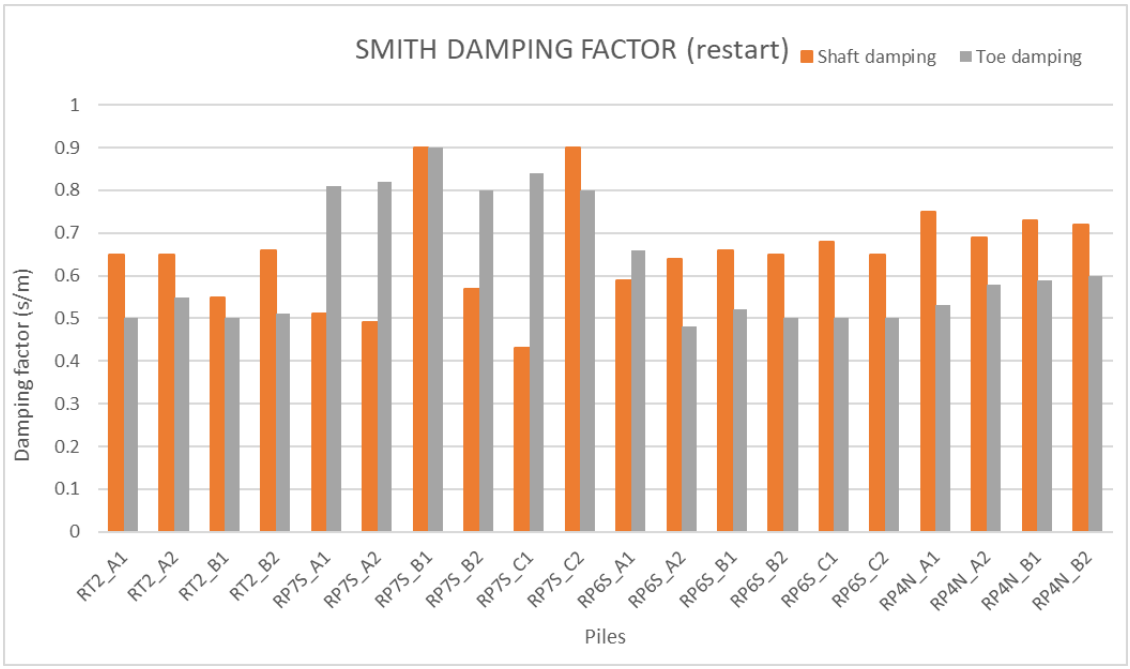

Figure 30 Damping factor for all jacket in restart condition

The figure below shows a comparison between the two shaft damping factors, before (EOD) and after (BOD) a set-up time. We can see that for most of the piles the damping factor decreases.

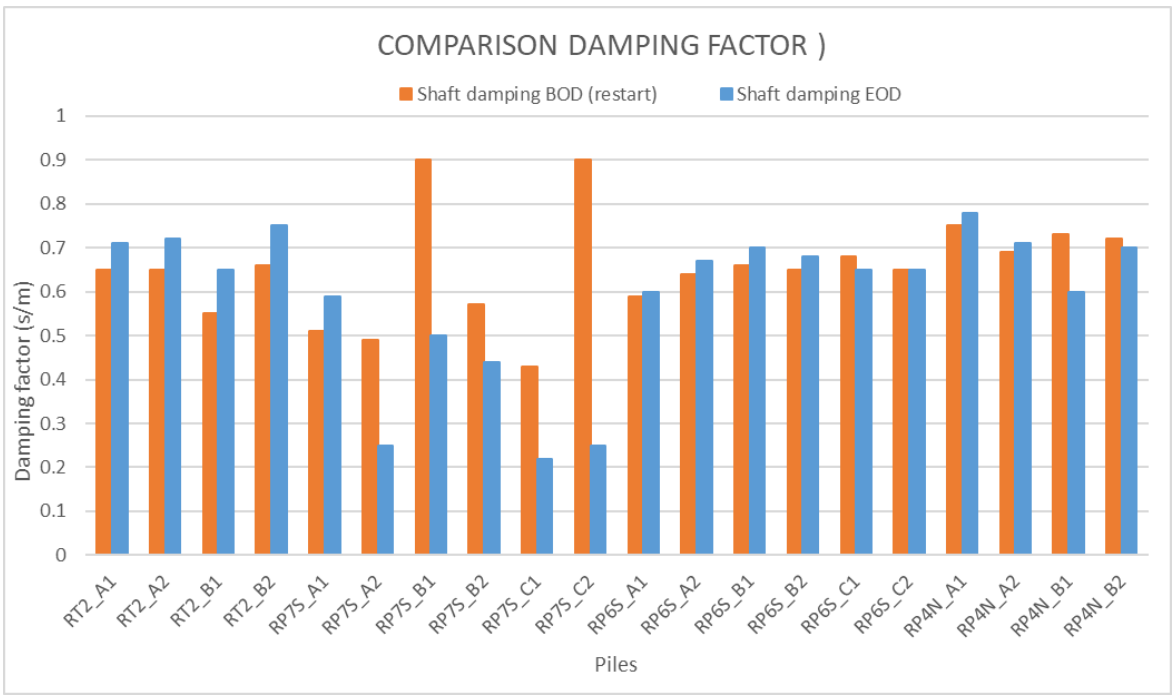

Furthermore, the CAPWAP analysis provides the trend of the total capacity along the depth. The capacity monitoring by Fugro at target penetration include the part along the shaft and end bearing. The last one, for pile with a big diameter (1.67m) and a high length, is about the 40% of the lateral friction as show in the figure below. So, we can conclude that the pile behaviour is plugged.

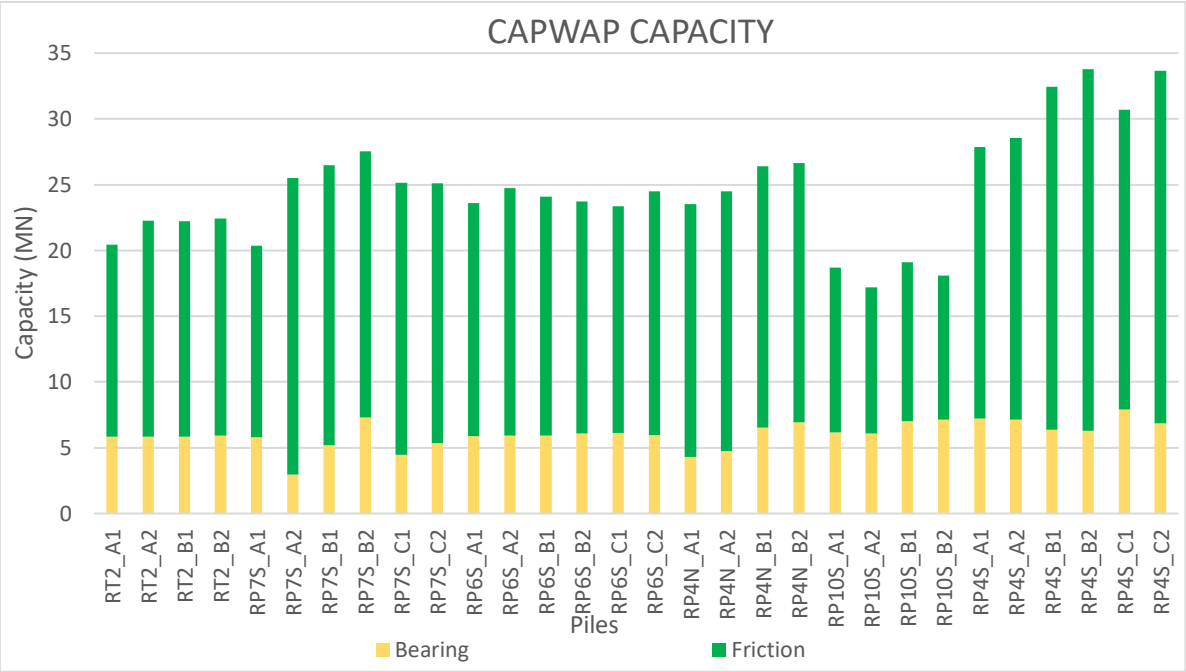

Figure 31 CAPWAP capacity

CHAPTER 4: METHODOLOGY

4.1 GRL weap

Wave equation analysis has become the standard method of evaluation of pile driving systems, with GRLWEAP the most widely used wave equation program.

Wave equation program models were developed based upon the original studies conducted by Smith (1960).

The program simulates what is happening in the hammer, pile and soil during and immediately after the ram impact.

It does this by modelling the system's components with masses, springs and dashpots and calculating the displacements and velocities of the masses and the forces in the springs.

Stresses are determined from forces divided by cross sectional area at points that are roughly one meter apart.

GRLWEAP can perform two types of analyses: bearing analysis option and driveability analysis option. Standard bearing graph analysis provides a thorough evaluation of pile and hammer system, while predicting the expected blow counts, pile stresses and hammer performance. However, these types of analyses may only be provided for a selected pile penetration, and the prediction of blow count versus pile penetration is not possible. The soil isn't modelled meter by meter and the user must provide a constant damping and quake factor with depth.

The driveability analysis option can be used to provide detailed predictions of blow count versus depth as well as predictions for the expected pile stresses and hammer performance. The soil in this case is modelled meter by meter, the dynamic parameters can be changed for each depth and a set-up time can be considered in the analysis.

The required INPUT data for bearing graph/driveability options are showing in the figure below and include:

- Hammer and driving system data (hammer type, striking energy, efficiency, helmet weight, hammer cushion);
- Pile data (pile section length, outside diameter, wall thickness, yield strength, target penetration);
- Soil Data (SRD, quake and damping parameters);

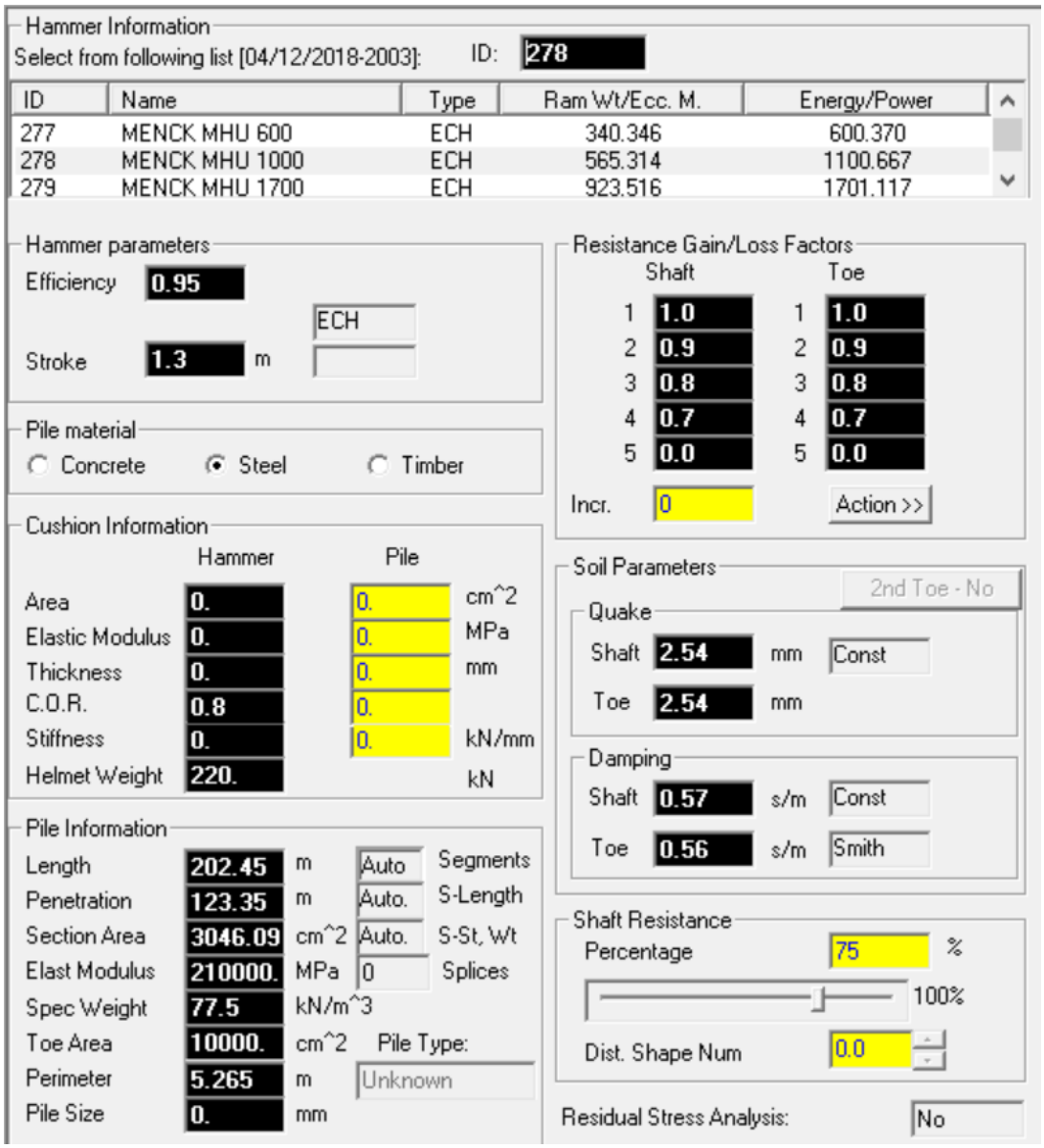

Figure 32 Software input screen

In the program the pile is modelled by a series of rigid masses connected by elastic springs; this allows considering both the inertia and the elasticity of the pile (as showed in Figure 33).

The ram and the anvil are generally rigid elements and are simply represented by their masses. The cushion, when present, is an elastic element with fully internal hysteresis.

The interaction between the pile and the surrounding soil is solved considering the two components of soil behaviour: one elastoplastic (linear) and one viscous.

The first component is represented by a spring and a friction block, with a maximum elastic displacement (quake), which correspond to a limit static resistance of soil.

The viscous component is assumed proportional to instant velocity and to the static resistance since greater pile dimensions correspond to a greater damping. It should be noted that radiation damping (the radial loss of energy) is not currently accounted for since only one-dimensional effects are considered.

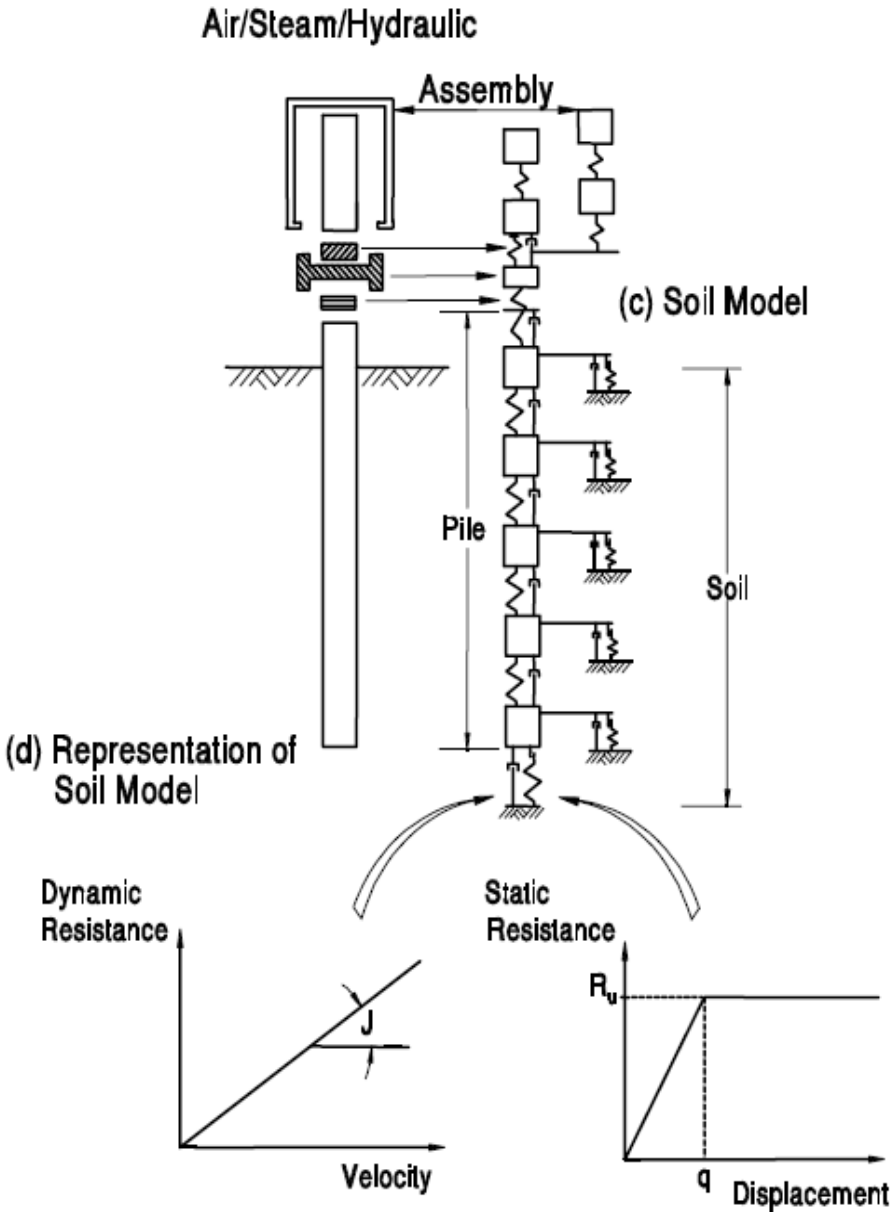

Figure 33 GRLWEAP model

The program computes:

- The blow count (number of hammer blows/unit length of permanent set) of a pile for several assumed ultimate resistance values, given a hammer and driving system.
- The axial stresses in a pile (tension and compression) averaged over the cross section for a certain pile penetration and associated ultimate capacity values.
- The energy transferred by the hammer to the pile for certain pile penetration and associated capacity values (ENTHRU).

4.2 SOFTWARE PROCEDURE AND ANALYSIS STEPS

The program models several subsystems: hammer, driving system (cushions, helmet), pile and soil are represented with a very basic and simple lumped mass model. It is mathematically stable only if the computational time increment is chosen shorter than the critical wave travel time of any segment i.

The critical time increment is the time that it takes the stress wave to travel through the pile segment:

$$\Delta t_{cri} = L_i/c_i \qquad \text{Eq. 38}$$

where:

- L_i is the length of the pile segment
- c_i is the wave speed of the segment $c_i = E_i/\rho_i$ with ρ_i, the unit mass of the segment.

For a lumped mass element, the critical time increment is equal to:

$$\Delta t_{cri} = (m_i/k_i)^{1/2} \qquad \text{Eq. 39}$$

where:

- k_i is the stiffness in segment i;

-m_i is the mass.

To avoid instability, the computational time increment Δt is chosen as:

$$\Delta t = \min(\Delta t_{cri})/\varphi \qquad \text{Eq. 40}$$

with φ =1.6

Established the time increment, the computation starts with a pre-integration.

Velocity value, v_{ij}, at segment i and time step j, are calculated in a simple Euler integration from accelerations, a_{ij}.

Displacements, u_{ij}, are predicted from v_{ij-1} and u_{ij-1}, from their value at the previous time increment.

For example, the ram of a hammer may be a simple mass, m_r, that has an initial velocity equal to the ram impact velocity, v_{ri}. Furthermore, at the beginning of the computations (j = 1) the first ram segment (i = 1) acceleration becomes $a_{11} = g_H$ with g_H being the gravitational acceleration of the hammer. In this case the pre-integration produces:

$$v_{12} = v_{ri} + a_{11}\Delta t \qquad \text{Eq. 41}$$

$$u_{12} = u_{11} + v_{ri}\,\Delta t \qquad \text{Eq. 42}$$

This process is repeated for all hammer, driving system and pile segments.

Then the force of the top spring on a segment is calculated from spring stiffness and the difference between the displacements of neighbouring segments.

$$F_{sij}{}^{t} = k_i(u_{i-1} - u_i) \qquad \text{Eq. 43}$$

Then the force at the top dashpot is calculated from the pile damping factor and the difference in the velocity of the neighbouring segments:

$$F_{dij}{}^{t} = c_p(v_{i-1} - v_i) \qquad \text{Eq. 44}$$

The force of the bottom spring is:

$$F_{sij}{}^{b} = k_{i+1}(u_i - u_{i+1}) \qquad \text{Eq. 45}$$

The force of the bottom dashpot is:

$$F_{dij}{}^{b} = c_p(v_i - v_{i+1}) \qquad \text{Eq. 46}$$

In the figure below is reported a schematic model of segment i with all forces and the external resistance forces.

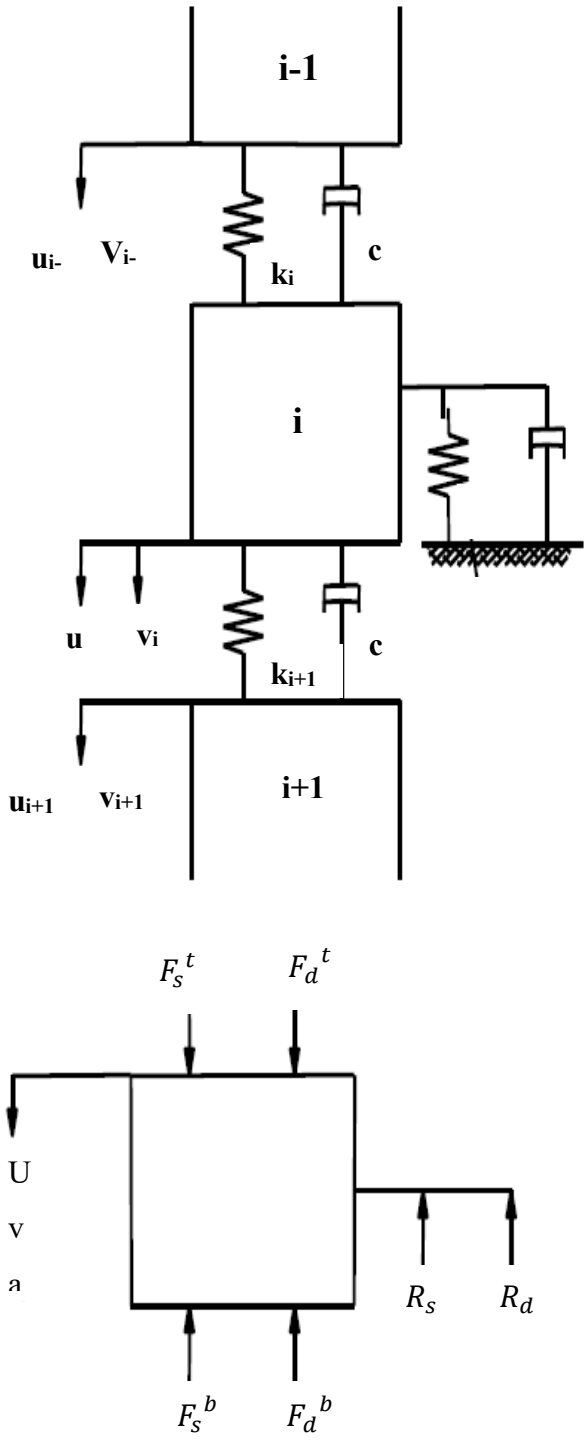

Figure 34 Schematic of model of segment i

Using the external resistance forces, R_{sij} and R_{dij}, calculated at the end of a previous time step, and the gravitational acceleration of the segment, g, it is now possible to compute the acceleration of a pile segment, i, during the current time step, j :

$$a_{ij} = g + ({F_{sij}}^t - {F_{dij}}^t + {F_{sij}}^b - {F_{dij}}^b - R_{sij} - R_{dij})/m_i \quad \text{Eq. 47}$$

with g = g_P for pile segment calculations and g = g_H for hammer or driving system segments. After the acceleration value has been calculated for a segment, its velocity and displacement values are corrected by integration under the assumption of a linearly varying acceleration:

$$v_{ij} = v_{ij-1} + \frac{(a_{ij}+a_{ij-1})\Delta t}{2} \quad \text{Eq. 48}$$

$$u_{ij} = u_{ij-1} + v_{ij-1}\Delta t + \frac{(2a_{ij-1}+a_{ij})\Delta t^2}{6} \quad \text{Eq. 49}$$

Since the displacements are now more accurately known than after the initial prediction, the spring forces F^t_{sij} and F^b_{sij} are recalculated. The changes of dashpot forces F^t_{dij} and F^b_{dij} are also recalculated. Thus, for the calculation of the spring forces on the next lower segment, i+1, updated force values are available.

Figure 35 shows the flow chart of GRLweap methodology. Is an iteration process. It starts with a velocity and accelerations prediction; then forces, acting on element i is computing. Forces are recomputed, from a compute and integration acceleration value. Finally current velocity and predicted value are compared. If these values are matching, resistance forces are computed. Instead, if the iterations exceeded it must return at initial steps.

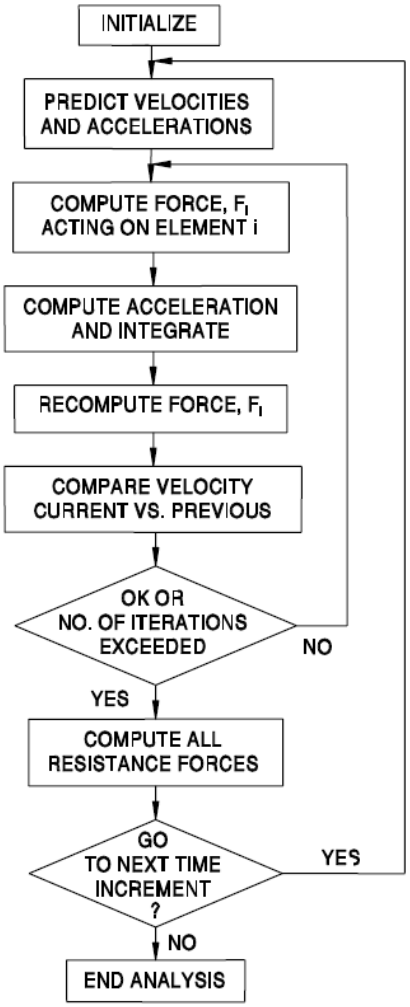

Figure 35 Analysis steps

For blow count calculations, the difference between the maximum toe displacement, u_{mt}, and the average quake is calculated. The average quake is:

$$q_{av} = \frac{\sum(R_{ui} * q_i)}{R_{ut}} \quad \text{Eq. 50}$$

where

- R_{ut} is the total ultimate capacity
- R_{ui} is the individual ultimate capacity value
- q is the quake

A summation is made over all elements from i = 1 to N+1 (N is the number of pile segments). Resistance number N+1 represents the end bearing.

The predicted permanent pile set is then:

$$s = u_{mt} - q_{av} \quad \text{Eq. 51}$$

So, the blow count is:

$$B_{ct} = \frac{1}{s} \quad \text{Eq. 52}$$

In the following section the two different analyses will be adopted and discussed.

4.2.1 BEARING ANALYSIS TYPE

The bearing analysis is useful for calculate blow count, compressive stress, tension stress, transferred energy (enthru) for several (at most 10) bearing capacity values.

There are three different ways in which end bearing and shaft capacity can be apportioned:

- PROPORTIONAL SHAFT RESISTANCE: since equal uncertainty usually exists about shaft resistance and end bearing, it may be best to analyse all capacity values with the same percentage of shaft resistance and end bearing. For example, for the jacket 1 the shaft resistance percentage is 80%; this it means that if the capacity value to be analysed are 500, 1000 and 2000 kN, then the shaft resistance (end bearing) would be 375 (125),750 (250),1500 (500) kN.
- CONSTANT SHAFT RESISTANCE: for a pile driving into rock; in this case the uncertainty will be about the rock capacity; so, we can consider the same shaft resistance and a variable toe resistance (it increases).
- CONSTANT END BEARING: for a long pile driving into clay; in this case the uncertainty will be about the shaft resistance; the end bearing is certain know (it is relatively small).

From the data recorded, the Capacity is back calculated using the so called “Global Analysis” method and presented versus penetration.

The global analysis method is based on the back analysis of field observations and measurements. The Energy delivered to the pile (ENTHRU) extracted from the pile monitoring data is combined with the measured blow count and processed through GRL-WEAP models (Bearing analysis) to calculate the actual Soil Resistance to Driving.

The analysis was conducted for six jackets considering two values of damping as recommended by previous experience [1]: shaft damping of 0.7 s/m and 0.4 s/m.

For the quake the same value for the shaft and the toe, equal to 2.54 mm, was considered.

The second step is to define the hammer: the energy recorded at sensors level (EMX) during driving the piles is useful to define the stroke in input.

Then the pile was modelled as it showed in Figure 36: separate analyses were carried out to consider the pile driving steps (lead section + 1st add on (a); lead section + 1st add on + 2nd add on (b); lead section + 1st add on + 2nd add on + 3rd add on (c)).

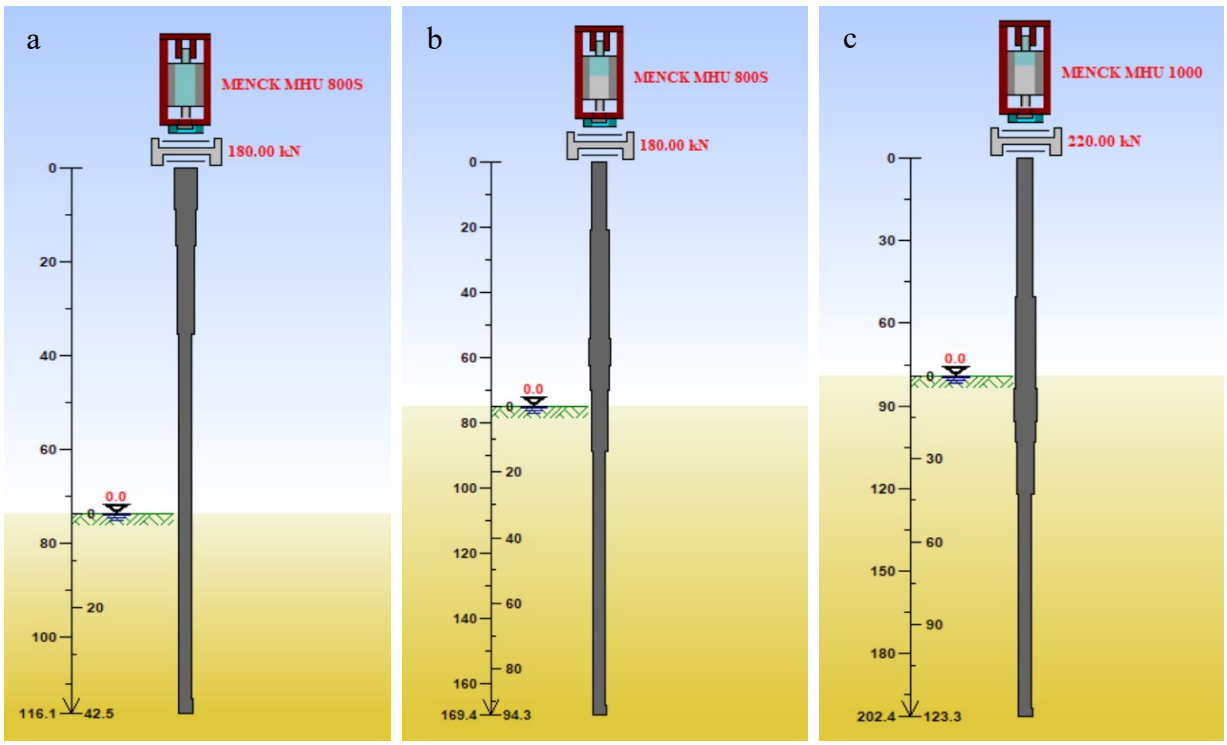

Figure 36 Pile section modelling

After accepting hammer, driving system, pile and soil input the bearing graph shows as a main result the ultimate capacity (kN) and the stroke vs blow count (bl/m) and as second graph the compressive (or tension) stress (MPa) vs blow count (bl/m) (Figure 37).

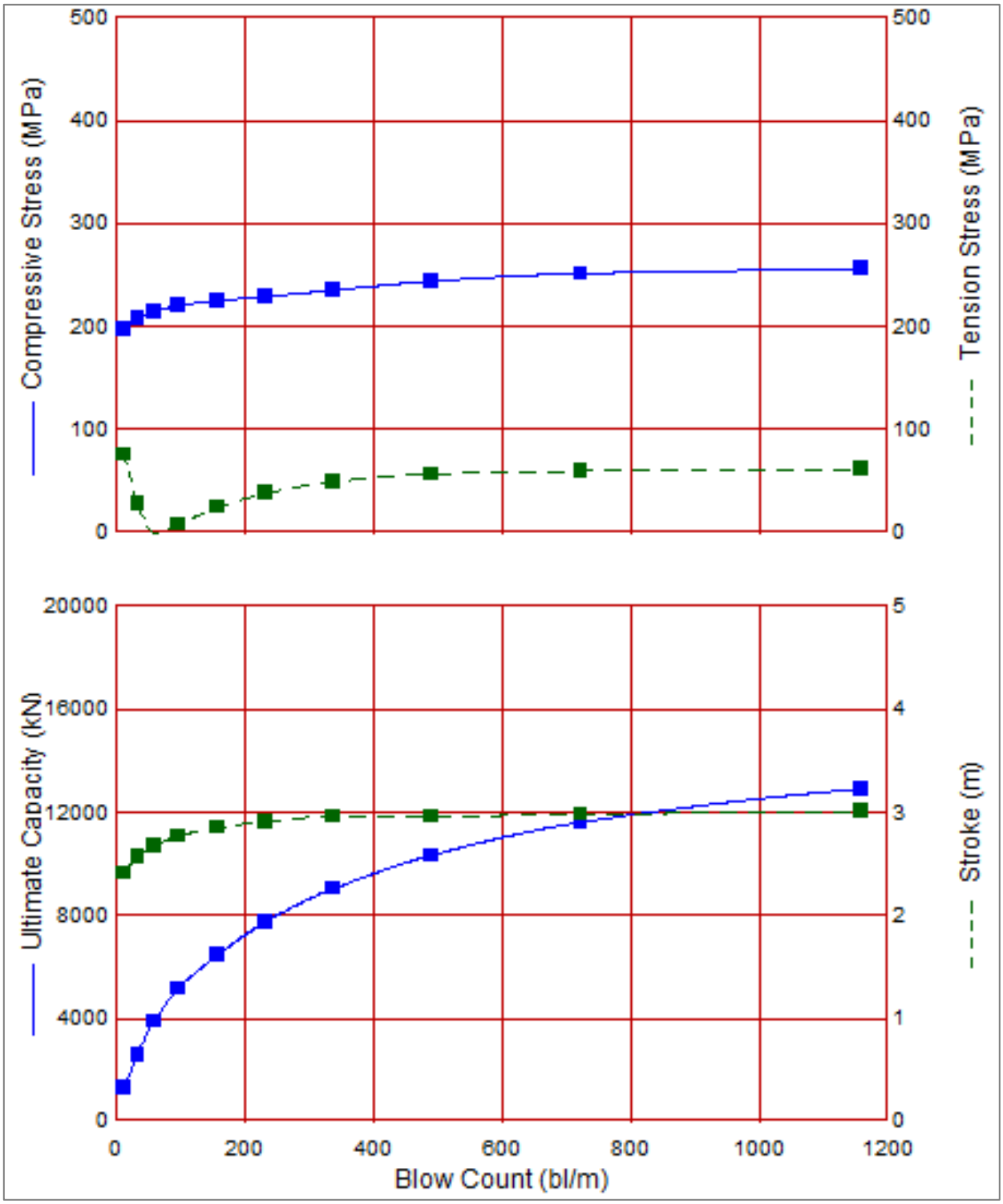

Figure 37 Bearing analysis results in term of ultimate capacity vs blow count

In this second graph, fixed the real blow count, for each blow count was calculated the ultimate capacity with an interpolation. Finally, the results is a graph capacity vs depth.

The assessments of pile resistances were performed using the Case Pile Wave Analysis Program (CAPWAP) at the final penetration of each pile. The CAPWAP method of analysis is a trial-and-error matching of force and velocities versus time records. Results include more detailed estimate of SRD and the friction distribution along the pile.
It was then possible to compare the interpolated capacity values with the actual measured at the end of driving (EOD).

4.2.2 DRIVABILITY ANALYSIS TYPE

This analysis calculates blow count, stresses and transferred energy vs pile penetration without running separate bearing graph analysis for each depth.

Input consists of unit shaft resistance and bearing value obtained by static soil analysis along with soil layer specific quake and damping value. The table below reports the input parameters.

Table 6 input parameters for drivability analysis

Depth	Unit Shaft resistance	Unit Toe resistance	Skin quake	Toe quake	Skin damping	Toe damping	Setup factor	Set up time	Toe Area
m	kPa	kPa	mm	mm	s/m	s/m	-	hours	cm^2

In GRLweap, to perform a dynamic analysis, the static resistance must be estimated by geotechnical analysis of the soil. The result of this analysis is the Long Term Static Resistance (LTSR).

However, during pile driving the soil properties change and the pile encounters the Static Resistance to Driving (SRD).

The conversion of LTSR to SRD is accomplished in GRLWEAP by means of Gain/Loss Factors, f_R, and Setup Factors, f_S.

While the Gain/Loss factors control the absolute change of static soil resistance, the Setup Factor controls the relative change of soil resistance among the various soil layers.

In general, for all soil type:

$$LTSR = f_S \cdot SRD \quad \text{Eq. 53}$$

if SRD is soil resistance occurring after the pile has been driven a certain distance, called limit distance, LL. In theory, driving the pile a distance equal to LL assures that SRD has been achieved. The LTSR will be occurring some time after driving which is called the setup time, t_S.

The reduction factor during driving would therefore be $f_{RD} = (1.0/f_s)$ if we would want to reduce the LTSR to the SRD to represent full resistance loss. If we would want to analyze the restrike situation with full setup, $f_{RD} = 1.0$ would be appropriate. For incomplete setup we could also analyze $f_{RD} = 0.7$. For each depth analyzed, with the three gain/loss factors f_{GL} specified as an input, a bearing graph would be calculated by the drivability analysis with three ultimate capacity values, one bearing graph for each depth analyzed.

Let now assume that two soil layers exist, with different setup factors like a clay layer and a sand layer with setup factor respectively $f_S = 2.5$ and $f_S = 1.25$. We would expect that full loss of setup resistance would reduce the sand LTSR to an SRD of $1/ f_S = 1/1.25$ or to 80% of its long term capacity and would reduce the clay LTSR to an SRD of 1/2.5=0.4.

We would therefore want to use $f_{RD} = 0.8$ for sand and $f_{RD} = 0.4$ for clay.
This is a dilemma which GRLWEAP solves by considering the gain/loss factor, f_{GL}, specified by the user to be consistent with the most sensitive layer. For less sensitive layers the reductions of resistance would be proportionate to the ratio of setup factors.

To avoid any confusion or risk or error, the approach chosen in this thesis consist in setting all the setup factor and gain/loss factor equal to 1 and prepare several input using different unit shaft resistance corresponding to different gain/loss conditions.

For each analysis depth, and depending on hammer and pile type, the following optional information can also be provided:

Table 7 Driveability analysis –Table for hydraulic hammer

Depth	Temp length	Wait time	stroke	Efficiency
	m	hours	m	

For each analysis depth, the drivability analysis also considers several driving system modifications in terms of:

- *(Ram) Stroke:* an effective way to modify pile driving energy of external combustion hammers (ECH) to control stresses.
- *(Hammer) Efficiency:* when there is a very hard driving situation (or driving to deep penetrations) it can be necessary a higher efficiency. For a correct modeling with increased or decreased efficiency values, experience based on measurements is often necessary.

When the driveability analysis type runs, the following output is obtained.

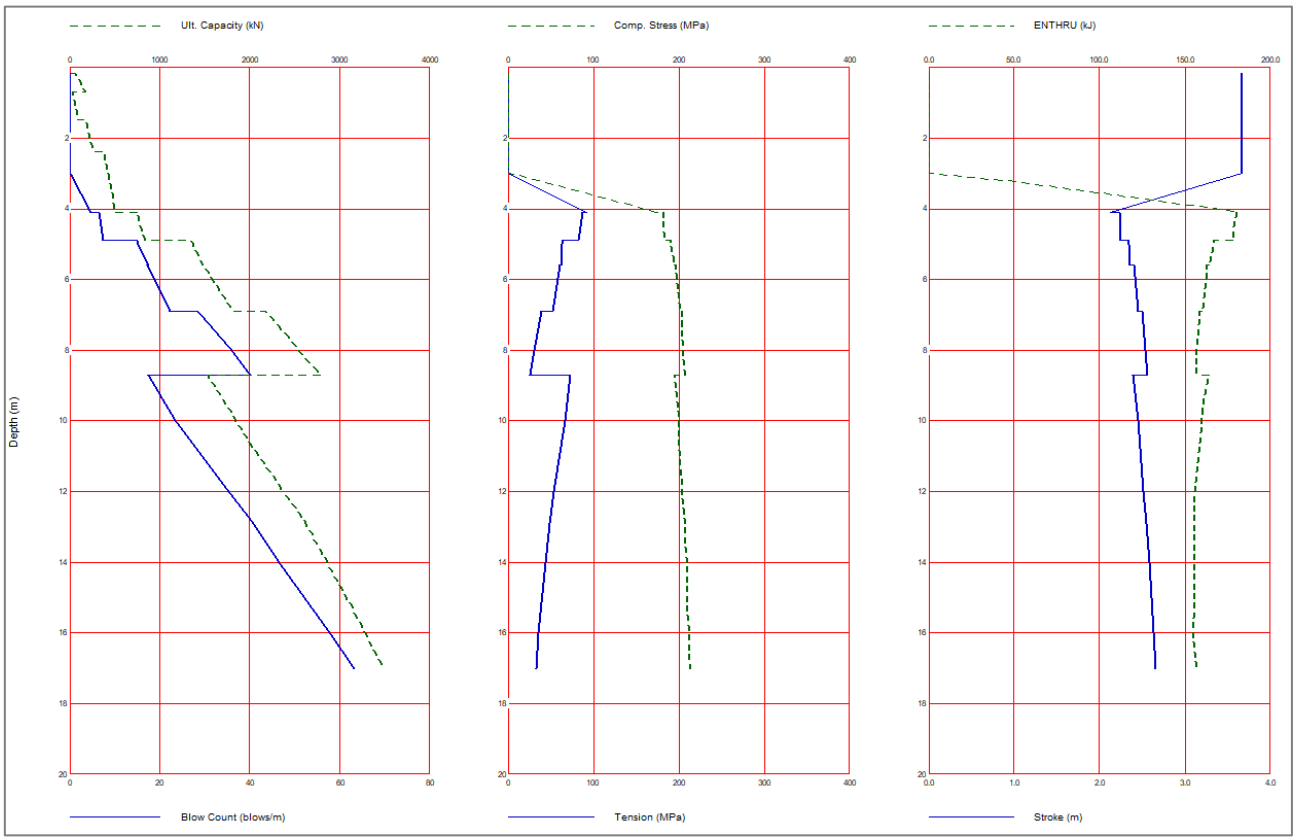

Figure 38 GRLWEAP driveability analysis output

The drivability graph shows as main result the ultimate capacity (kN), blow count (bl/m), compressive and tensile strength, enthru energy and stroke versus depth.

4.3 OTHER SOFTWARES

In addition to GRLweap there are other softwares that can be used for drivability analysis:

- TIPWHIP

- ALLWAVE

The first one [11] is a rotationally symmetric finite element analysis that can solve the same problems considered by the simpler one-dimensional program GRLWEAP. It can simulate a static test based on either static geotechnical properties from soil borings or parameters gained from dynamic signal matching. The static analysis is particularly useful for open ended piles which, depending on their diameter, wall thickness, and soil properties may not plug during pile driving but can plug during static loading where they behave like closed ended piles with full end bearing.

The pile soil interface is represented by thin elements which obey the Mohr Coulomb failure criterion.

$$\tau = \sigma' \cdot tan\delta \qquad \text{Eq. 54}$$

The soil properties (friction angle, elastic modulus, specific weight) for the static analysis may be obtained from CPT soil investigation.

The second one [12] is a powerful tool for driveability studies for impact driving. To install deep foundations, mono piles, offshore wind foundations require advanced software to predict the behavior of the total of pile, soil and hammer during installation. AllWave-PDP helps to select the hammer type, the expected penetration depth, blow counts and soil resistance.

The program enables the modelling of the impact hammer, the pile and soil resistance in a realistic way.

Accurate input values for all these parameters can be obtained from the database integrated in the program, which contains models for hammers (hydraulic, diesel and more) and also static and dynamic parameters for a variety of soils.

One of the considerable is the advanced implementation of soil fatigue modelling. The soil model is updated with the soil fatigue at each simulated penetration level. Without proper soil fatigue modelling it is almost impossible to predict the blow counts and the depth of refusal of a pile in a reliable way.

In the figure below are reported the typical results of an AllWave-PDP driveability analysis:

- Blow count versus depth diagram. This graph shows if the pile can be driven up to design depth. Blow counts exceeding predefined criteria for both hammer and pile indicate refusal.
- Maximum penetration depth. Essential for hammer selection and also provides the pile driving contractor an indication of the time required to drive the pile to target penetration. For field tests the graph can be used to check whether the pile behaves "normally".
- Maximum stresses in the pile, both in compression and tension, as input for fatigue analysis.

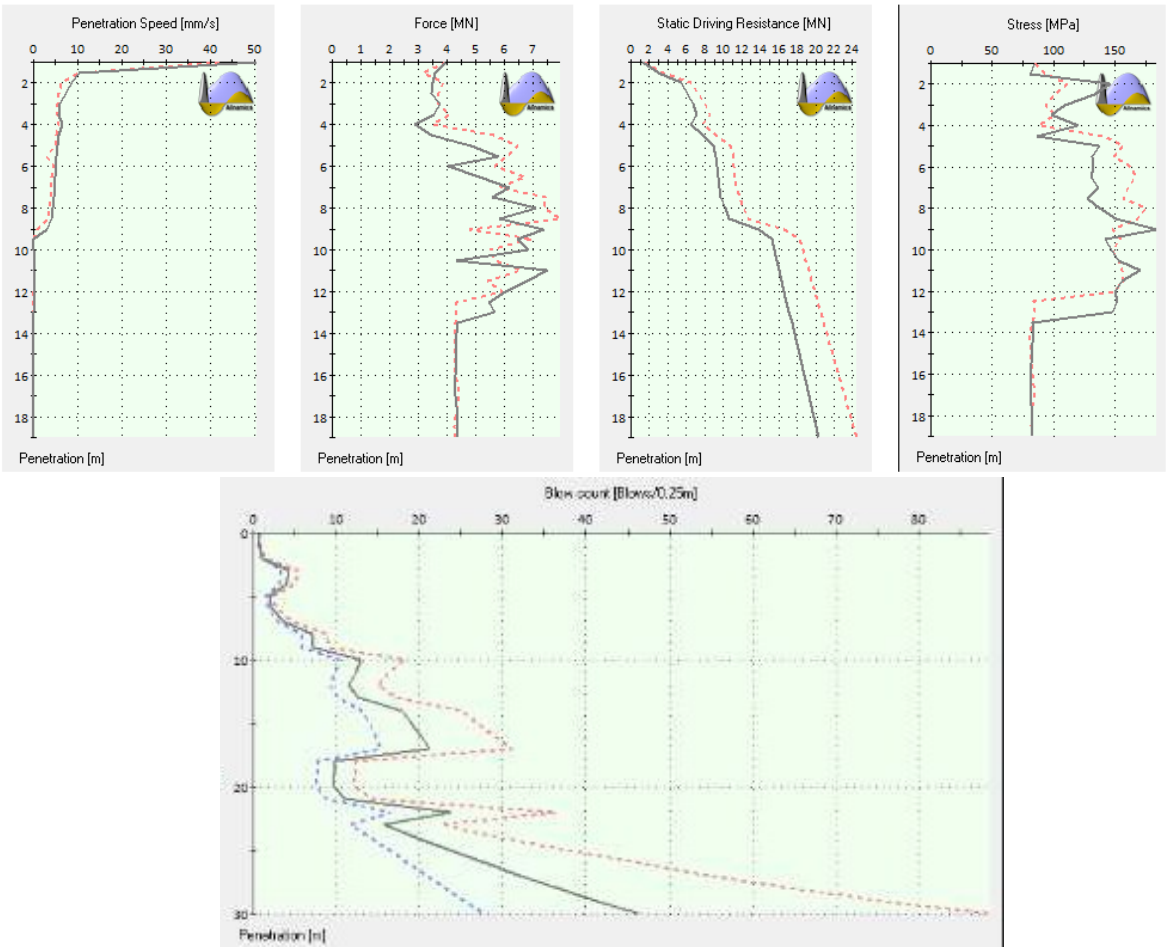

Figure 39 Allwave output

CHAPTER 5: RESULTS

In this section the following results will be shown:

- the prediction of the ultimate capacity of the pile from blow count (capacity vs depth). It was obtained from bearing analysis starting from the definition of the used hammer with its medium monitored energy and dynamic parameters assumption (damping and quake); the predicted ultimate capacity was then compared to the capacity trend obtained from CAPWAP analysis.

Figure 40 Flow chart for bearing analysis from monitored blow counts

- the prediction of the drivability analysis (blow count vs depth). It was obtained starting with some assumption in terms of soil degraded resistance and dynamic parameters; the calculated blow counts were then compared to the monitored blow counts.

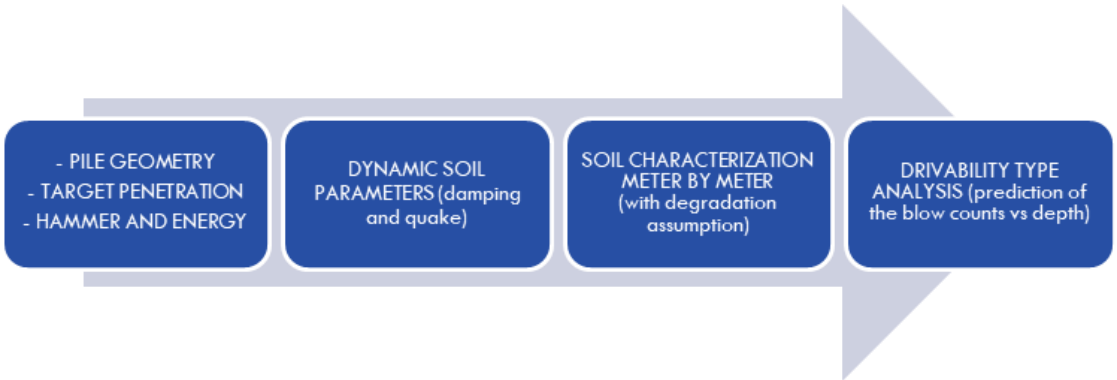

Figure 41 Flow chart for drivability analysis

- the influence of the set-up time for drivability and ultimate capacity of pile;

- the prediction of the ultimate capacity of the pile from CPT (capacity vs depth), starting from the definition of a degradation factor and with the hypothesis of plugged behaviour of pile.

Figure 42 Flow chart for bearing analysis from CPT data

- comparison between calculated and measured capacity. The calculated capacities are the following:
  - AXIAL STATIC CAPACITY: the bearing capacity of pile in static condition calculated as reported in Section 2.4
  - DEGRADED AXIAL CAPACITY: the bearing capacity of the pile during continuous driving considering a degradation (as it shown in Figure 19).

5.1 RESULTS OF BEARING ANALYSIS TYPE

After accepting hammer, driving system, pile and soil input the bearing analysis gives a graph showing the ultimate capacity (kN) vs blow count (bl/m).

Each step of pile penetration was analysed separately:

1. lead section + 1st add on + hammer
2. lead section + 1st add on + 2nd add on + hammer
3. lead section + 1st add on + 2nd add on + 3rd add on + hammer

Then, for each analysis, the capacity curves vs blow counts were obtained.

For example, if the jacket was composed by four piles A1, A2, B1, B2, each pile is modelled considering the insertion steps and the correct target penetration.

For pile A1, after the analysis considering a damping shaft equal to 0.7 s/m, the following results were obtained:

Table 8 Results of bearing analysis

	Ultimate Capacity	Blow counts	Stroke	Tension Stresses	Compression Stresses	Energy
	kN	bl/m	m	MPa	MPa	kJ
lead section + 1st add on + hammer800S (P1P2MHU800S)	50	0	0.2	0	0	0
	3377	30	0.2	-54	86	99
	6705	140	0.2	-28	86	84
	10033	301	0.2	-14	86	82
	13361	498	0.2	-10	86	82
	16688	929	0.2	-10	86	82
	20016	2410	0.2	-11	86	82
	23344	9999	0.2	-10	86	82
lead section + 1st add on + 2nd add on + hammer800S (P1P2P3MHU800S)	50	0	0.9	0	0	0
	6711	39	0.9	-74	167	352
	13372	109	0.9	-32	167	344
	20033	234	0.9	-18	167	341
	26694	522	0.9	-17	167	340
	33355	2208	0.9	-18	167	340
	40016	9999	0.9	-20	167	339
lead section + 1st add on + 2nd add on + 3rd add on + hammer1000S (P1P2P3P4MHU800S)	1000	0	1.3	0	0	0
	12000	45	1.3	-57	241	655
	23000	143	1.3	-28	241	645
	34000	595	1.3	-24	241	645
	36439	874	1.3	-23	241	645
	45000	9999	1.3	-20	241	645

The ultimate capacity, the blow count, the stroke (considering a medium energy of hammer for each section of pile), the tension and compression stress along the pile and the energy delivered to the pile (ENTHRU) are shown in the table above.

The capacity and the blow counts reported in the table are shown in the graphs below.

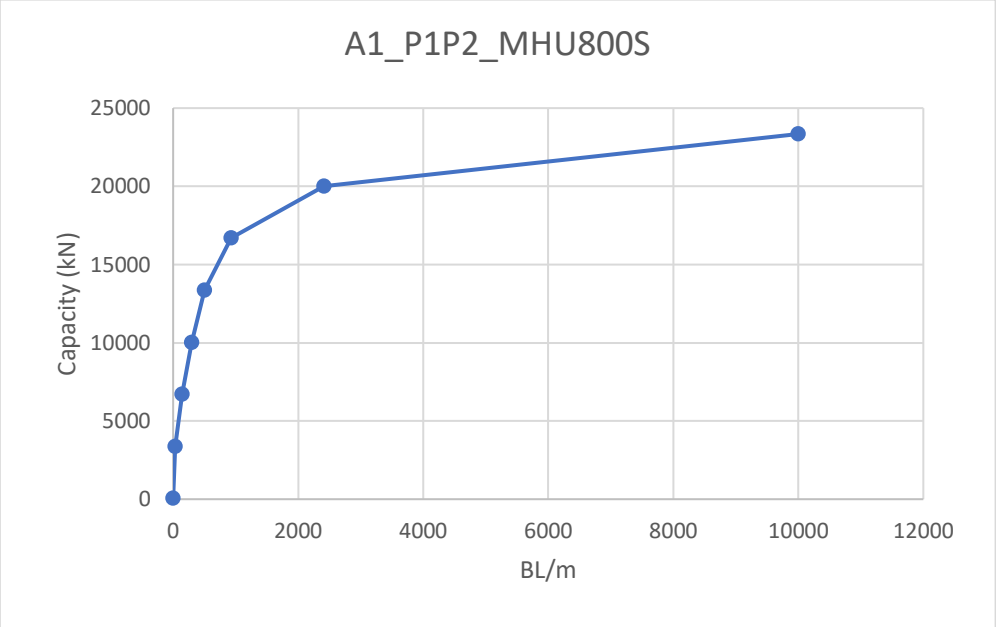

Figure 43 Capacity vs blow count for first penetration

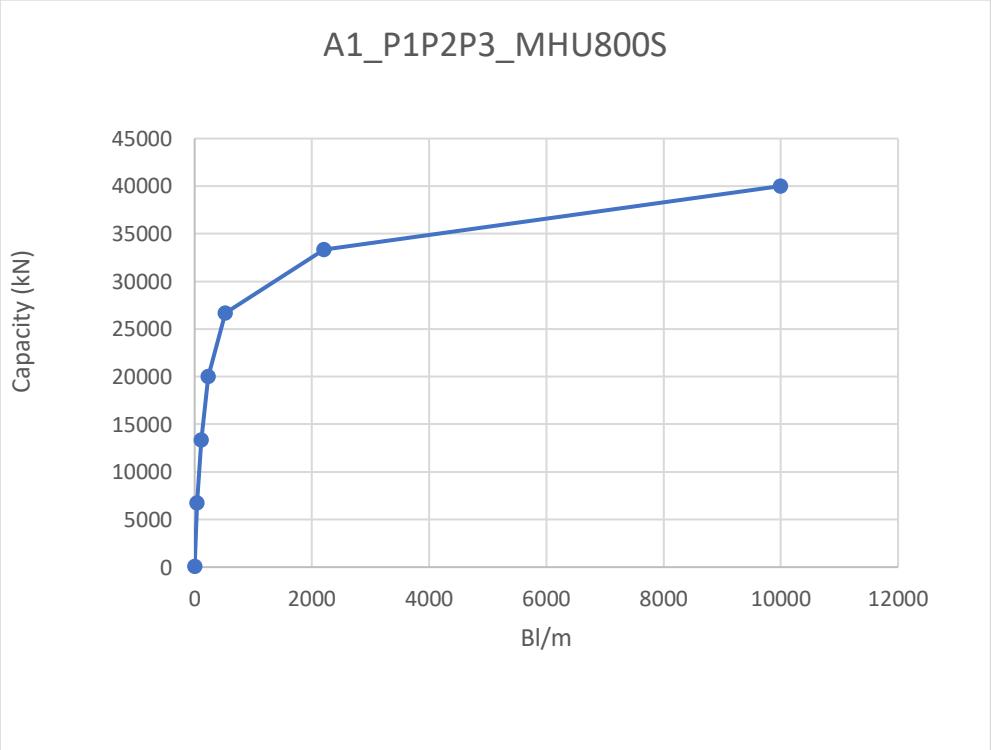

Figure 44 Capacity vs blow count for second penetration step

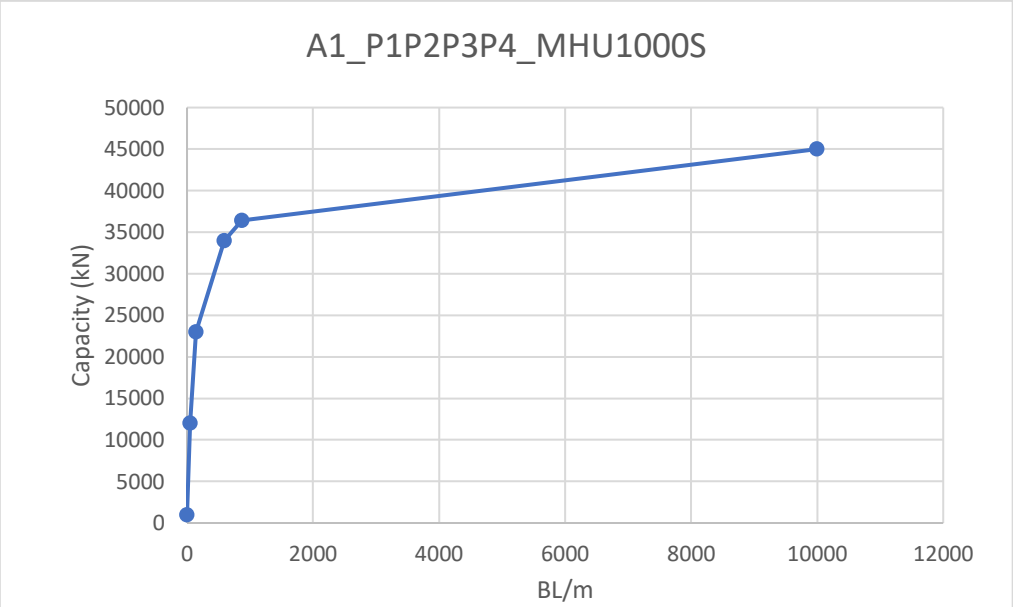

Figure 45 Capacity vs blow count for the last penetration step

Then, fixed the real blow counts (obtained by the monitoring system), for each blow count, the ultimate capacity was calculated with an interpolation and the values are shown in Table 9.

Table 9 Interpolated capacity value from monitoring blow counts

Depth (m)	Blow counts (bl/m)	Capacity (MN)	Depth (m)	Blow counts (bl/m)	Capacity (MN)
14.75	76	4.75	79.00	64	9.07
15.00	68	4.51	79.25	64	9.07
15.25	64	4.39	79.50	60	8.70
15.50	80	4.88	79.75	64	9.07
15.75	40	3.66	80.00	68	9.45
16.00	12	1.35	80.25	68	9.45
17.00	4	0.48	80.50	68	9.45
17.25	24	2.66	80.75	68	9.45
17.50	44	3.78	81.00	68	9.45
24.75	0	9.99	81.25	72	9.83
25.00	40	3.66	81.50	68	9.45
25.25	52	4.02	81.75	68	9.45
25.50	16	1.79	82.00	68	9.45
29.75	0	9.99	82.25	68	9.45
30.00	16	1.79	82.50	76	10.21
30.25	16	1.79	82.75	72	9.83
30.50	20	2.22	83.00	60	8.70

Depth (m)	Blow counts (bl/m)	Capacity (MN)	Depth (m)	Blow counts (bl/m)	Capacity (MN)
30.75	16	1.79	83.25	72	9.83
31.00	16	1.79	83.50	64	9.07
31.25	16	1.79	83.75	76	10.21
31.50	16	1.79	84.00	60	8.70
31.75	12	1.35	84.25	68	9.45
32.50	8	0.92	84.50	76	10.21
32.75	40	3.66	84.75	64	9.07
33.00	84	5.00	85.00	60	8.70
34.50	4	0.48	85.25	64	9.07
35.00	12	1.35	85.50	68	9.45
35.25	16	1.79	85.75	80	10.55
35.50	20	2.22	86.00	120	13.94
35.75	24	2.66	86.25	140	15.00
36.00	16	1.79	86.50	80	10.59
36.25	28	3.09	86.75	72	9.83
36.50	20	2.22	87.00	60	8.70
36.75	20	2.22	87.25	56	8.32
37.00	24	2.66	87.50	60	8.70
37.25	24	2.66	87.75	60	8.70
37.50	24	2.66	88.00	60	8.70
37.75	28	3.09	88.25	60	8.70
38.00	28	3.09	88.50	64	9.07
38.25	32	3.42	88.75	64	9.07
38.50	32	3.42	89.00	60	8.70
38.75	32	3.42	89.25	60	8.70
39.00	36	3.54	89.50	64	9.07
39.25	40	3.66	89.75	68	9.45
39.50	40	3.66	90.00	64	9.07
39.75	44	3.78	90.25	64	9.07
40.00	44	3.78	90.50	64	9.07
40.25	44	3.78	90.75	64	9.07
40.50	56	4.15	91.00	60	8.70
40.75	52	4.02	91.25	64	9.07
41.00	52	4.0	91.50	64	9.07
41.25	56	4.15	91.75	60	8.70
41.50	68	4.51	92.00	56	8.32
41.75	64	4.39	92.25	60	8.70
42.00	48	3.90	92.50	64	9.07
42.25	64	4.39	92.75	64	9.07
42.50	64	4.39	93.00	72	9.83

Depth (m)	Blow counts (bl/m)	Capacity (MN)	Depth (m)	Blow counts (bl/m)	Capacity (MN)
42.75	148	15.46	93.25	68	9.45
43.00	124	14.15	93.50	68	9.45
43.25	140	15.00	93.75	80	10.59
43.50	144	15.22	94.00	64	9.07
43.75	164	16.28	94.25	84	10.97
44.00	104	12.87	94.26	84	10.97
44.25	108	13.24	94.27	84	10.97
44.50	124	14.15	94.29	84	10.97
44.75	124	14.15	94.31	84	10.97
45.00	116	13.72	94.50	212	24.66
45.25	104	12.87	94.75	144	23.01
45.50	84	10.97	95.00	184	23.98
45.75	80	10.59	95.25	232	25.15
46.00	68	9.45	95.50	140	22.60
46.25	64	9.07	95.75	140	22.60
46.50	52	7.94	96.00	120	20.36
46.75	60	8.70	96.25	116	19.91
47.00	44	7.18	96.50	120	20.36
47.25	40	6.80	96.75	136	22.15
47.50	48	7.56	97.00	104	18.56
47.75	56	8.32	97.25	104	18.56
48.00	60	8.70	97.50	124	20.81
48.25	56	8.32	97.75	128	21.26
48.50	64	9.07	98.00	120	20.36
48.75	56	8.32	98.25	108	19.01
49.00	56	8.32	98.50	120	20.36
49.25	64	9.07	98.75	108	19.01
49.50	64	9.07	99.00	108	19.01
49.75	64	9.07	99.25	112	19.46
50.00	56	8.32	99.50	84	16.32
50.25	60	8.70	99.75	148	23.13
50.50	56	8.32	100.00	112	19.46
50.75	60	8.70	100.25	96	17.66
51.00	64	9.07	100.50	116	19.91
51.25	64	9.07	100.75	128	21.26
51.50	68	9.45	101.00	104	18.56
51.75	60	8.70	101.25	108	19.01
52.00	56	8.32	101.50	152	23.20
52.25	60	8.70	101.75	128	21.26
52.50	76	10.21	102.00	116	19.91

Depth (m)	Blow counts (bl/m)	Capacity (MN)	Depth (m)	Blow counts (bl/m)	Capacity (MN)
52.75	72	9.83	102.25	116	19.91
53.00	64	9.07	102.50	124	20.81
53.25	72	9.83	102.75	108	19.01
53.50	64	9.07	103.00	112	19.46
53.75	68	9.45	103.25	112	19.46
54.00	64	9.07	103.50	108	19.01
54.25	68	9.45	103.75	124	20.81
54.50	72	9.83	104.00	112	19.46
54.75	72	9.83	104.25	108	19.015
55.00	72	9.83	104.50	100	18.11
55.25	64	9.07	104.75	108	19.01
55.50	72	9.83	105.00	100	18.11
55.75	72	9.83	105.25	104	18.56
56.00	80	10.59	105.50	104	18.56
56.25	64	9.07	105.75	112	19.46
56.50	64	9.07	106.00	108	19.01
56.75	76	10.21	106.25	112	19.46
57.00	72	9.83	106.50	112	19.46
57.25	136	14.79	106.75	104	18.56
57.50	68	9.45	107.00	84	16.32
57.75	40	6.80	107.25	104	18.56
58.00	36	6.19	107.50	100	18.11
58.25	64	9.07	107.75	104	18.56
58.50	64	9.07	108.00	104	18.56
58.75	80	10.59	108.25	108	19.01
59.00	84	10.97	108.50	100	18.11
59.25	68	9.45	108.75	108	19.01
59.50	52	7.94	109.00	92	17.21
59.75	56	8.32	109.25	92	17.21
60.00	56	8.32	109.50	160	23.40
60.25	56	8.32	109.75	112	19.46
60.50	64	9.07	110.00	112	19.46
60.75	68	9.45	110.25	116	19.91
61.00	68	9.45	110.50	116	19.91
61.25	64	9.03	110.75	132	21.70
61.50	56	8.32	111.00	120	20.36
61.75	56	8.32	111.25	116	19.91
62.00	60	8.70	111.50	96	17.66
62.25	56	8.32	111.75	108	19.01
62.50	52	7.94	112.00	140	22.60

Depth (m)	Blow counts (bl/m)	Capacity (MN)	Depth (m)	Blow counts (bl/m)	Capacity (MN)
62.75	56	8.32	112.25	116	19.91
63.00	56	8.32	112.50	116	19.91
63.25	56	8.32	112.75	128	21.26
63.50	60	8.70	113.00	116	19.91
63.75	56	8.32	113.25	100	18.11
64.00	52	7.94	113.50	104	18.56
64.25	56	8.32	113.75	116	19.91
64.50	56	8.32	114.00	124	20.81
64.75	52	7.94	114.25	120	20.36
65.00	64	9.07	114.50	124	20.81
65.25	60	8.70	114.75	104	18.56
65.50	60	8.70	115.00	116	19.91
65.75	64	9.07	115.25	136	22.15
66.00	60	8.70	115.50	124	20.81
66.25	68	9.45	115.75	116	19.91
66.50	64	9.07	116.00	112	19.46
66.75	68	9.45	116.25	120	20.36
67.00	64	9.07	116.50	140	22.60
67.25	64	9.07	116.75	140	22.60
67.50	68	9.45	117.00	120	20.36
67.75	76	10.21	117.25	140	22.60
68.00	72	9.83	117.50	140	22.60
68.25	88	11.35	117.75	128	21.26
68.50	76	10.21	118.00	128	21.26
68.75	68	9.45	118.25	132	21.70
69.00	64	9.07	118.50	132	21.70
69.25	64	9.07	118.75	136	22.15
69.50	64	9.07	119.00	136	22.15
69.75	64	9.07	119.25	140	22.60
70.00	64	9.07	119.50	132	21.70
70.25	68	9.45	119.75	132	21.70
70.50	64	9.07	120.00	132	21.70
70.75	76	10.21	120.25	132	21.70
71.00	68	9.45	120.50	132	21.70
71.25	76	10.21	120.75	132	21.70
71.50	68	9.45	121.00	132	21.70
71.75	84	10.97	121.25	132	21.70
72.00	80	10.59	121.50	140	22.60
72.25	80	10.59	121.75	136	22.15
72.50	84	10.97	122.00	156	23.30

Depth (m)	Blow counts (bl/m)	Capacity (MN)	Depth (m)	Blow counts (bl/m)	Capacity (MN)
72.75	80	10.59	122.25	136	22.15
73.00	72	9.83	122.50	120	20.36
73.25	80	10.59	122.75	112	19.46
73.50	76	10.21	123.00	112	19.46
73.75	84	10.97	123.25	116	19.91
74.00	80	10.59	123.50	144	23.01
74.25	84	10.97	123.51	144	23.01
74.50	84	10.97	123.51	144	23.01
74.75	80	10.59	123.52	144	23.01
75.00	64	9.07	123.53	144	23.01
75.25	112	13.51	123.53	144	23.01
75.50	32	5.51	123.54	144	23.01
75.75	72	9.81	123.55	144	23.01
76.00	56	8.32	123.56	144	23.01
76.25	68	9.45	123.56	144	23.01
76.50	60	8.70	123.57	144	23.01
76.75	64	9.07	123.58	144	23.01
77.00	68	9.45	123.58	144	23.01
77.25	68	9.45	123.59	144	23.01
77.50	56	8.32	123.60	144	23.01
77.75	60	8.70	123.60	144	23.01
78.00	64	9.07	123.61	144	23.01
78.25	60	8.70	123.62	144	23.01
78.50	56	8.32	123.63	144	23.01
78.75	72	9.83			

The graph with monitoring blow counts vs depth is shown below with the strata description from the borehole results.

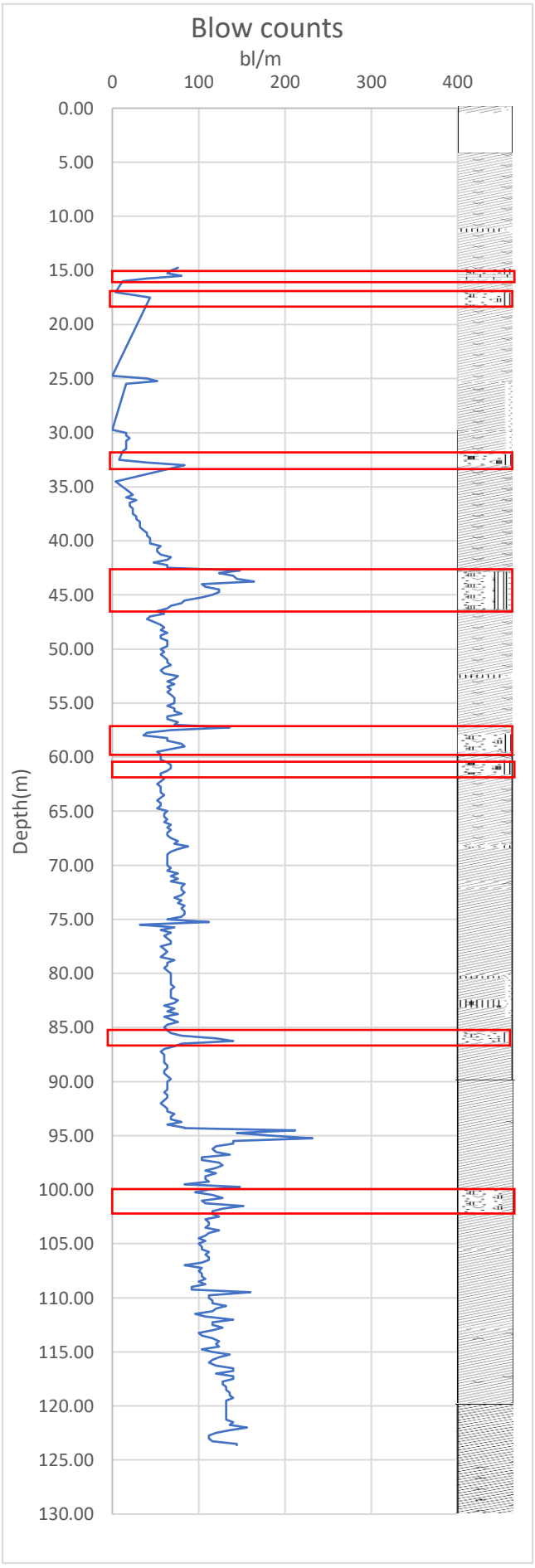

STRATA DESCRIPTION

From 0.00 m to 0.60 m - very soft sandy Clay

From 0.00 m to 4.30 m - Light greenish grey silty carbonate fine to medium SAND

From 4.30 m to 43.00 m - Firm to very stiff greenish grey carbonate CLAY

From 11.30 m to 11.60 m - greenish grey sandy carbonate Silt.

From 15.00m to 15.50m – moderately cemented light grey silty siliceous carbonate fine to medium SAND

From 15.50m to 16.00- moderately weak highly weathered light grey siliceous calcarenite

From 17.20 m to 18.50m- cemented silty sand

From 25.50 m to 27.00 m – with sand

From 32.00 m to 33.00 m – cemented silty sand.

From 43.00 m to 46.50 m - Moderately to well cemented light greenish grey silty carbonate SAND

From 46.50 m to 130.10 m - Very stiff to very hard greenish grey to brown carbonate CLAY

From 57.00 m to 59.60 m - slightly to moderately cemented silty Sand

From 82.60 m to 83.30 m - slightly to moderately cemented sandy Silt

From 85.60 m to 86.50 m - slightly cemented light brownish grey to light greenish grey silty carbonate Sand

From 97.70 m to 98.50 m - with pockets of sand

From 105.65 m to 113.00 m - with partings of sand

From 121.20 m to 122.00 m – with partings of sand

At 130.10 m - End of Borehole

Figure 46 Blow counts vs depth with strata description.

The rectangles in red identify the sand layers.

The interpolated capacity obtained from monitoring blow counts is shown in the figure below.

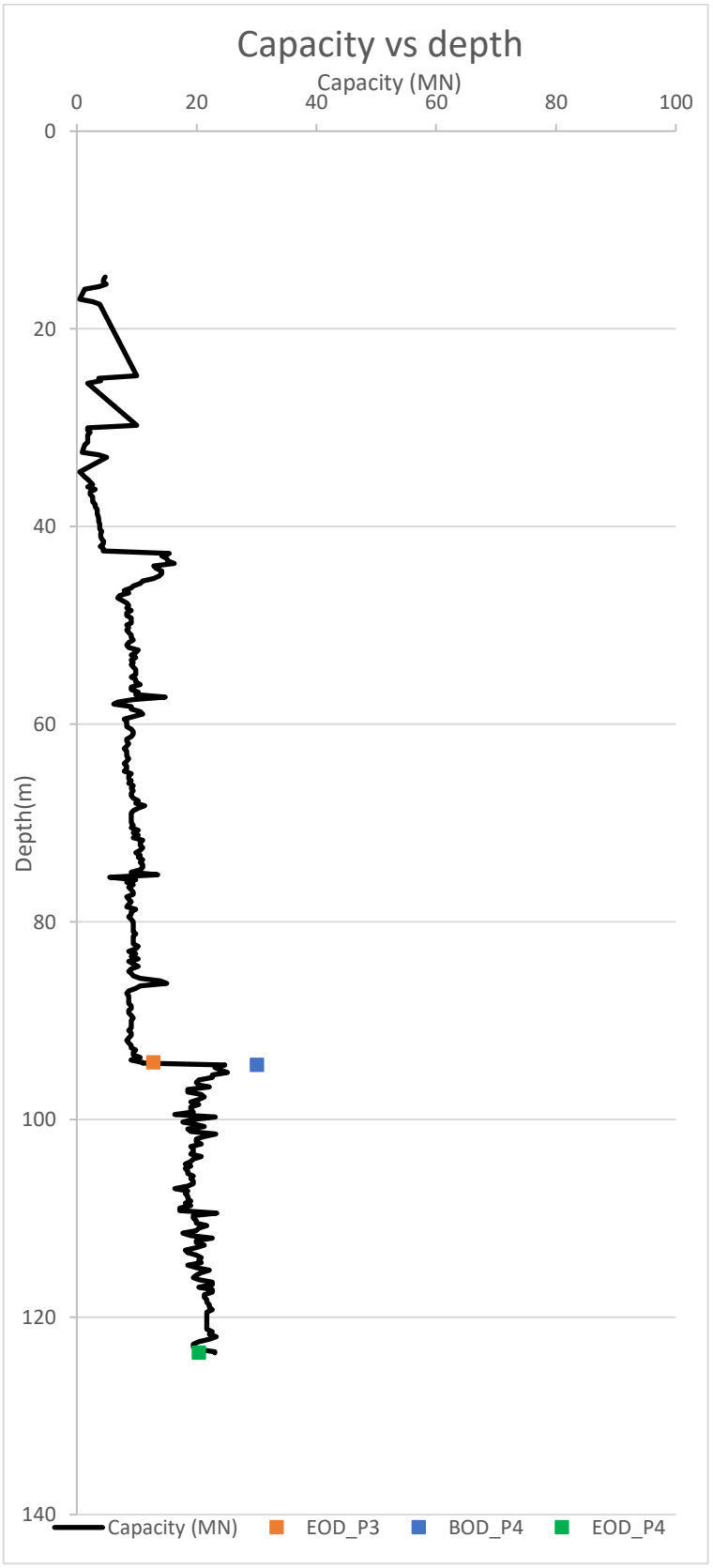

Figure 47 Interpolated capacity vs depth

The main result is that the back calculated capacity matches well the measured capacity by Fugro (see the two points, EOD_P3 in orange and EOD in green at target penetration).

Instead, after a set-up time for the last add-on (BOD_P4; the blue point in the figure) the capacity interpolated from blow counts does not match the capacity monitored by Fugro because in this first analysis the damping shaft equal to 0.7 s/m does not represent properly the restart condition but consider the continuous driving, without interruption.

For this reason, the analysis was repeated considering a damping shaft equal to 0.4 s/m as recommended by Delimi and Clavaud for restart of driving [1]. The output is the same and it was compared to the first results (damping shaft 0.7 s/m).

Both values of capacity, at continuous driving and at restart were shown in the figure below.

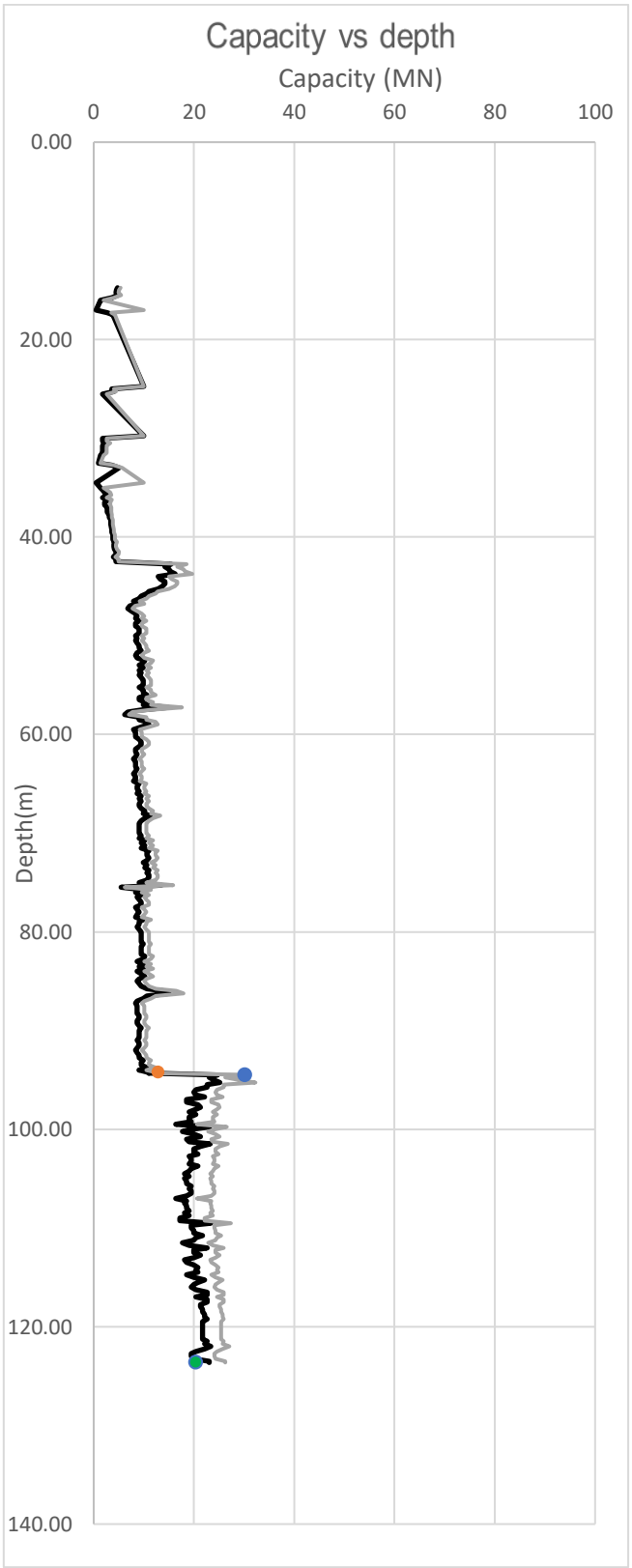

Figure 48 Capacity vs depth considering different damping values

In this case of restart of driving (Figure 48), the capacity at restart is matched by the interpolated value.

The interpolated capacity trends were compared with those obtained from CAPWAP analysis in the figure below.

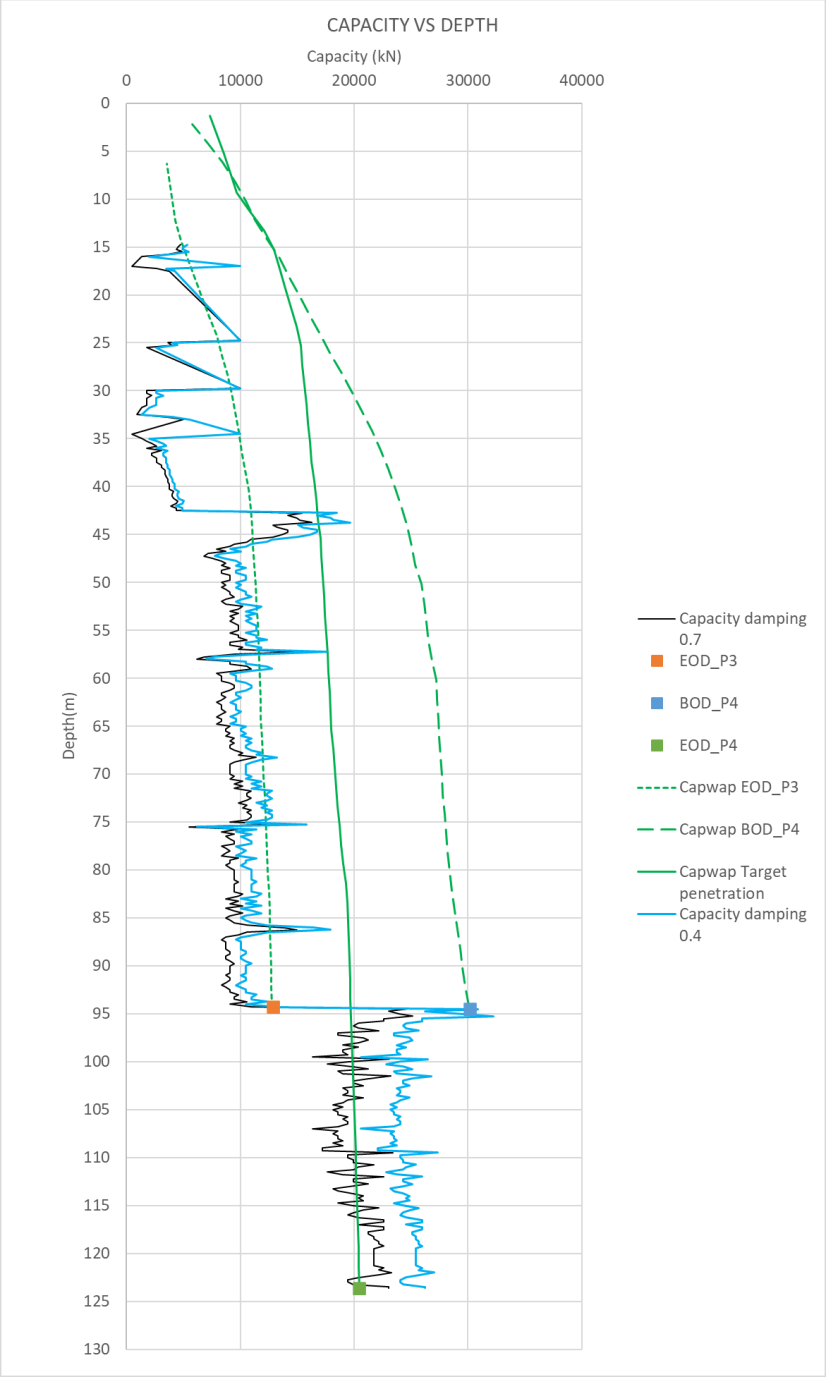

Figure 49 Comparison between continuous capacity and restart capacity

The back calculated capacity from measured blow counts produces a good match with the CAPWAP trend capacity. The continuous driving methods underestimate the capacity at restart, so both analyses are necessary in case of predictions. At 42 m and 94 m it can be observed a higher capacity due to the welding process (set-up effect). For the restart condition, soil appears to be still degraded, but the capacity profile is greater than continuous driving curve.

Calcareous clays, encountered offshore, are characterized by severe friction degradation during driving (low blow counts) and a strong and rapid increase in driving resistance during delays. The selection of hammer for pile installation is governed by the set-up effect since it may lead to premature refusal of pile. The restart analysis (using a lower damping factor, 0.4 s/m) is useful to represent the gain of resistance during driving interruptions. It follows the trends obtained by CAPWAP analysis after a set-up time.

The same considerations and analyses were carried out for all the 6 jacket piles. Below a histogram regarding the EOD for each pile obtained from the two analyses (damping 0.7 s/m and 0.4 s/m) is reported and it was compared with that measured by Fugro monitoring.

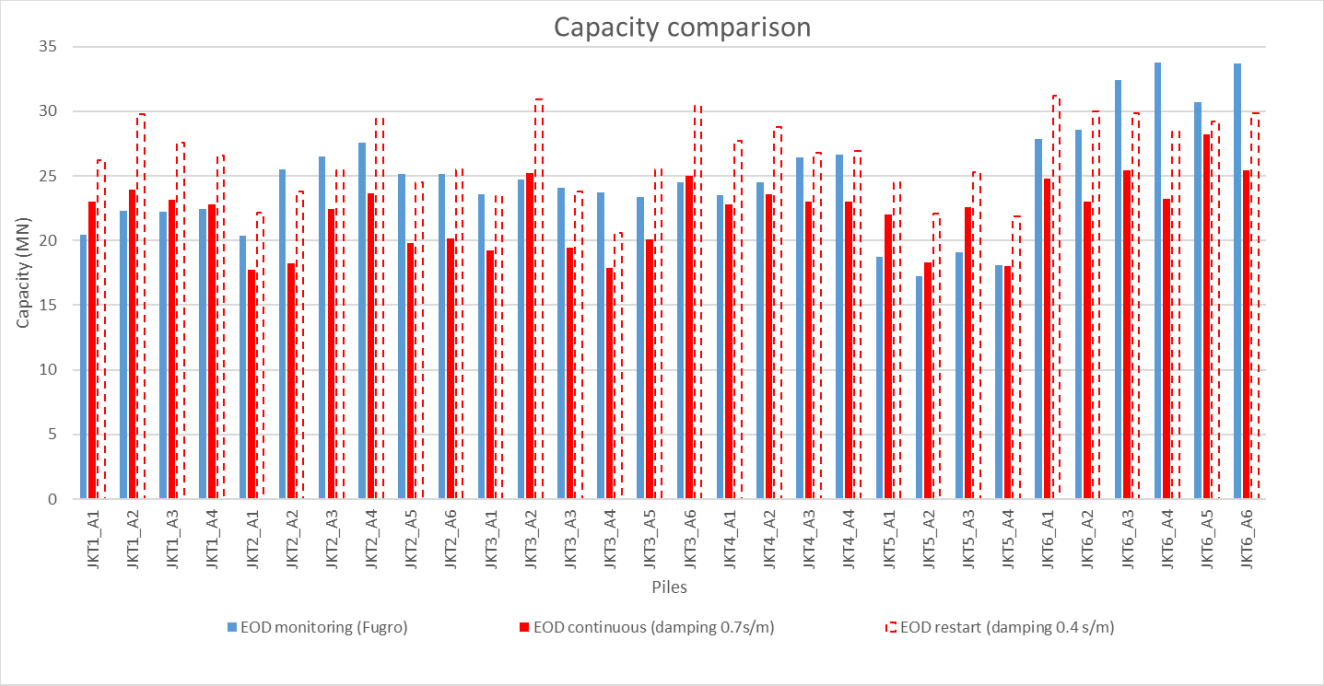

Figure 50 Capacity comparison between monitoring value (by Fugro) and calculated value

From the comparison between monitored values and predictions of the analysis, a good match was found using a damping factor value from 0.4 s/m to 0.7 s/m. This is in accordance with Delimi's suggestion [1].

5.2 RESULTS OF DRIVIBILITY ANALYSIS

After accepting hammer, driving system, pile and soil input the drivability graph shows as a main result the ultimate capacity (kN), blow count (bl/m), compressive and tensile strength, enthru enery and stroke versus depth.

Each step of pile penetration was analysed separately:

1. lead section + 1st add on + hammer
2. lead section + 1st add on + 2nd add on + hammer
3. lead section + 1st add on + 2nd add on + 3rd add on + hammer

Then for each analysis the main outputs were obtained.

For pile A1, after the analysis considering a gain loss factor and a set-up factor equal to 1, details about the outputs numerical value are provided as shown in Table 10.

Table 10 Numerical output detail

Depth	Ultimate Capacity	Friction	End Bearing	Blow Count	Compression Stresses	Tension Stresses	Stroke	Energy
m	kN	kN	kN	bl/m	MPa	MPa	m	kJ
1	18.1	2.8	15.3	0	0	0	0.2	0
3	124.6	26.4	98.2	0	0	0	0.2	0
5	504.6	86.5	418	0	0	0	0.2	0
7	903.5	240.4	663.1	0	0	0	0.2	0
9	1152.5	443.4	709.2	0	0	0	0.2	0
11	1439.1	685.2	753.9	0	0	0	0.2	0
13	1754.7	957.4	797.3	0	0	0	0.2	0
15	2155	1260.6	894.4	0	0	0	0.2	0
17	2570.4	1606.5	963.9	0	0	0	0.2	0
19	2923.9	1972.5	951.4	0	0	0	0.2	0
21	3291.2	2352.3	938.9	0	0	0	0.2	0
23	3671.6	2745.3	926.4	33.5	87.065	-61.236	0.2	99.6
25	4078.1	3150.9	927.2	35.6	87.033	-58.964	0.2	97.8

Depth	Ultimate Capacity	Friction	End Bearing	Blow Count	Compressio n Stresses	Tension Stresses	Stroke	Energy
m	kN	kN	kN	bl/m	MPa	MPa	m	kJ
27	4569.8	3576.2	993.6	51.2	87.009	-55.883	0.2	93.7
29	5150.2	4039.9	1110.4	62.6	86.985	-52.087	0.2	91.1
31	5767.1	4543.6	1223.5	82.3	86.954	-48.183	0.2	87.4
33	6418.9	5085.9	1333	93.4	86.917	-44.221	0.2	85.5
35	7104.2	5665.4	1438.8	107	86.876	-40.24	0.2	85.3
37	7821.4	6280.6	1540.9	124	86.826	-36.321	0.2	84.6
39	8569.4	6930.1	1639.3	145.8	86.771	-32.471	0.2	84.3
41	9346.6	7612.6	1734	173.5	86.708	-30.06	0.2	83.8
42.2	10079	8050.2	2028.8	207.5	86.669	-27.547	0.2	83.5
42.5	10401.9	8124.9	2277	226.1	86.656	-25.717	0.2	83.4
42.5	10401.9	8125.1	2276.8	50.7	167.188	-64.893	0.88	348.1
43	11018.5	8245.2	2773.3	55.7	167.188	-58.983	0.88	347.9
45	12259.7	8413.4	3846.3	66.8	167.188	-50.203	0.88	348.2
47	11515.3	8589.6	2925.7	58.9	167.188	-58.209	0.88	346.6
49	11197.8	9288.4	1909.4	53.9	167.189	-66.277	0.88	346.4
51	11955.6	10077.5	1878.1	58.2	167.188	-65.516	0.88	344.9
53	12716.4	10869.6	1846.8	62.6	167.188	-62.309	0.88	343.9
55	13479.3	11663.8	1815.5	67.2	167.188	-59.968	0.88	343.1
57	14243.6	12459.3	1784.3	71.7	167.188	-59.362	0.88	343
59	15318.6	13165.8	2152.8	79.6	167.188	-55.562	0.88	343.4
61	15786.9	13421.5	2365.4	83.6	167.188	-55.934	0.88	343.1
63	16281.6	14108.2	2173.4	86.1	167.189	-58.201	0.88	342.6
65	17002.7	14869.5	2133.2	91.4	167.188	-58.476	0.88	342.5
67	17709.6	15616.6	2093	97.4	167.188	-58.501	0.88	342.3
69	18402.3	16349.5	2052.8	103.9	167.189	-56.462	0.88	342.2
71	19080.8	17068.1	2012.6	110	167.188	-56.668	0.88	342
73	19745	17772.6	1972.4	114.9	167.188	-57.259	0.88	341.8
75	20395	18462.8	1932.2	118.2	167.188	-57.78	0.88	341.7
77	21030.9	19138.9	1892	121.6	167.188	-58.244	0.88	341.5
79	21652.5	19800.7	1851.8	125	167.188	-58.687	0.88	341.3
81	22558.4	20448.3	2110.1	131.8	167.188	-56.278	0.88	341.2
83	23443.5	21081.7	2361.8	138.6	167.188	-54.381	0.88	341
85	24009	21700.8	2308.2	141.4	167.188	-55.338	0.88	340.9
87	24560.4	22305.8	2254.6	144.2	167.188	-56.194	0.88	340.8
89	25278.6	22896.5	2382.1	149.6	167.188	-55.338	0.88	340.6
91	25978.3	23473	2505.3	155.1	167.188	-54.471	0.88	340.4
93	26478.1	24035.3	2442.7	157.8	167.188	-55.304	0.88	340.2
94.2	26763.8	24357.7	2406.1	159.3	167.188	-55.801	0.88	340.1
94.3	26807.4	24406.9	2400.5	159.5	167.188	-55.882	0.88	340.1
94.3	26807.4	24406.9	2400.5	84.8	241.487	-72.508	1.3	645.7

Depth	Ultimate Capacity	Friction	End Bearing	Blow Count	Compressio n Stresses	Tension Stresses	Stroke	Energy
m	kN	kN	kN	bl/m	MPa	MPa	m	kJ
95.3	27047.2	24677.9	2369.2	86	241.487	-72.997	1.3	645.7
96.3	27283.4	24945.4	2338	87.2	241.487	-73.627	1.3	645.7
97.3	27516	25209.3	2306.7	88.5	241.488	-74.252	1.3	645.7
98.3	27745.1	25469.7	2275.4	89.3	241.487	-74.871	1.3	645.7
99.3	27970.6	25726.5	2244.1	90.2	241.487	-75.479	1.3	645.7
100.3	28192.6	25979.7	2212.9	91	241.488	-76.097	1.3	645.7
101.3	28411.1	26229.5	2181.6	91.9	241.487	-76.695	1.3	645.7
102.3	28625.9	26475.6	2150.3	92.7	241.487	-77.235	1.3	645.7
103.3	28837.3	26718.2	2119.1	93.5	241.487	-77.778	1.3	645.7
104.3	29045.1	26957.3	2087.8	94.2	241.488	-78.374	1.3	645.7
105.3	29249.3	27192.8	2056.5	94.9	241.487	-78.965	1.3	645.7
106.3	29450	27424.7	2025.2	95.7	241.487	-79.538	1.3	645.7
107.3	29647.1	27653.1	1994	96.4	241.487	-80.09	1.3	645.7
108.3	29840.6	27877.9	1962.7	97	241.487	-80.607	1.3	645.7
109.3	30030.6	28099.2	1931.4	97.7	241.488	-81.156	1.3	645.7
110.3	30217.1	28317	1900.1	98.4	241.487	-81.684	1.3	645.7
111.3	30400	28531.1	1868.9	99	241.488	-82.265	1.3	645.7
112.3	30579.3	28741.7	1837.6	99.6	241.487	-82.876	1.3	645.7
113.3	30755.1	28948.8	1806.3	100.1	241.487	-83.463	1.3	645.7
114.3	30927.4	29152.3	1775.1	100.6	241.488	-84.079	1.3	645.7
115.3	31096.1	29352.3	1743.8	101.1	241.487	-84.71	1.3	645.7
116.3	31261.2	29548.7	1712.5	101.5	241.487	-85.346	1.3	645.7
117.3	31422.8	29741.5	1681.2	101.9	241.488	-85.998	1.3	645.7
118.3	31580.8	29930.8	1650	102.3	241.488	-86.681	1.3	645.7
119.3	31735.3	30116.6	1618.7	102.6	241.488	-87.358	1.3	645.7
120.3	31886.2	30298.8	1587.4	102.9	241.487	-88.011	1.3	645.7
121.3	32033.6	30477.4	1556.2	103.2	241.488	-88.639	1.3	645.7
122.3	32177.4	30652.5	1524.9	103.4	241.487	-89.254	1.3	645.7
123.3	32317.6	30824	1493.6	103.6	241.488	-89.869	1.3	645.7
123.6	32356.3	30871.4	1484.9	103.7	241.488	-90.044	1.3	645.7

In Figure 51, blow counts and hammer energy are plotted versus depth.

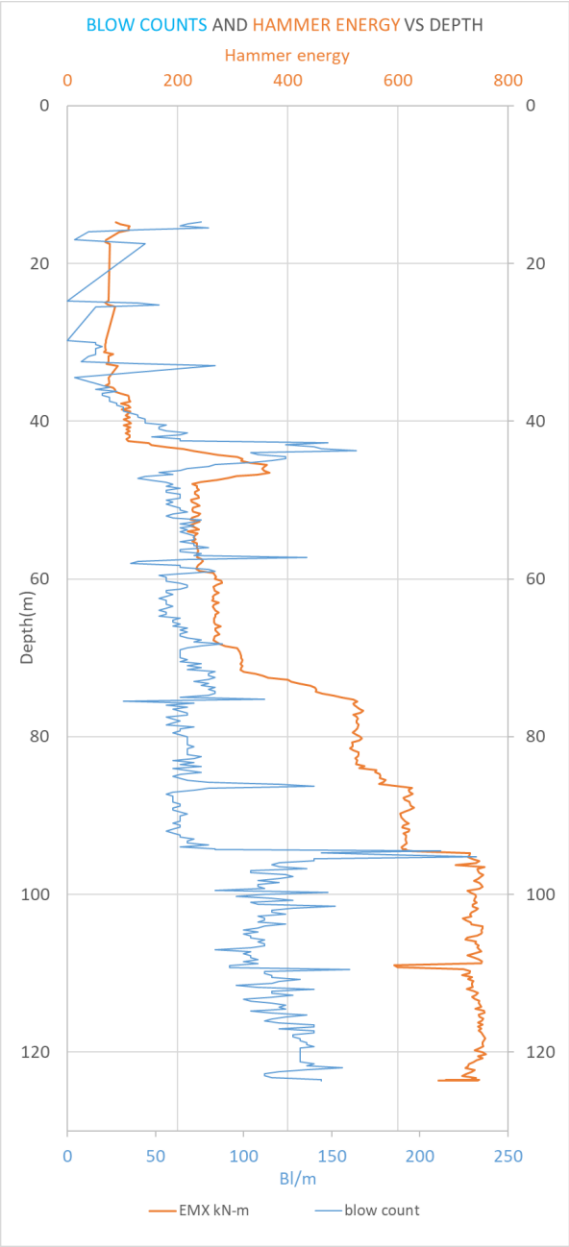

Figure 51 Blow count and hammer energy vs depth

The blue line represents the blow count measured by Fugro during the installation pile.

The field blow counts during final driving are constant with depth with little scatter because of variations in soil conditions and hammer efficiency.

The pile driving curves clearly highlighted the friction degradation effect with blow counts becoming constant with pile penetration for long driving sequences.

The figure above implicitly takes into account the set-up. The high blow count monitored at 42 m and 94 m considers the welding time and the related gain of resistance.

The figure below compares the predicted and the monitored blow counts.

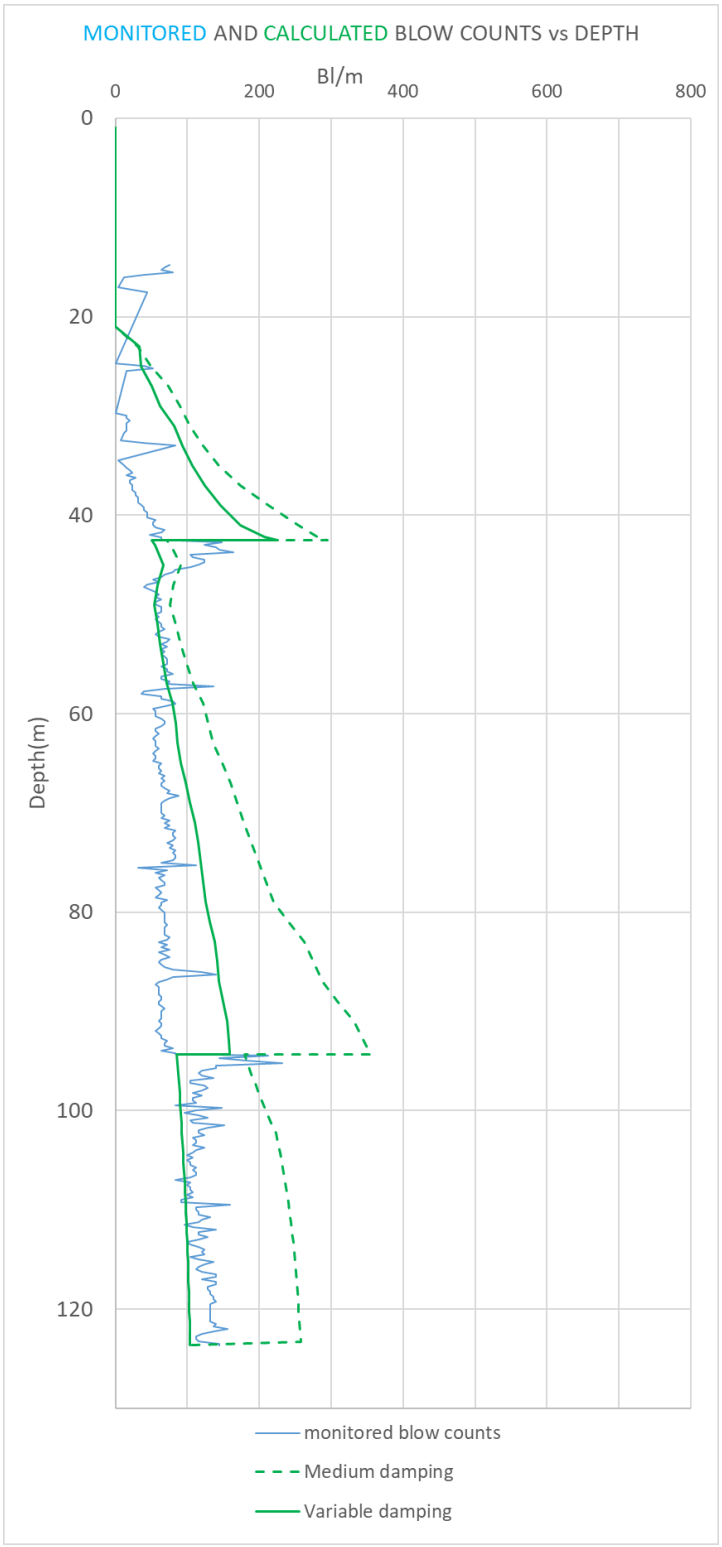

Figure 52 Output of drivability analysis in comparison with measured blow counts

The scatters in the predicted blow count (green curves) are due to the hammer energy variation. At the welds, in particular at 42m the blow counts curve has a big reduction because the hammer striking energy changes: we pass from a medium energy of 10% to 48% (as is show in the Figure 51 with orange line).

In the second case, at a depth of 94m, the lower blow counts are due to the hammer changing: we pass from a MENCK 800S to a MENCK 1000S, characterized by a higher efficiency.

Our predicted range in blow counts is in good agreement with the scatter observed in the field.

The green continuous line represents the blow count considering a variable damping along depth, reported in Table 11:

Table 11 Variable soil damping

Depth (m)	Skin damping (s/m)	Soil type	Depth (m)	Skin damping (s/m)	Soil type	Depth (m)	Skin damping (s/m)	Soil type
0.10	0.36	CLAY	60.00	0.26	SAND	110.00	0.10	CLAY
2.00	0.26	SAND	62.00	0.16	CLAY	111.00	0.10	CLAY
4.00	0.26	SAND	64.00	0.16	CLAY	112.00	0.10	CLAY
6.00	0.23	CLAY	66.00	0.16	CLAY	113.00	0.10	CLAY
8.00	0.23	CLAY	68.00	0.16	CLAY	114.00	0.10	CLAY
10.00	0.23	CLAY	70.00	0.16	CLAY	115.00	0.10	CLAY
12.00	0.23	CLAY	72.00	0.16	CLAY	116.00	0.10	CLAY
14.00	0.23	CLAY	74.00	0.16	CLAY	117.00	0.10	CLAY
16.00	0.26	CLAY	76.00	0.16	CLAY	118.00	0.10	CLAY
18.00	0.20	CLAY	78.00	0.16	CLAY	119.00	0.10	CLAY
20.00	0.20	CLAY	80.00	0.16	CLAY	120.00	0.10	CLAY
22.00	0.20	CLAY	82.00	0.10	CLAY	121.00	0.10	CLAY
24.00	0.20	CLAY	84.00	0.10	CLAY	122.00	0.10	CLAY
26.00	0.20	CLAY	86.00	0.10	CLAY	123.00	0.10	CLAY
28.00	0.20	CLAY	88.00	0.10	CLAY	124.00	0.10	CLAY
30.00	0.20	CLAY	90.00	0.10	CLAY	125.00	0.10	CLAY
32.00	0.20	CLAY	92.00	0.10	CLAY	126.00	0.10	CLAY
34.00	0.20	CLAY	94.00	0.10	CLAY	127.00	0.10	CLAY
36.00	0.20	CLAY	96.00	0.10	CLAY	128.00	0.10	CLAY
38.00	0.20	CLAY	98.00	0.10	CLAY	129.00	0.10	CLAY
40.00	0.20	CLAY	100.00	0.10	CLAY	130.00	0.10	CLAY
42.00	0.20	CLAY	101.00	0.10	CLAY	131.00	0.10	CLAY
44.00	0.26	SAND	102.00	0.10	CLAY	132.00	0.10	CLAY

Depth (m)	Skin damping (s/m)	Soil type	Depth (m)	Skin damping (s/m)	Soil type	Depth (m)	Skin damping (s/m)	Soil type
46.00	0.26	SAND	103.00	0.10	CLAY	133.00	0.10	CLAY
48.00	0.16	CLAY	104.00	0.10	CLAY	134.00	0.10	CLAY
50.00	0.16	CLAY	105.00	0.10	CLAY	135.00	0.10	CLAY
52.00	0.16	CLAY	106.00	0.10	CLAY	136.00	0.10	CLAY
54.00	0.16	CLAY	107.00	0.10	CLAY	137.00	0.10	CLAY
56.00	0.16	CLAY	108.00	0.10	CLAY	138.00	0.10	CLAY
58.00	0.16	CLAY	109.00	0.10	CLAY	139.00	0.10	CLAY
						140.00	0.10	CLAY

The green dotted line represents the blow count considering a constant damping along depth equal to 0.56 s/m for both soil, clay and sand.

It can be seen that lower and variable damping factor, at the same unit shaft resistance and unit toe resistance, produces a better match between monitored and calculated blow count.

5.3 INFLUENCE OF SET-UP

The set-up factor and the set-up time for the four jackets are resumed in the following table.

Table 12 capacity considering the restart and the set-up time

Jacket	Pile		Capacity		Set-up time	Set-up factor	bl/0.25m	
			EOD_P3	BOD_P4	hours	-	EOD_P3	BOD_P4
RT2	A1	JKT1_A1	12.87	30.18	89.5	2.34	16	52
	A2	JKT1_A2	12.9	20.73	46.8	1.60	17	21
	B1	JKT1_A3	12.72	24.7	42.6	1.94	17	39
	B2	JKT1_A4	12.94	30.16	81.4	2.33	15	41
RP7S	A1	JKT2_A1	9.84	26.38	48.6	2.68	17	80
	A2	JKT2_A2	10.89	27.65	52.2	2.53	12	58
	B1	JKT2_A3	12.12	22.57	57	1.86	11	86
	B2	JKT2_A4	11.32	29.62	57.6	2.61	16	99
	C1	JKT2_A5	14.11	26.39	42.5	1.87	17	31
	C2	JKT2_A6	13.91	24.47	47.4	1.75	10	57
RP6S	A1	JKT3_A1	14.4	30.4	59.9	2.11	22	74
	A2	JKT3_A2	14	30.97	56.4	2.21	22	64
	B1	JKT3_A3	14.18	31.29	63.8	2.20	24	78
	B2	JKT3_A4	13.64	32.09	-	2.35	21	77
	C1	JKT3_A5	14.02	31.04	61.3	2.22	23	71
	C2	JKT3_A6	14.27	30.85	57.4	2.16	21	73
RP4N	A1	JKT4_A1	17.03	30.44	184.1	1.78	28	110
	A2	JKT4_A2	18.26	31.06	214.6	1.701	27	160

Jacket	Pile		Capacity		Set-up time	Set-up factor	bl/0.25m	
			EOD_P3	BOD_P4	hours	-	EOD_P3	BOD_P4
	B1	JKT4_A3	18.32	30.29	182.4	1.65	28	162
	B2	JKT4_A4	18.57	28.89	221.4	1.55	32	150

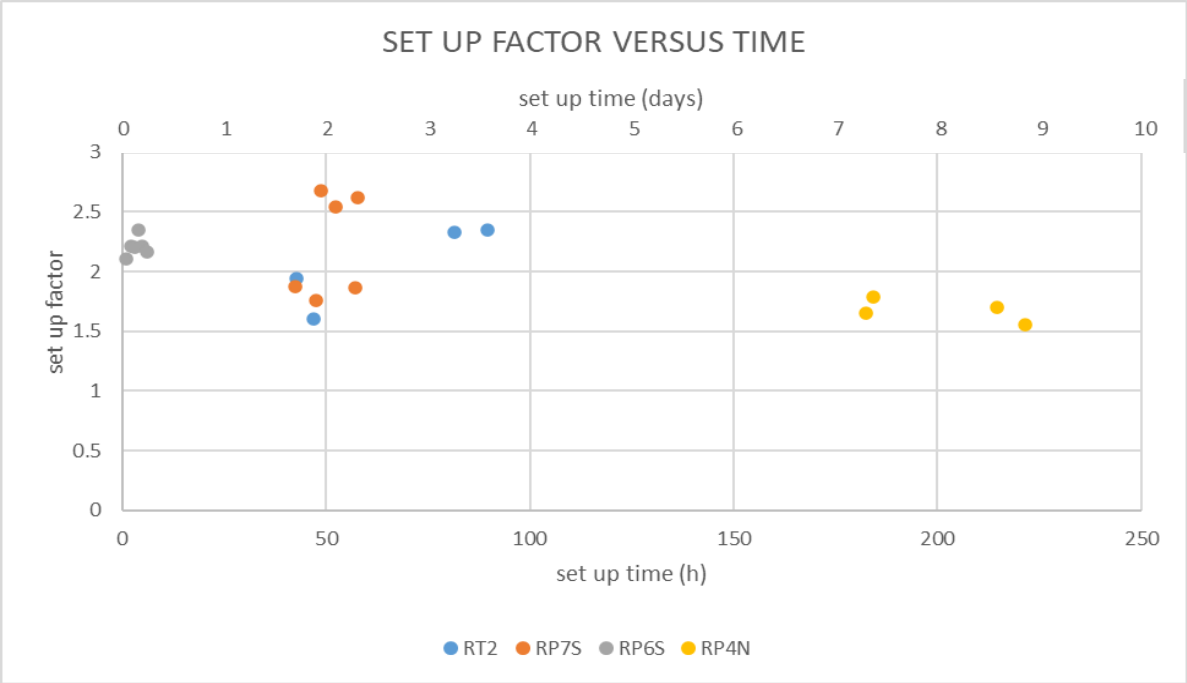

Figure 53 Set-up factor versus set-up time

The most of the set-up effect, or restoration of the clay strength, is obtained after only 40-50 hours of delay in pile driving. For this reason, it was recommended the full set-up resistance when interruptions in pile driving are planned, irrespective of the expected time of interruption.

The jacket RP4N is an exception: the set-up factor is lower than what might be expected after 10 days.

The set-up effect in clays suggests that the loss of shaft capacity is only temporary and that the soil may recover its initial strength properties.

In the figure below is reported with yellow histogram the soil resistance to driving without stopping and in green the SRD after a time interruption for welding the last add on element.

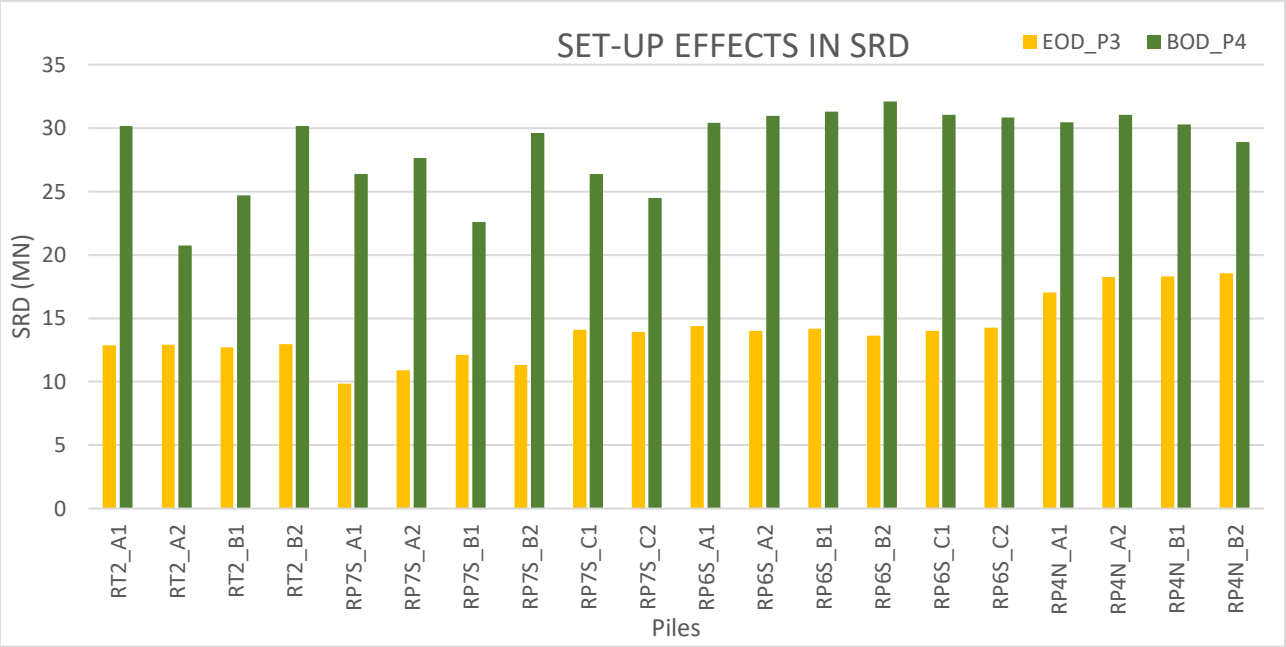

Figure 54 Set-up effect in SRD

The percentage of mobilized resistance at begin of driving of P4 and the resistance at end of driving of P3 versus set-up time is shown in the figure below.

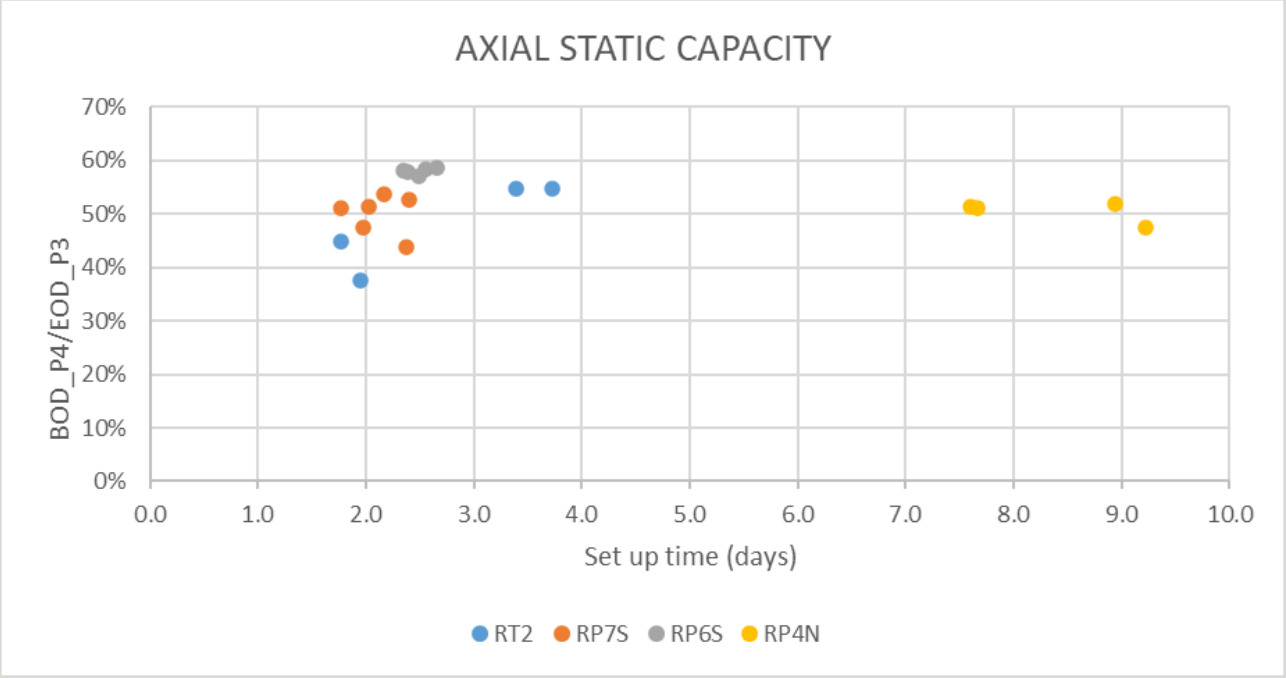

Figure 55 Percentage of begin of driving resistance after restart/axial static capacity at the same depth vs set-up time.

After the first two-three days the calcareous clay will have around the 40% - 60% of its static resistance during driving (axial static capacity). Only for one jacket (RP4N) the time needed to recover the 50% of the axial capacity is around eight-ten days.

Higher strength means higher blow counts which can lead to premature refusal of piles.

The figure below shows the comparison between recorded blow counts before and after restart.

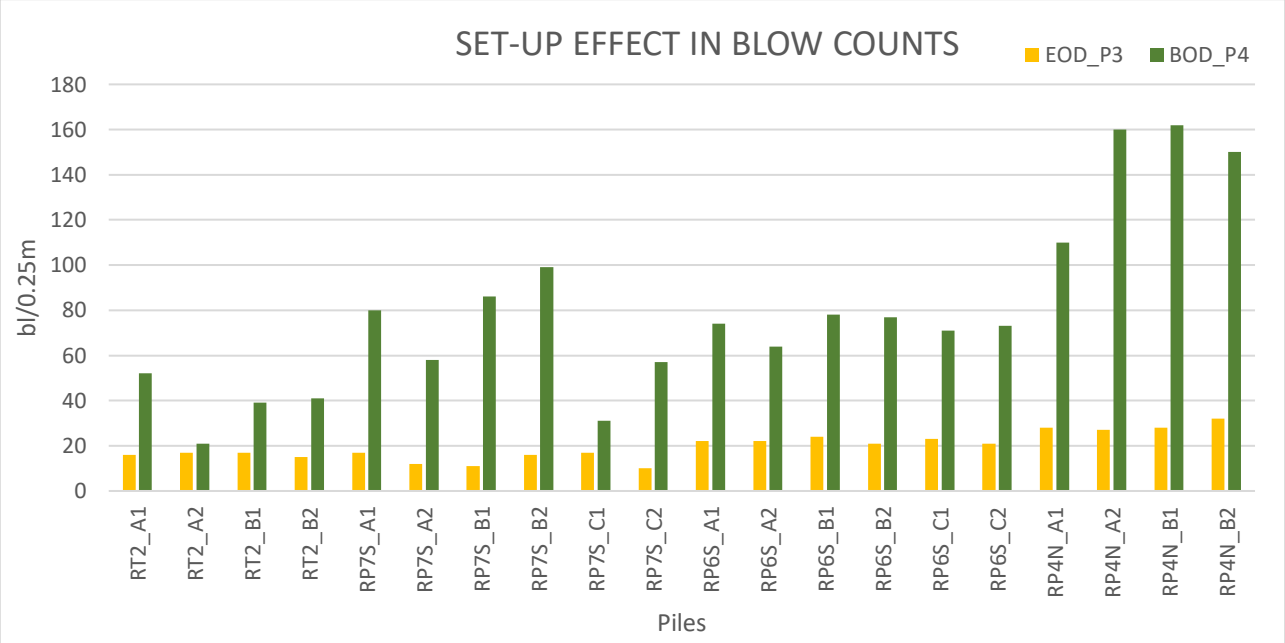

Figure 56 Set-up effects in blow counts

So, the set-up can be seen as a phenomenon useful to recover the soil strength. This information is useful in the project phases to decide the type of hammer to be used. We must have to consider that calcareous clay, after a set-up time, can reach the 60% of its static resistance; so, it must be chosen an hammer and an hammer energy able to drive the pile in this soil condition. This is the reason why, at restart, after the welding, it was necessary to change the hammer with one more efficient or the hammer energy (it must be higher than the previous one).

5.4 RESULT OF CPT METHOD

The method proposed by Alm & Hamre led to the calculation of SRD from CPT results.

The unit skin friction during driving f_d, the residual unit skin friction (f_{sres}) and the initial unit skin friction (f_{si}) were calculated with formulations reported in Section 2.8.3 and values were showed in the following table.

Table 13 Summary of CPT method results

z	Ground Behaviour	qt	fsi_CPT	fsi	f_s_res	f_d
m		MPa	kPa	kPa	kPa	kPa
0	Cohesive	0	0	0	0	0
1	Frictional	2.27	33.1	5.79	1.15	1.15
2	Frictional	4.19	25.8	11.70	2.34	2.34
3	Frictional	6.95	6.4	20.44	4.08	4.08
4	Frictional	6.95	6.4	21.21	4.24	4.24
5	Cohesive	0.72	15.6	15.6	2.76	2.77
6	Cohesive	0.66	14.1	14.1	2.57	2.61
7	Cohesive	0.77	16.2	16.2	2.97	3.02
8	Cohesive	0.77	16.2	16.2	2.98	3.05
9	Cohesive	0.92	22.2	22.2	3.57	3.66
10	Cohesive	0.99	20.8	20.8	3.85	3.94
11	Cohesive	1.01	19.3	19.3	3.93	4.03
12	Cohesive	1.01	19.3	19.3	3.94	4.07
13	Cohesive	1.13	19	19	4.42	4.54
14	Cohesive	1.13	16.7	16.7	4.44	4.56
15	Cohesive	1.73	35.7	35.7	6.69	6.82
16	Frictional	6.69	208.9	52.76	10.55	10.55
17	Cohesive	2.60	31.2	31.2	9.92	9.96
18	Cohesive	7.22	213.4	213.4	25.33	25.34
19	Cohesive	1.45	26.7	26.7	5.68	5.97
20	Cohesive	1.45	26.7	26.7	5.68	6.03
21	Cohesive	1.39	30.3	30.3	5.48	5.98
22	Cohesive	1.41	30.9	30.9	5.53	6.10
23	Cohesive	1.45	33.2	33.2	5.81	6.44
24	Cohesive	1.48	33.2	33.2	5.82	6.52
25	Cohesive	1.76	32.3	32.3	6.91	7.43
26	Cohesive	2.09	37.1	37.1	8.17	8.66
27	Cohesive	2.09	37.1	37.1	8.18	8.73
28	Cohesive	1.68	37.4	37.4	6.62	7.59
29	Cohesive	2.02	52.1	52.1	7.91	9.03
30	Cohesive	2.01	37.7	37.7	7.87	8.72
31	Cohesive	2.01	37.7	37.7	7.88	8.81
32	Cohesive	1.80	24.8	24.8	7.07	7.80

z	Ground Behaviour	qt	fsi_CPT	fsi	f_s_res	f_d
m		MPa	kPa	kPa	kPa	kPa
33	Cohesive	22.51	332.7	332.7	71.56	71.56
34	Cohesive	2.74	70.2	70.2	10.69	12.12
35	Cohesive	2.74	70.2	70.2	10.70	12.27
36	Cohesive	2.62	44.2	44.2	10.26	11.31
37	Cohesive	2.69	50.9	50.9	10.53	11.84
38	Cohesive	2.81	61.5	61.5	11.01	12.67
39	Cohesive	2.81	61.5	61.5	11.02	12.82
40	Cohesive	3.02	81.7	81.7	11.83	14.23
41	Cohesive	2.99	83.1	83.1	11.73	14.43
42	Cohesive	3.13	90	90	12.27	15.22
43	Cohesive	3.13	90	90	12.28	15.47
44	Frictional	3.13	90	13.18	2.636	3.10
45	Frictional	34.60	94.2	145.88	29.17	29.18
46	Frictional	24.01	186.6	101.60	20.32	20.34
47	Cohesive	3.84	72.2	72.2	15.00	17.36
48	Cohesive	3.55	82	82	13.91	17.30
49	Cohesive	3.48	79.6	79.6	13.67	17.28
50	Cohesive	3.61	80.7	80.7	14.14	17.84
51	Cohesive	3.81	92.1	92.1	14.93	19.17
52	Cohesive	3.73	75.1	75.1	14.61	18.27
53	Cohesive	4.12	75.6	75.6	16.12	19.45
54	Cohesive	4.35	120	120	17.00	22.70
55	Cohesive	3.90	152.5	152.5	15.28	24.71
56	Cohesive	3.84	75.1	75.1	15.06	19.53
57	Cohesive	4.07	168.3	168.3	15.96	27.10
58	Cohesive	5.54	140.4	140.4	21.56	27.59
59	Frictional	25.77	659.2	112.80	22.56	22.72
60	Frictional	5.59	193.5	24.58	4.91	6.03
61	Frictional	8.76	400.2	38.56	7.71	8.65
62	Cohesive	4.89	74.5	74.5	19.13	23.47
63	Cohesive	5.00	57.5	57.5	19.55	22.62
64	Cohesive	4.42	77.8	77.8	17.36	23.36
65	Cohesive	4.42	77.8	77.8	17.37	23.71
66	Cohesive	5.01	112.1	112.1	19.61	28.51
67	Cohesive	5.24	127.1	127.1	20.50	30.80
68	Cohesive	4.75	69.8	69.8	18.64	24.47
69	Cohesive	5.98	196.9	196.9	23.37	39.44
70	Cohesive	4.76	111.3	111.3	18.71	30.37
71	Cohesive	5.49	230.8	230.8	21.49	45.42
72	Cohesive	16.34	230.8	230.8	61.25	65.65
73	Cohesive	16.34	230.8	230.8	61.31	66.13

z	Ground Behaviour	qt	fsi_CPT	fsi	f_s_res	f_d
m		MPa	kPa	kPa	kPa	kPa
74	Cohesive	6.76	410.6	410.6	26.36	67.58
75	Cohesive	11.11	412	412	42.63	65.32
76	Cohesive	15.91	250	250	59.97	67.31
77	Cohesive	15.91	250	250	60.02	68.00
78	Cohesive	4.39	101.6	101.6	17.31	33.94
79	Cohesive	4.48	105.6	105.6	17.64	35.47
80	Cohesive	4.83	112	112	19.02	37.53
81	Cohesive	4.83	112	112	19.03	38.34
82	Cohesive	8.60	283.2	283.2	33.43	65.93
83	Cohesive	18.33	438.1	438.1	68.88	89.30
84	Cohesive	6.68	187.3	187.3	26.15	55.60
85	Cohesive	6.68	187.3	187.3	26.16	57.05
86	Cohesive	14.76	351.7	351.7	56.29	83.48
87	Cohesive	8.67	603.4	603.4	33.74	130.27
88	Cohesive	6.97	236.4	236.4	27.30	71.88
89	Cohesive	8.01	297.7	297.7	31.26	84.68
90	Cohesive	6.37	116.1	116.1	24.98	47.69
91	Cohesive	11.86	325.2	325.2	45.78	90.25
92	Cohesive	9.69	424.8	424.8	37.66	115.14
93	Cohesive	9.11	370.9	370.9	35.50	109.56
94	Cohesive	8.66	417.2	417.2	33.79	126.08
95	Cohesive	10.84	358	358	42.03	109.76
96	Cohesive	8.46	282.5	282.5	33.06	100.05
97	Cohesive	7.20	184.8	184.8	28.24	76.81
98	Cohesive	7.28	203.6	203.6	28.55	84.82
99	Cohesive	7.88	234.5	234.5	30.84	96.16
100	Cohesive	8.59	244.4	244.4	33.58	100.79
101	Cohesive	8.39	313.2	313.2	32.82	127.45
102	Cohesive	8.39	313.2	313.2	32.83	131.61
103	Cohesive	9.38	269.8	269.8	36.67	117.57
104	Cohesive	12.67	342.4	342.4	49.03	139.37
105	Cohesive	9.81	227.1	227.1	38.26	108.33
106	Cohesive	9.81	227.1	227.1	38.27	111.53
107	Cohesive	8.35	82.7	82.7	32.70	54.44
108	Cohesive	10.41	353.8	353.8	40.56	169.83
109	Cohesive	8.12	153.1	153.1	31.83	89.54
110	Cohesive	8.12	153.1	153.1	31.83	91.83
111	Cohesive	10.91	274.6	274.6	42.49	149.84
112	Cohesive	12.82	262.8	262.8	49.74	146.59
113	Cohesive	14.38	303.4	303.4	55.56	168.65
114	Cohesive	14.38	303.4	303.4	55.58	174.42

z	Ground Behaviour	qt	fsi_CPT	fsi	f_s_res	f_d
m		MPa	kPa	kPa	kPa	kPa
115	Cohesive	9.26	262.3	262.3	36.27	166.60
116	Cohesive	10.40	295.3	295.3	40.63	188.74
117	Cohesive	10.06	392.1	392.1	39.31	254.89
118	Cohesive	10.06	392.1	392.1	39.32	263.68
119	Cohesive	9.42	150.9	150.9	36.91	113.33
120	Cohesive	9.28	124.7	124.7	36.35	98.05
121	Cohesive	11.00	294.4	294.4	42.95	220.09
122	Cohesive	11.00	294.4	294.4	42.96	227.37
123	Cohesive	9.05	189.8	189.8	35.50	156.27
124	Cohesive	11.86	266.3	266.3	46.23	219.46
125	Cohesive	12.95	392.6	392.6	50.38	328.47
126	Cohesive	12.95	392.6	392.6	50.39	340.46
127	Cohesive	12.24	415.4	415.4	47.74	373.80
128	Cohesive	10.40	370.3	370.3	40.72	346.95
129	Cohesive	10.01	306.2	306.2	39.24	296.78
130	Cohesive	10.01	306.2	306.2	39.25	306.2

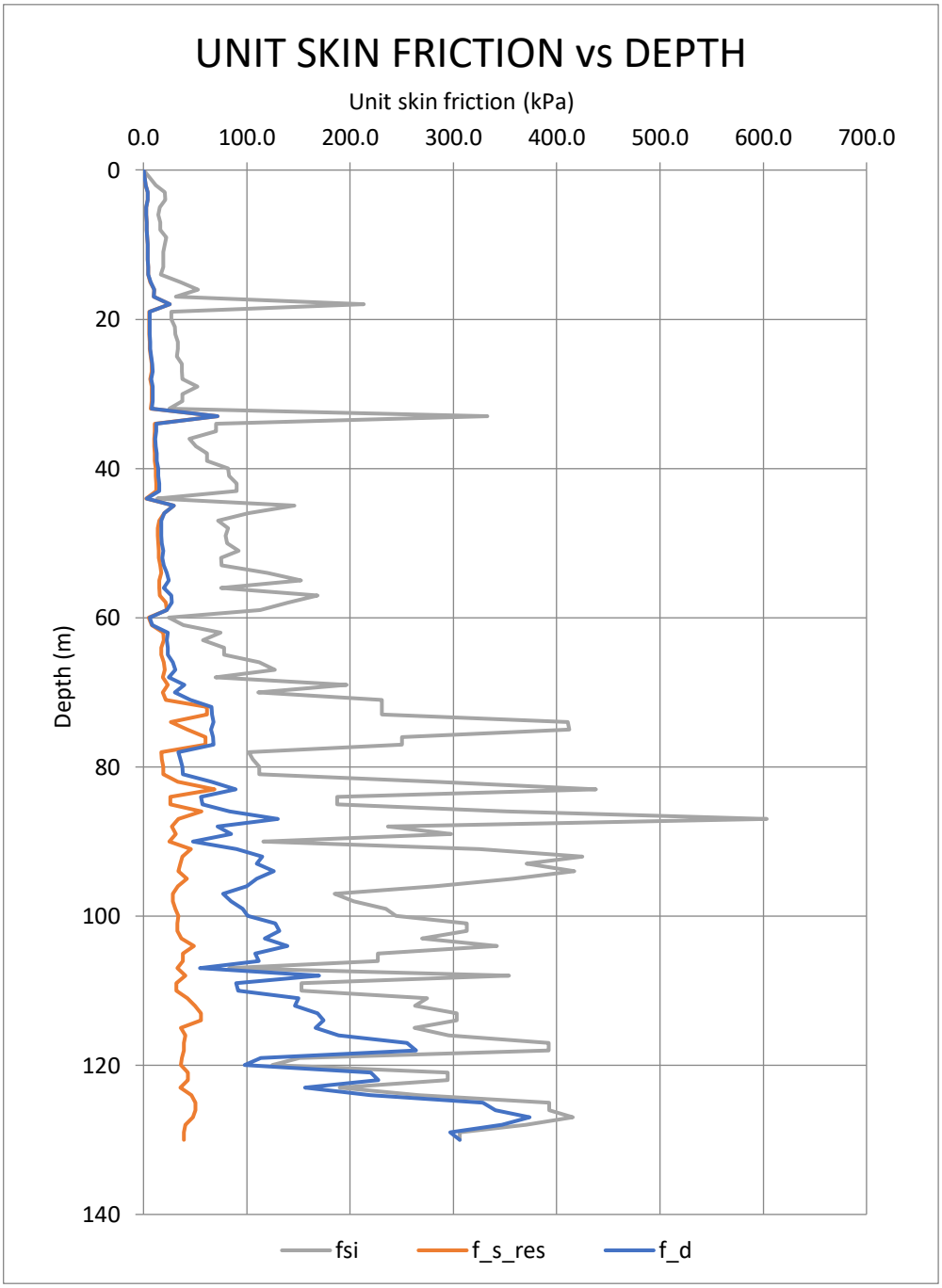

Figure 57 Unit skin friction vs depth based on CPT results.

This figure represents the initial unit skin friction that for cohesive soil comes from CPT test; instead for frictional soils it depends on the vertical effective stress, the soil-steel friction angle and the coefficient of lateral earth pressure K.

Then, the unit skin friction during driving (f_d) is not the sum of residual and initial unit skin friction. The last one is reduced considering a degradation (taking into account with a shape factor k).

The degradation factor is reported in the figure below.

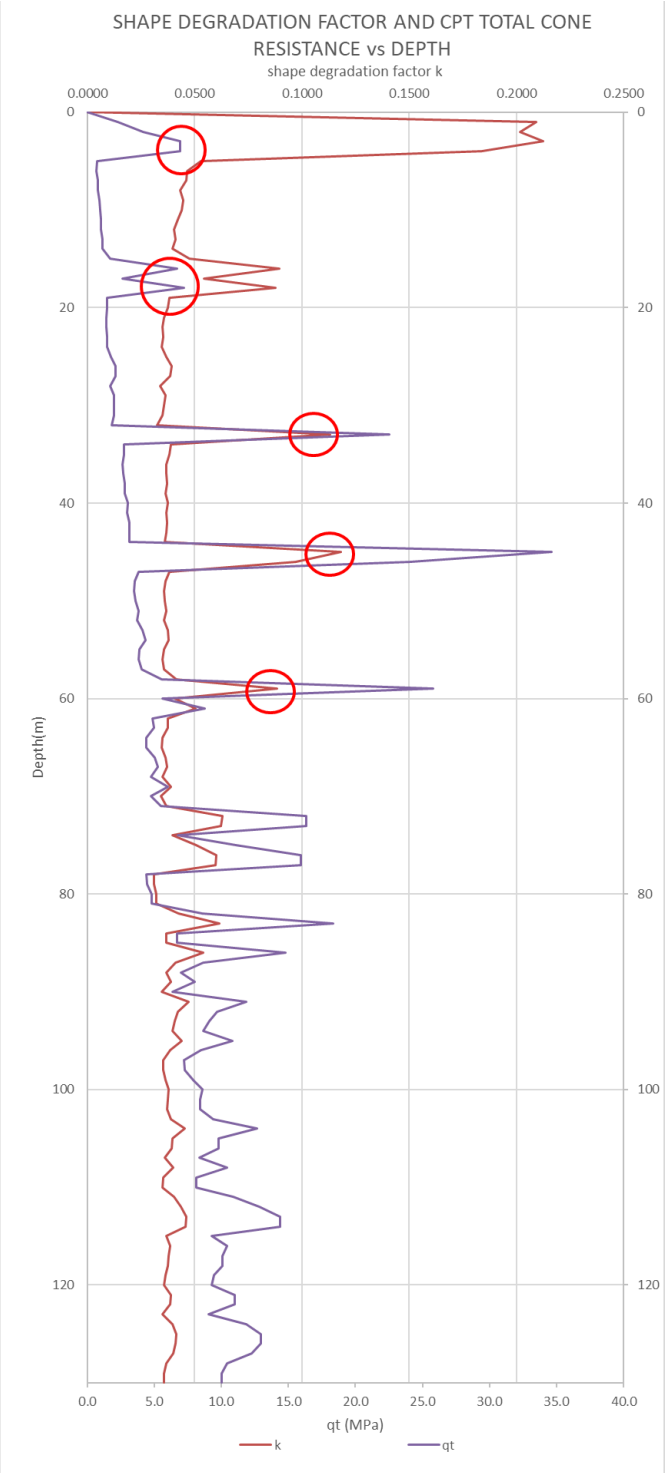

Figure 58 Shape degradation factor and cpt total cone resistance vs depth.

The degradation factor is proportional to the total cone resistance. For sand layers, a higher friction degradation occurs.

From the graph we can talk about a rapid degradation (k higher) for dense sands, while the opposite is for soft clays.

The results in terms of soil resistance to driving, considering the degradation above, is presented in the following figure.

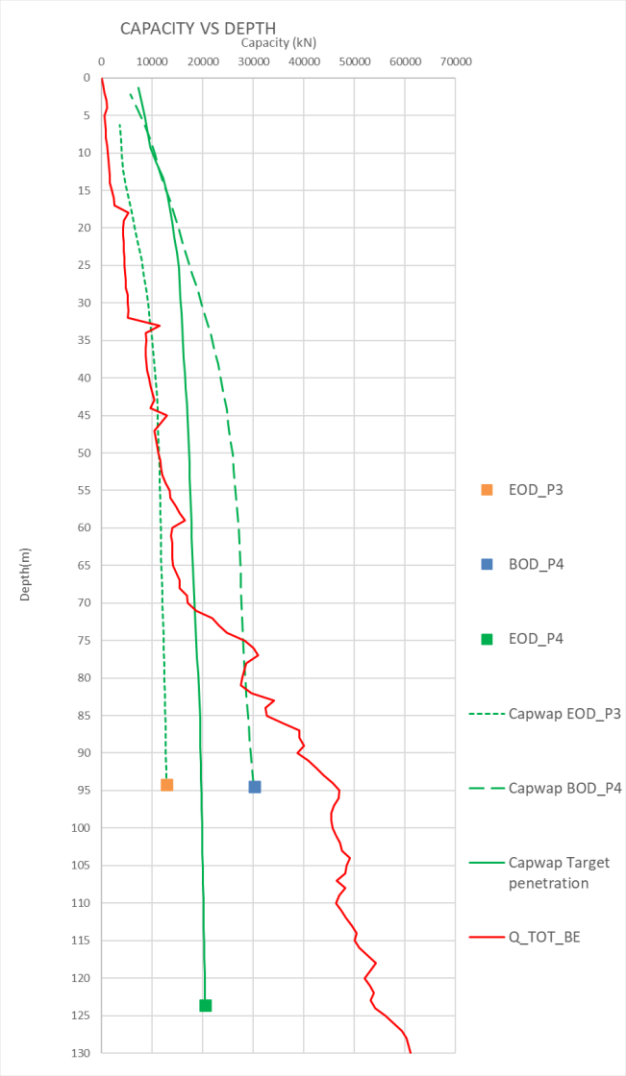

Figure 59 Results of CPT analysis in comparison with monitoring and interpolated value

The Figure 59 shows the comparison between SRD calculated with two different methods:

- CPT method
- CAPWAP ANALYSIS described in Section 2.11.1

The method considers unplugged behaviour of pile.

But, as reported in Figure 31, the end bearing is about the 40% of the lateral friction, so we can conclude that the pile behaviour is plugged.

If we consider a plugged pile (to estimate SRD we include only external shaft resistance and the end bearing area (the gross area of the pile)), the results are shown below.

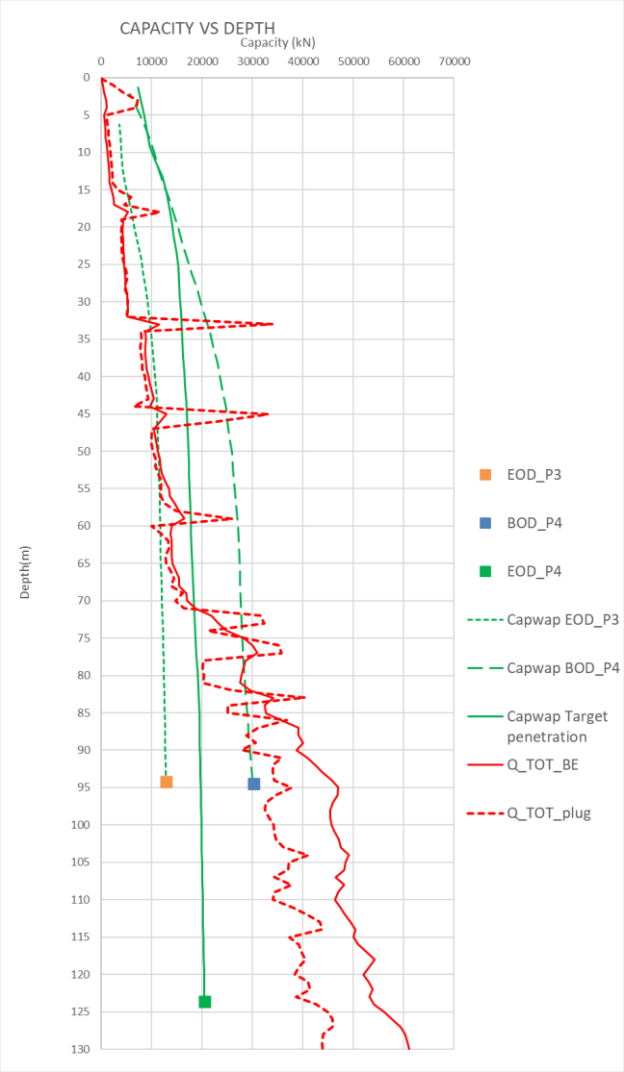

Figure 60 Results of CPT sensitivity analysis

With the assumption of plugged behaviour the SRD from CPT method is similar to capacity trend evaluated by the CAPWAP and the interpolated trends.

5.5 COMPARISON BETWEEN CALCULATED AND MEASURED SRD

For all jackets the pile static capacity for axial compression (as it reported in Section 2.4) was calculated. Then the continuous resistance to driving was obtained from axial capacity

considering a friction degradation (Delimi). These two results are reported in the figure below, the first one with the dotted line and the second one with a continuous line.

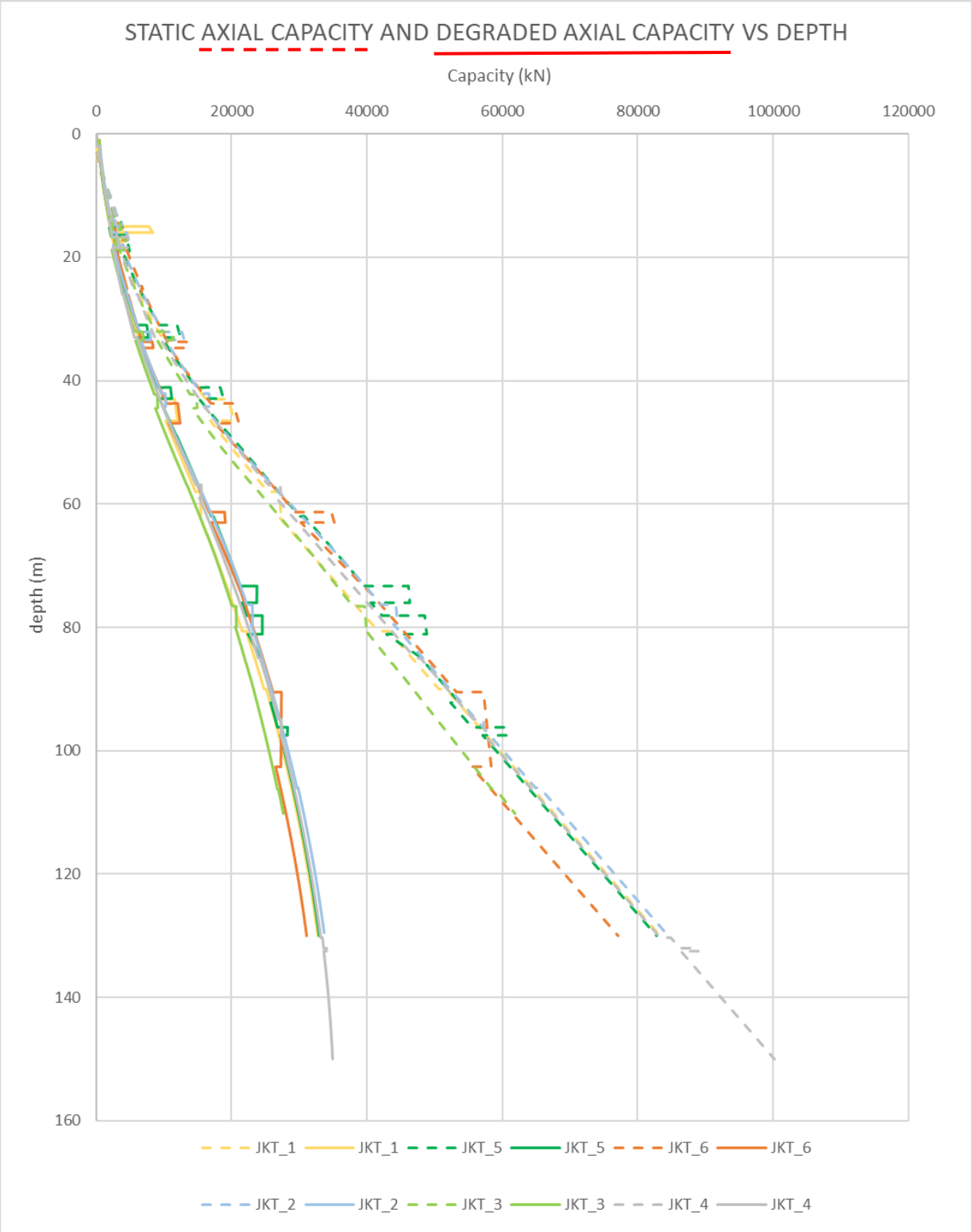

Figure 61 Axial static capacity and degraded axial capacity versus depth.

Then the monitoring data was compared with the results above at different depth:

- End of driving of the second add on (EOD_P3)
- Begin of driving of the third add on (BOD_P4)
- Target penetration of pile

We focus the attention on the percentage of monitoring soil resistance to driving (by Fugro) ratio the axial capacity (at first time) and the continuous predicted driving (in the second time).

At end of driving of second add on, the results of the resistance in percentage are reported in the figure below.

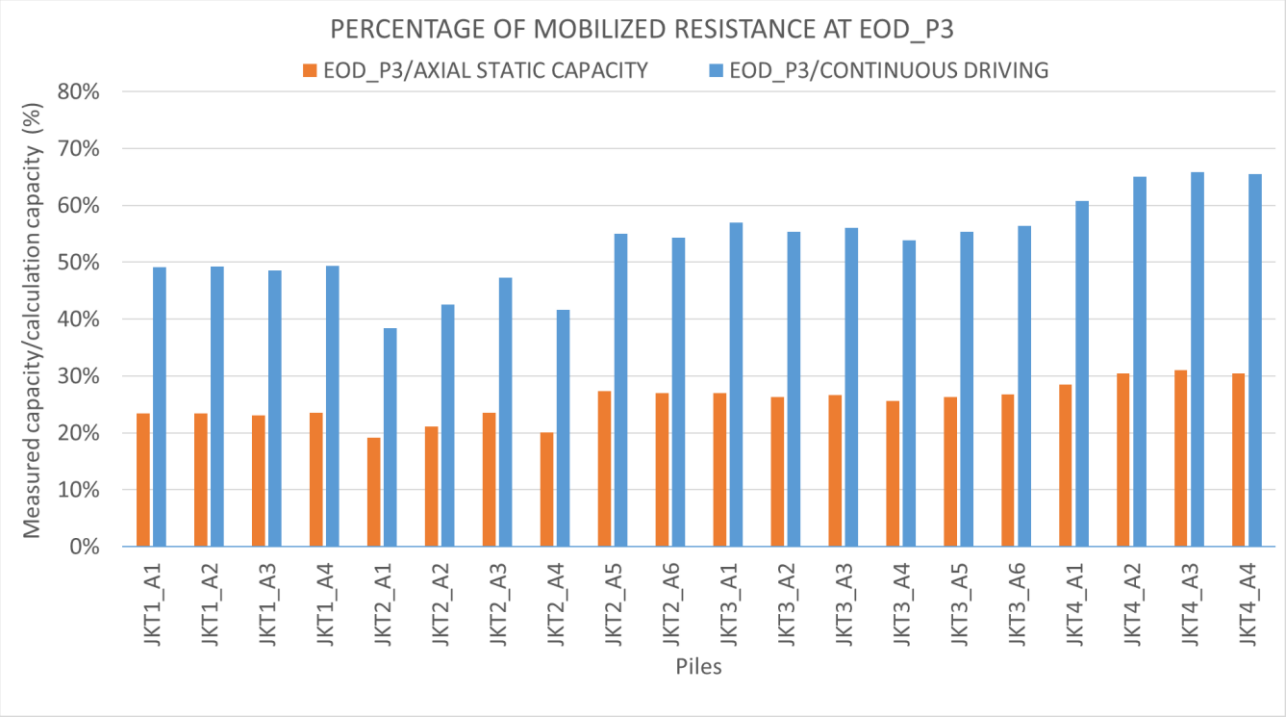

Figure 62 Percentage of mobilized resistance at end of driving of third add on compared to axial pile capacity and continuous driving

In this case a high soil friction degradation has been observed in calcareous clay: for all the piles the soil resistance to driving mobilized is more or less the 20%-30% of piles axial capacity and between 40% and 70% of the continuous predicted driving.

After a set-up time (showed in Table 14), at the same depth the soil resistance to driving increases (see Figure 63). It becomes the 40%-60% of axial pile capacity and almost always

is higher than the 100% of the continuous driving value. A gain of resistance has been observed after stopping driving.

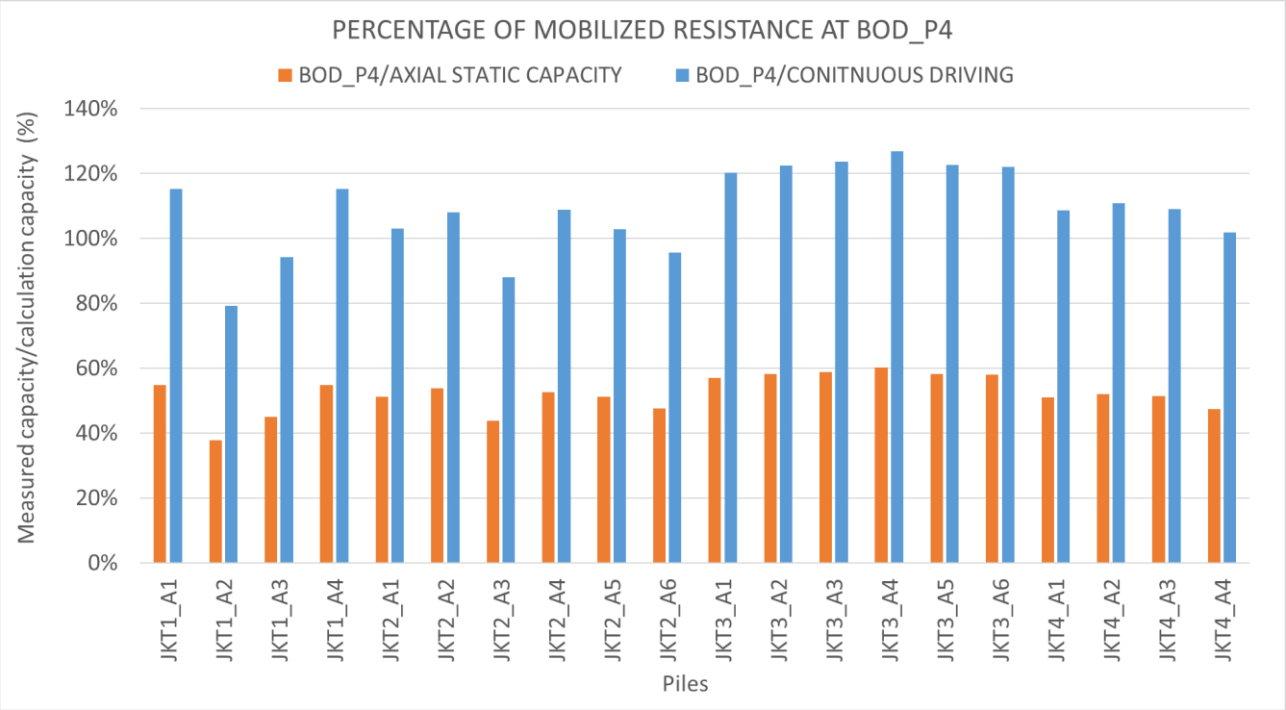

Figure 63 Percentage of mobilized resistance at begin of driving of fourth add on compared to axial pile capacity and continuous driving.

For the driving of the last pile section (third add on) an increase of soil resistance has been observed with respect to the driving up to the second add on.

The percentage of mobilized resistance at target penetration is shown in the figure below.

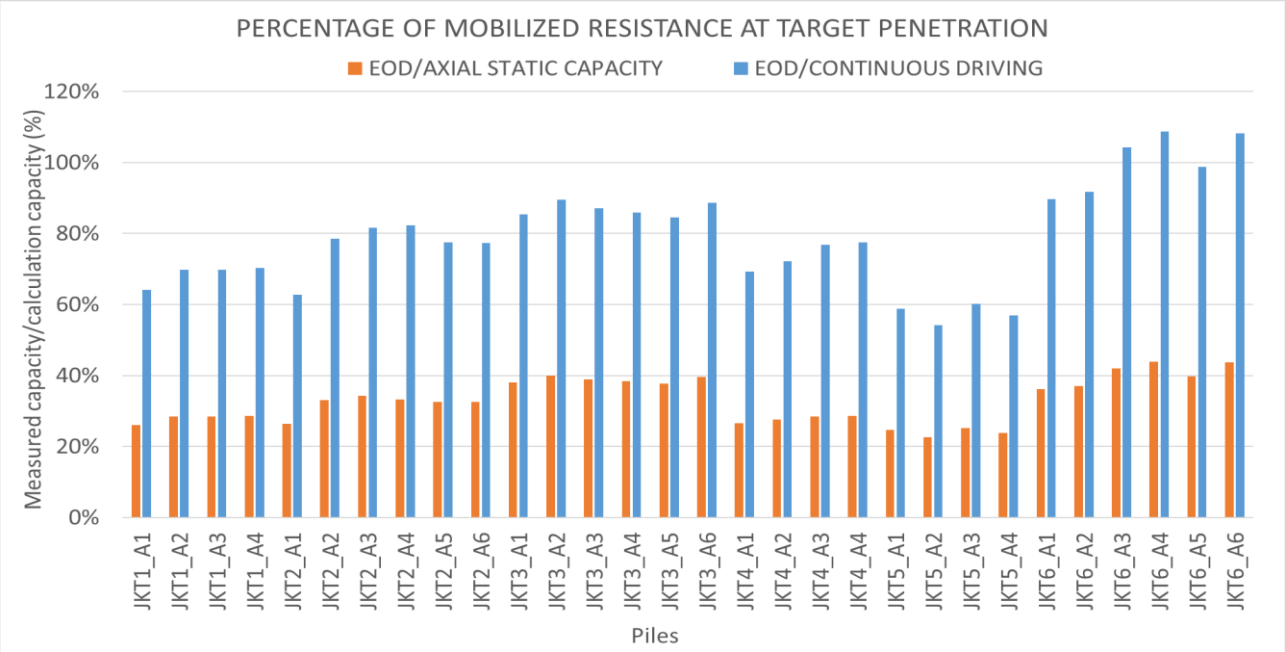

Figure 64 Percentage of mobilized resistance at target penetration compared to axial pile capacity and continuous driving.

For all the piles the soil resistance to driving mobilized is more or less the 30% - 40% of piles axial capacity.

Instead, compared to the continuous predicted driving (considering a friction degradation), the percentage of SRD mobilized is near the maximum value; that it means that all the predicted resistance was mobilized during continuous driving.

For the piles of JKT_6 the soil resistance to driving monitoring by Fugro is higher than the predicted value due to the set-up effect.

The set-up time during which the installation was interrupted is reported in the table below.

Table 14 Set-up time

Piles	Set-up time
	days
JKT1_A1	3.7
JKT1_A2	2.0

Piles	Set-up time days
JKT1_A3	1.8
JKT1_A4	3.4
JKT2_A1	2.0
JKT2_A2	2.2
JKT2_A3	2.4
JKT2_A4	2.4
JKT2_A5	1.8
JKT2_A6	2.0
JKT3_A1	2.5
JKT3_A2	2.4
JKT3_A3	2.7
JKT3_A4	-
JKT3_A5	2.6
JKT3_A6	2.4
JKT4_A1	7.7
JKT4_A2	8.9
JKT4_A3	7.6
JKT4_A4	9.2

For the last jacket the time stop was longer than for the others; that is the reason of the higher percentage of measured capacity/continuous driving.

CHAPTER 6: CONCLUSION AND FUTURE STUDIES

Research in the Arabian Gulf is constantly evolving. In recent years, the possibility of collecting real field data allowed to better understand the phenomenon of degradation and gain of soil resistance after pile driving in calcareous clay.

In this chapter the results of the thesis are discussed and some recommendations for further work on this field are pointed out.

6.1 CONCLUSION

The availability of monitoring data during the installation of large offshore tubular piles made it possible to investigate the behaviour of calcareous clays during the driving process, in terms of bearing capacity and set-up with time. Calcareous clays are a fine-grained soil characterized by low plasticity index and high carbonate content, a composition that makes not typical its behaviour during installation by driving of piles. A low driving resistance observed during continuous driving (thanks to the friction degradation) and a relevant set-up effect during driving interruptions (due to welding; hammer braking; bad weather conditions) are the two main phenomena that characterize this soil.

Calcareous clay shows an important friction degradation during pile installation: on one hand this phenomenon helps pile installation process, because the soil resistance to driving is lower; but, on the other hand, it could be a problem for the achievement of the bearing capacity of the pile required by the project.

However, a relevant set-up effect is also observed: it means that the bearing capacity of the pile increase with time, mainly due to the consolidation process that develops around the pile. The short time required to gain bearing capacity can lead to premature refusal of the pile during driving interruptions, if not well considered during design.

Thanks to the availability of monitoring data recovered in a past project regarding the installation of six jackets, a back analysis was performed: from the monitoring blow counts the soil resistance to driving was back calculated and compared with the capacity value directly measured during installation. A sensitivity analysis of dynamic soil parameters (damping and quake), to obtain the best match, was conduct. The main results of this analysis are in agreement with previous experiences from literature (i.e. Delimi's report) indicating

that, to find a good match between monitored and calculated capacity during driving in calcareous clay, a damping factor between to 0.4 s/m and 0.7 s/m should be assumed.

Taking into account the following definitions:

- Static axial capacity: the bearing capacity of the pile in static condition
- Degraded axial capacity: the bearing capacity of the pile during continuous driving
- Restart condition: the blow count recorded after a short set-up time

we can conclude that:

1. Calcareous clay shows an important friction degradation during installation:
   - The soil resistance to driving measured at the end of driving of the second add on (EOD_P3), is 20% - 30% of its static axial capacity.
   - The soil resistance to driving measured at the end of driving of the second add on (EOD_P3), is 40% - 70% of degraded axial capacity (continuous driving assumption).
2. Thanks to set-up phenomenon piles can recover some axial capacity:
   - The soil resistance to driving measured at the beginning of last add on (BOD_P4 in restart condition) is 40% - 60% of static axial capacity.
   - The soil resistance to driving measured at the beginning of last add on (BOD_P4 in restart condition) is 80% - 130% of degraded axial capacity (continuous driving assumption).
3. At target penetration both phenomena are visible:
   - The measured soil resistance to driving is 20% - 40% of piles static axial capacity, that is larger than the value obtained during continuous driving, showing a gain of capacity after set-up time.
   - The measured soil resistance to driving is 60% - 100% of degraded axial capacity (continuous driving assumption), that means less degradation with respect to the continuous driving up to the welding of the last add on is recorded.

6.2 FUTURE STUDIES

Future studies are now suggested:

- When the soil is submitted to rapid motions, some excess pore pressures can be generated in the soil. However, this behaviour is extremely difficult to consider. It is

therefore proposed to perform further investigations in order to assess the influence of drained/undrained behaviour of the soil.

- Use other soil parameters in the signal matching analysis.
- Test the formulations with the proposed damping and quake parameters in other locations with a same soil and verify the match in terms of SRD and in terms of blow counts.
- For CPT METHOD is necessary to investigate if the overestimation of SRD is due to the uncertainty of degradation phenomenon or due to the plugged behaviour of pile. If the first one has a greater impact it is possible to verify if the new formulation for degradation factor provides a good prediction and can be used for other types of soil.
- Test other type of pile and soil to identify alternative formulation (other than Delimi) for the degradation in other soil conditions.

REFERENCES

[1] Z. L. Delimi, M. Maron and R. Clavaud. Pile installation in Calcareous Clays. California.

[2] Likins G., Piscsalko G. & Roppel S (2008). PDA Testing: 2008 State of the art.

[3] Rausche, Nagy, Liang, Webster (2009). CAPWAP and refined wave equation analyses for driveability predictions and capacity assessment of offshore pile installations. USA

[4] J.F. Wilson (1933). Dynamics of offsore structures. USA

[5] A.S. Kharade, S.V. Kapadiya (2014). Offshore engineering: an overview of types and loadings on structures.

[6] L. Wisch, D. J. Puskar (2004). An Update on API RP 2A for the Assessment of Existing Platform.

[7] API recommended practice 2A- WSD (2014). Planning, designing, and Constructing Fixed Offshore Platforms – Working stress design.

[8] Colliant, Vergobbi and Puech (1993). Friction degradation and Set-up effects in hard clays offshore Congo and Angola. USA.

[9] F. Rausche, B. Robinson, G. Likins (2004). On the prediction of a long-term pile capacity from end-of-driving information. California

[10] F. Rausche, G. Likins, L. Liang, M. Hussein (2010). Static and Dynamic Models for CAPWAP Signal Marching.

[11] F.Rausch, M.Hussein (2000). Pile driving in calcareous sediments. USA

[12] Allnamics (official web site)

ACKNOWLEDGMENTS

Prima di ringraziare tutte le persone che mi sono state vicine in questi cinque anni e che hanno preso parte al mio percorso universitario, un ringraziamento speciale non può che essere dedicato al Prof. Paolo Ruggeri, relatore di questa tesi che mi ha guidato nella stesura scrupolosa dell'elaborato con estrema pazienza e disponibilità quotidiana.

Un ringraziamento speciale a tutta la società Saipem, e in particolare ad Andrea, il correlatore di questo lavoro. Mi hai sempre sostenuto e guidato in questo periodo, mi hai trasmesso la passione con la quale svolgi tutto il tuo lavoro. Grazie anche ad Alessia, Maurizio, Bibiana, Nicolas e Roberto, avete reso quest'esperienza di tirocinio indimenticabile. Mi avete accolta in un mondo del tutto nuovo, mi avete supportato dall'inizio alla fine di questo seppur breve percorso.

Non posso poi non nominare la mia famiglia che mi ha permesso di intraprendere questo percorso universitario, lasciandomi liberà di scelta e supportandomi in ogni mia decisione giorno dopo giorno. A mio papà, alla tua bontà d'animo e alla tua disponibilità; alla mia mamma, al tuo amore incondizionato verso di me. A voi dedico questo successo. Ci siete sempre stati e sempre ci sarete. Mi avete sempre spronato a puntare in alto, a non arrendermi mai, a non piangermi addosso anche quando l'ansia mi prendeva per la gola, mi chiudeva lo stomaco e mi faceva credere di non farcela più.

A mio Fratello, il mio punto debole. A te che sei così forte e così sensibile allo stesso tempo. A te che hai sempre la parola giusta al momento giusto. A te che "guai a chi ti tocca e spaccherei il mondo", proprio come so che faresti tu per me. Anche se non passiamo più molto tempo insieme, ci basta uno sguardo per capirci e senza dire nulla ci diamo la forza per conquistare ogni cosa che ci passa per la testa.

A tutti i miei parenti, a zia Manu che è stata il perfetto hotel per tutti i mesi di tirocinio; a nonna Filo che tutti le volte di un esame aspettava con ansia la fatidica telefonata, e a zia Paola. Mi dispiace per averti deluso quest'anno e non aver fatto i giri di duecento mila negozi per trovare un vestito. Sarà che mancava la parte fondamentale del trio, la mia cucu.

A te, la sorella che non ho avuto. A te che mi hai insegnato cos'è il sacrificio, cosa significa lottare per raggiungere un obiettivo quando tutti credono che non ce la fai. A noi che siamo sempre state insieme fin dalla nascita, sappi che, anche se adesso ci sono più di 400 km a dividerci, sono fiera di te e della tenace sognatrice che sei.

Ai miei amici, grazie per non avermi abbandonata nonostante i miei continui impegni e scleri. Grazie per essermi stati a fianco, per avermi dato spensieratezza e divertimento anche quando i pensieri erano tanti.

A Giulia, la persona che mi ha fatto capire che la famiglia non è solo quella di sangue. Grazie per aver creduto in me quando non ci credevo nemmeno io. Grazie per avermi sempre supportato e sopportato, per aver subito ogni mia ansia e paranoia prima e dopo ogni esame e per essere stata al mio fianco in ogni momento. Grazie per avermi spronata a dare sempre il meglio di me e per essere stata la persona su cui poter contare ogni giorno. Hai gioito per ogni mio esame più di quanto lo facessi io e hai sofferto quanto me quando qualcosa è andato storto.

A Omar, il mio punto debole e il mio punto di riferimento. Ti ringrazio per non avermi lasciata mai sola, per non essere né avanti né indietro, ma accanto ad ogni mio passo. Alla nostra telepatia, al nostro essere troppo simili in troppe cose, alla tua dolcezza e alla tua pazienza che in quest'ultimo periodo troppa ce n'è voluta. Alla nostra felicità, ai nostri successi e ai nostri progetti e traguardi, che insieme, mano per la mano, abbiamo conquistato e riusciremo a conquistare.

Siete esattamente quello che ho sempre desiderato, siete la parte mancante che completa il mio cuore. Noi siamo una squadra e ogni mia vittoria è anche la vostra.

Vi voglio bene.

APPENDIX A

SOIL BOREHOLE PLOT

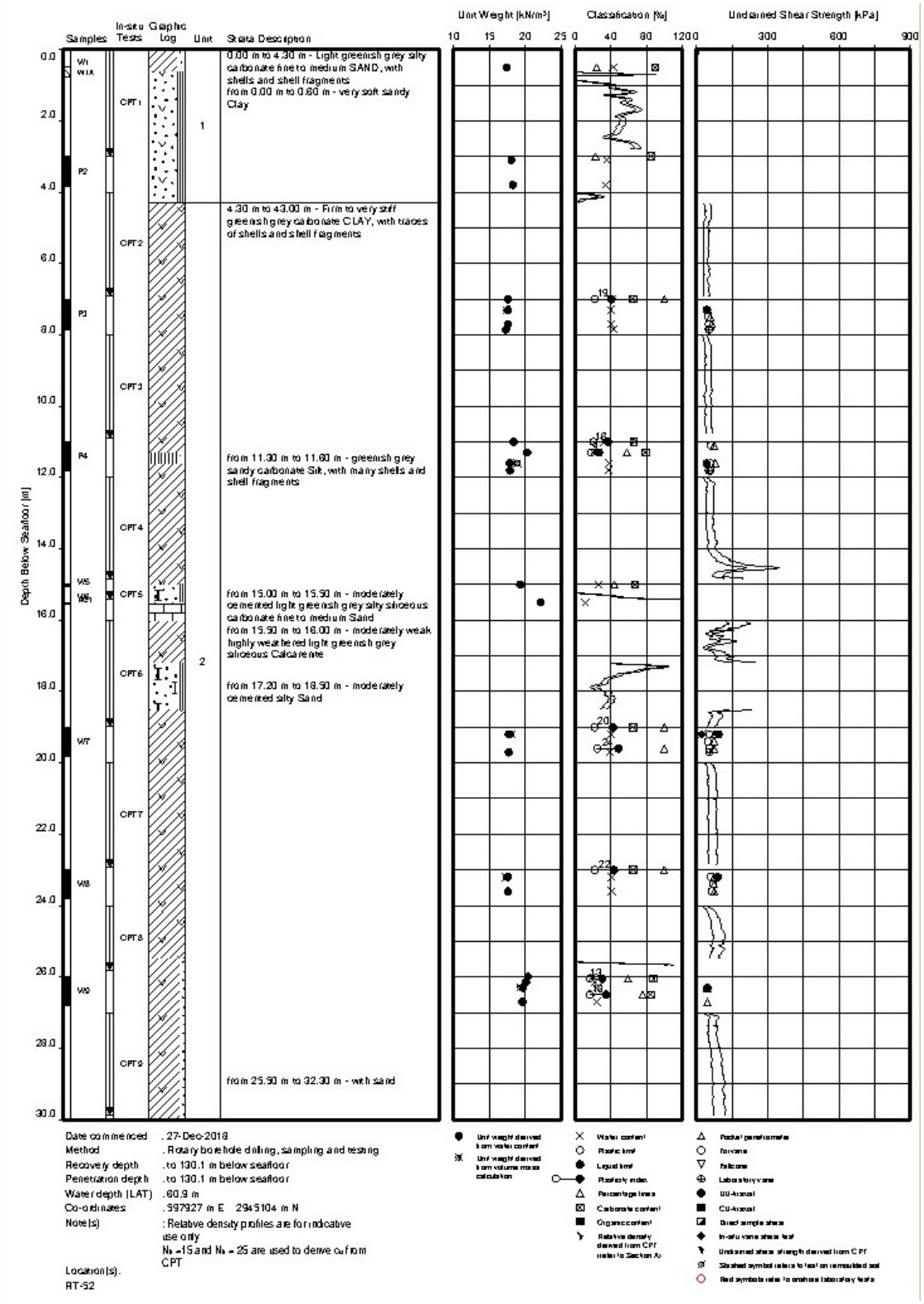

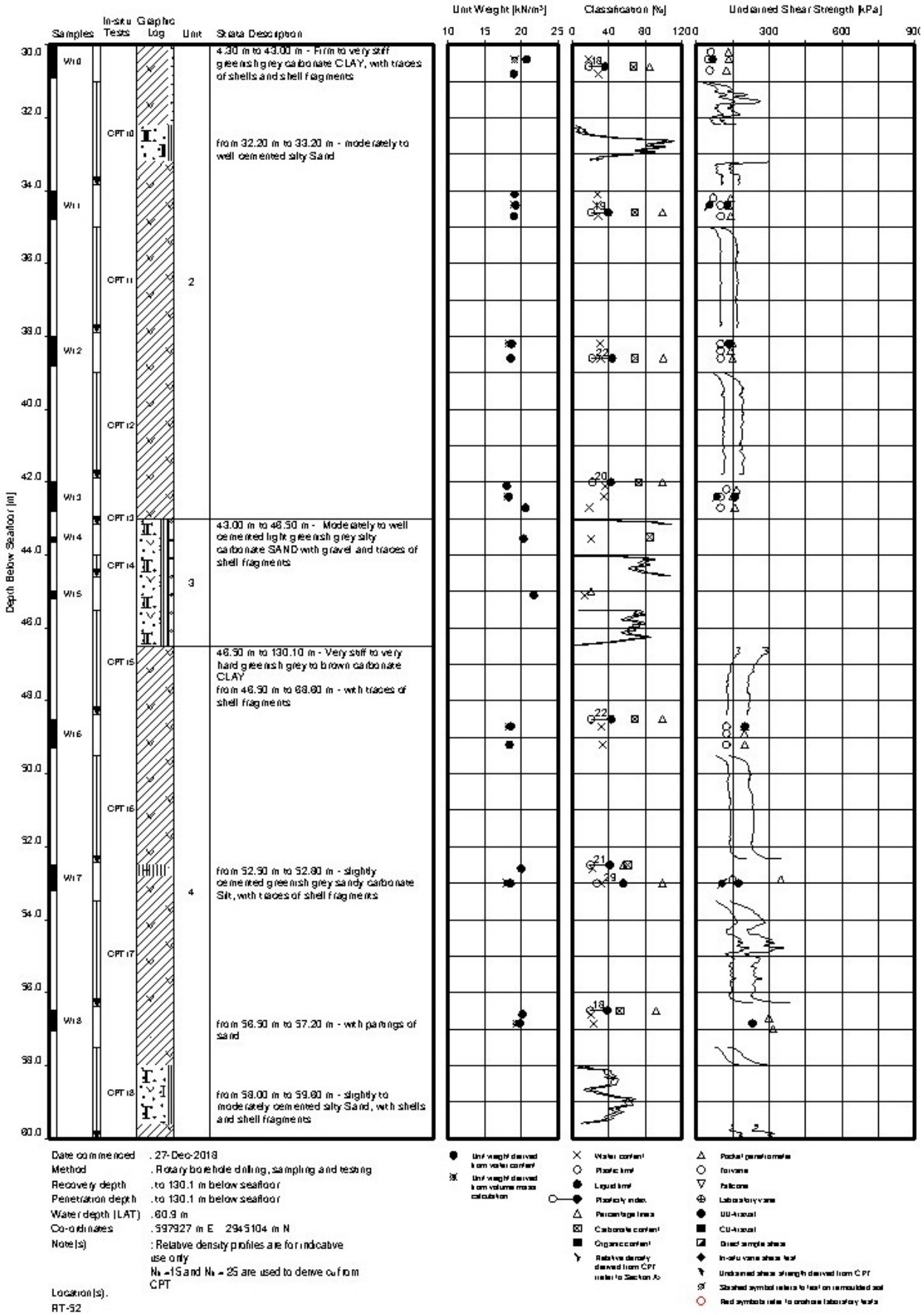
Samples
In-situ Tests
Graphic Log
Unit
Strata Description
Unit Weight [kN/m³]
Classification [%]
Undrained Shear Strength [kPa]
Depth Below Seafloor [m]
4.30 m to 43.00 m - Firm to very stiff greenish grey carbonate CLAY, with traces of shells and shell fragments
from 32.20 m to 33.20 m - moderately to well cemented silty Sand
43.00 m to 46.50 m - Moderately to well cemented light greenish grey silty carbonate SAND with gravel and traces of shell fragments
46.50 m to 130.10 m - Very stiff to very hard greenish grey to brown carbonate CLAY
from 46.50 m to 68.80 m - with traces of shell fragments
from 52.90 m to 52.80 m - slightly cemented greenish grey sandy carbonate Silt, with traces of shell fragments
from 56.90 m to 57.20 m - with partings of sand
from 58.00 m to 59.80 m - slightly to moderately cemented silty Sand, with shells and shell fragments
Date commenced . 27-Dec-2018
Method . Rotary borehole drilling, sampling and testing
Recovery depth . to 130.1 m below seafloor
Penetration depth . to 130.1 m below seafloor
Water depth (LAT) . 60.9 m
Co-ordinates . 597927 m E 2945104 m N
Note(s) : Relative density profiles are for indicative use only
Nk = 15 and Nk = 25 are used to derive cu from CPT
Location(s).
RT-S2
Unit weight derived from water content
Unit weight derived from volume mass calculation
Water content
Plastic limit
Liquid limit
Plasticity index
Percentage fines
Carbonate content
Organic content
Relative density derived from CPT refer to Section A
Pocket penetrometer
Torvane
Fallcone
Laboratory vane
UU-triaxial
CU-triaxial
Direct simple shear
In-situ vane shear test
Undrained shear strength derived from CPT
Slashed symbol refers to test on remoulded soil
Red symbols refer to onshore laboratory tests

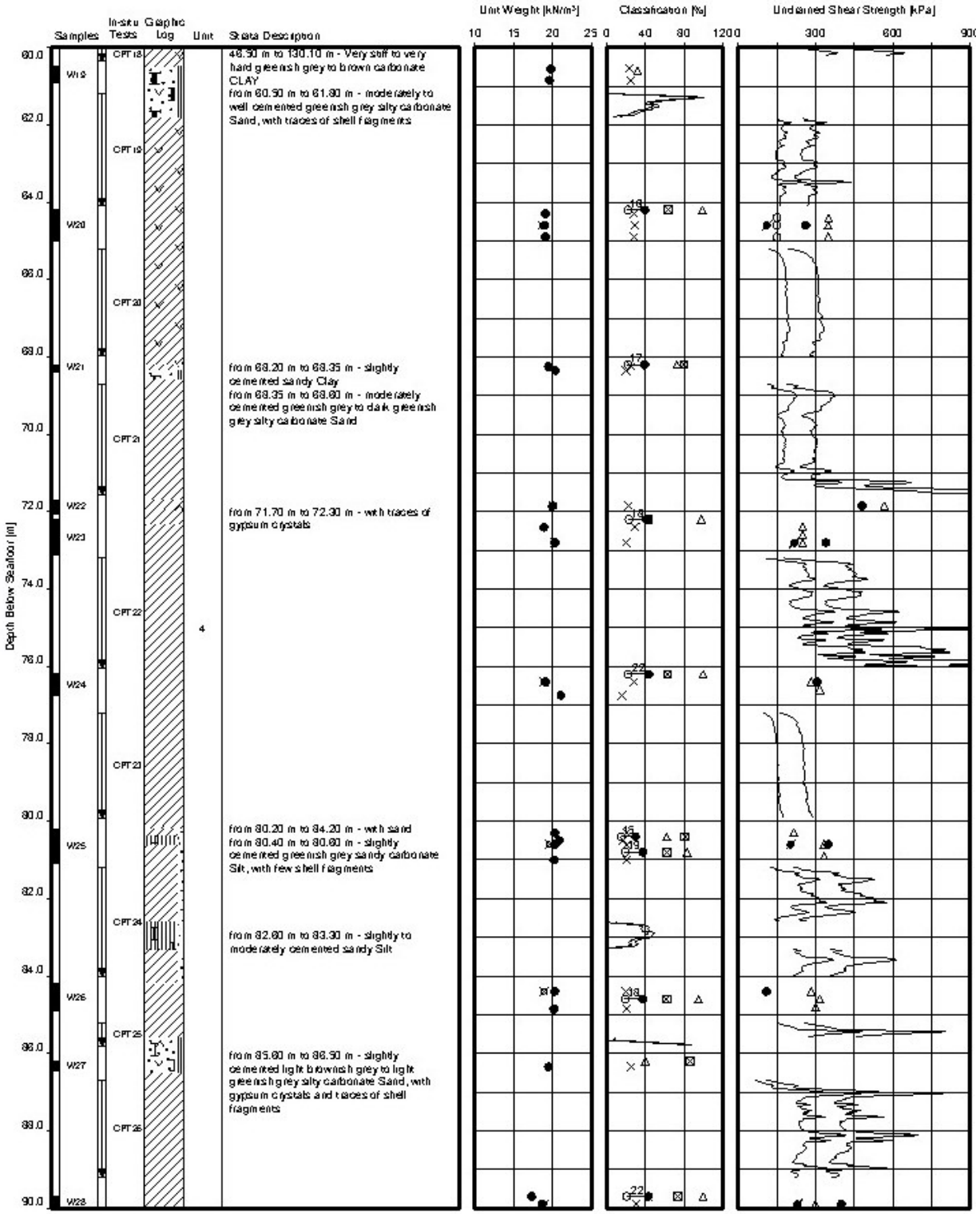
Samples
In-situ Tests
Graphic Log
Unit
Strata Description
Unit Weight [kN/m³]
Classification [%]
Undrained Shear Strength [kPa]
Depth Below Seafloor [m]
48.90 m to 130.10 m - Very stiff to very hard greenish grey to brown carbonate CLAY
from 60.90 m to 61.80 m - moderately to well cemented greenish grey silty carbonate Sand, with traces of shell fragments
from 68.20 m to 68.35 m - slightly cemented sandy Clay
from 68.35 m to 68.80 m - moderately cemented greenish grey to dark greenish grey silty carbonate Sand
from 71.70 m to 72.30 m - with traces of gypsum crystals
from 80.20 m to 84.20 m - with sand
from 80.40 m to 80.60 m - slightly cemented greenish grey sandy carbonate Silt, with few shell fragments
from 82.60 m to 83.30 m - slightly to moderately cemented sandy Silt
from 85.60 m to 86.90 m - slightly cemented light brownish grey to light greenish grey silty carbonate Sand, with gypsum crystals and traces of shell fragments
Date commenced . 27-Dec-2018
Method . Rotary borehole drilling, sampling and testing
Recovery depth . to 130.1 m below seafloor
Penetration depth . to 130.1 m below seafloor
Water depth (LAT) . 60.9 m
Co-ordinates . 597927 m E 2945104 m N
Note(s) : Relative density profiles are for indicative use only
Nk = 15 and Nk = 25 are used to derive cu from CPT
Location(s).
RT-S2

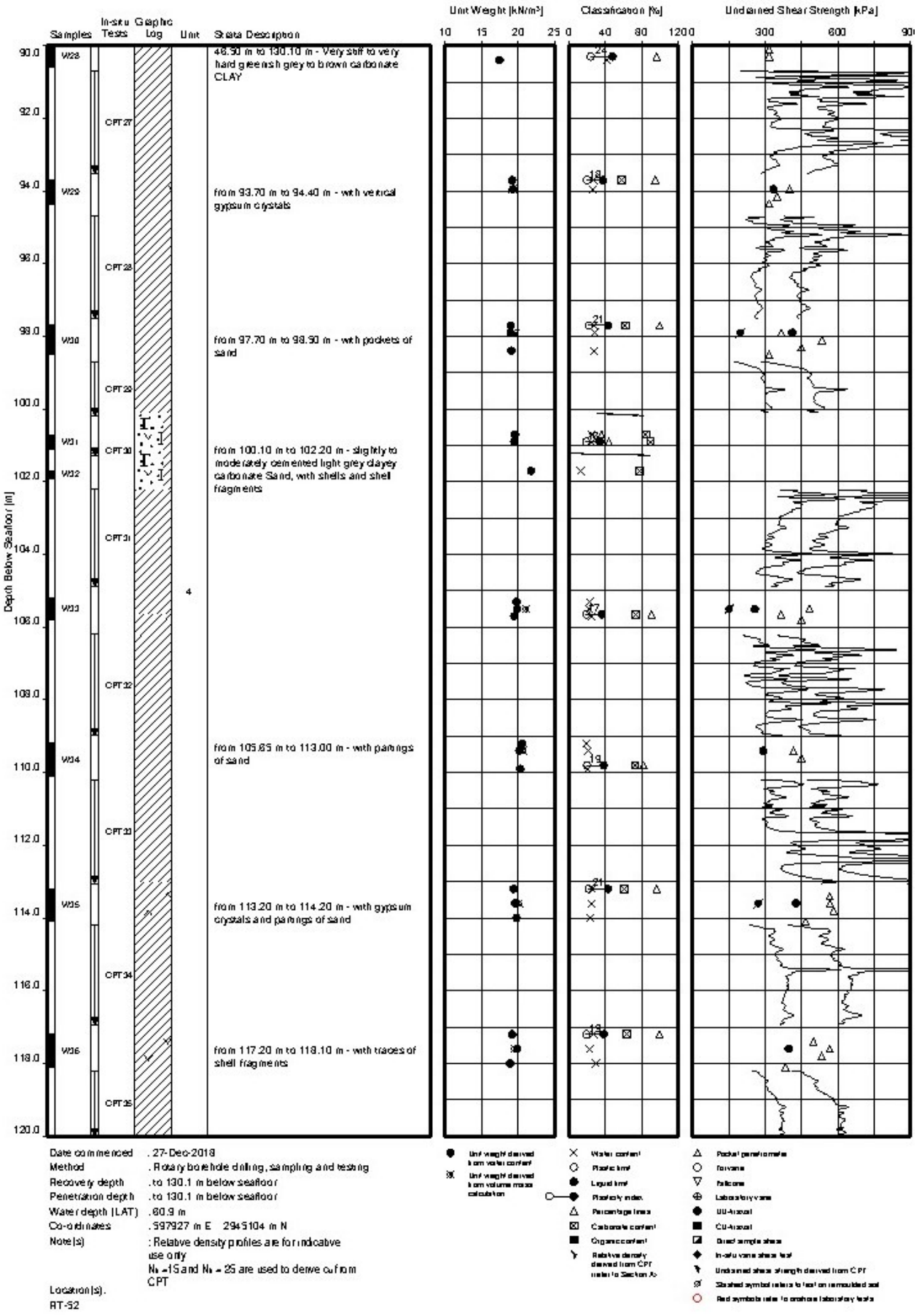
Samples
In-situ Tests
Graphic Log
Unit
Strata Description
Unit Weight [kN/m³]
Classification [%]
Undrained Shear Strength [kPa]
Depth Below Seafloor [m]
48.90 m to 130.10 m - Very stiff to very hard greenish grey to brown carbonate CLAY
from 93.70 m to 94.40 m - with vertical gypsum crystals
from 97.70 m to 98.90 m - with pockets of sand
from 100.10 m to 102.20 m - slightly to moderately cemented light grey clayey carbonate Sand, with shells and shell fragments
from 105.85 m to 113.00 m - with partings of sand
from 113.20 m to 114.20 m - with gypsum crystals and partings of sand
from 117.20 m to 118.10 m - with traces of shell fragments
W028
W029
W030
W031
W032
W033
W034
W035
W036
CPT27
CPT28
CPT29
CPT30
CPT31
CPT32
CPT33
CPT34
CPT35
Date commenced . 27-Dec-2018
Method . Rotary borehole drilling, sampling and testing
Recovery depth . to 130.1 m below seafloor
Penetration depth . to 130.1 m below seafloor
Water depth (LAT) . 60.9 m
Co-ordinates . 597927 m E 2945104 m N
Note(s) : Relative density profiles are for indicative use only
Nk = 15 and Nk = 25 are used to derive cu from CPT
Location(s).
RT-S2
Unit weight derived from water content
Unit weight derived from volume mass calculation
Water content
Plastic limit
Liquid limit
Plasticity index
Percentage fines
Carbonate content
Organic content
Relative density derived from CPT refer to Section A
Pocket penetrometer
fall cone
Laboratory vane
UU-triaxial
CU-triaxial
Direct simple shear
In-situ vane shear test
Undrained shear strength derived from CPT
Shaded symbol refers to test on remoulded soil
Red symbols refer to onshore laboratory tests

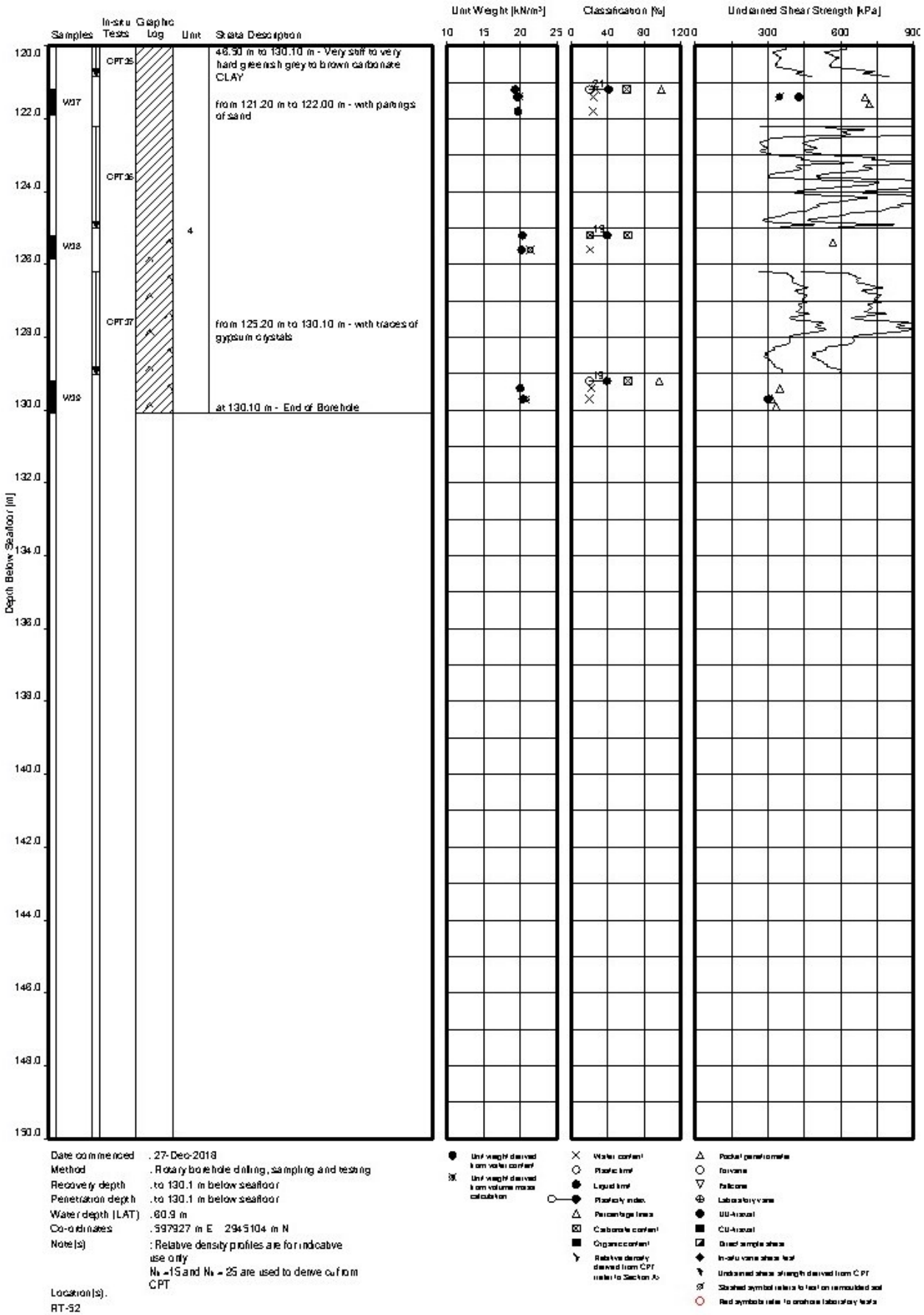
Unit Weight [kN/m³]
Classification [%]
Undrained Shear Strength [kPa]
Samples
In-situ Tests
Graphic Log
Unit
Strata Description
48.50 m to 130.10 m - Very stiff to very hard greenish grey to brown carbonate CLAY
from 121.20 m to 122.00 m - with partings of sand
from 125.20 m to 130.10 m - with traces of gypsum crystals
at 130.10 m - End of Borehole
CPT35
CPT36
CPT37
W37
W38
W39
4
Depth Below Seafloor [m]
120.0
122.0
124.0
126.0
128.0
130.0
132.0
134.0
136.0
138.0
140.0
142.0
144.0
146.0
148.0
150.0
10
15
20
25
0
40
80
120
300
600
900
Date commenced . 27-Dec-2018
Method . Rotary borehole drilling, sampling and testing
Recovery depth . to 130.1 m below seafloor
Penetration depth . to 130.1 m below seafloor
Water depth (LAT) . 60.9 m
Co-ordinates . 597927 m E 2945104 m N
Note(s) : Relative density profiles are for indicative use only
N_k =15 and N_k = 25 are used to derive cu from CPT
Location(s).
RT-S2
Unit weight derived from water content
Unit weight derived from volume mass calculation
Water content
Plastic limit
Liquid limit
Plasticity index
Percentage fines
Carbonate content
Organic content
Relative density derived from CPT refer to Section A-
Pocket penetrometer
fall vane
falcon
Laboratory vane
UU-triaxial
CU-triaxial
Direct simple shear
In-situ vane shear test
Undrained shear strength derived from CPT
Slashed symbol refers to test on remoulded soil
Red symbols refer to onshore laboratory tests